
**An X-ray diffraction approach:
Bulk mineral assemblages as provenance indicator of
sediments from the Arctic Ocean**

Dissertation zur Erlangung des akademischen Grades
eines Doktors der Naturwissenschaften

— Dr. rer. nat. —

am Fachbereich Geowissenschaften
der Universität Bremen

vorgelegt von

Hao Zou

Bremerhaven, March 2016

Gutachter der Dissertation

Prof. Dr. Rüdiger Stein

Prof. Dr. Gerhard Bohrmann

Tag des öffentlichen Kolloquiums

15th June 2016

Name :Hao.Zou.....Datum31.03.2016.....

Anschrift :Am Alten Hafen 26, 27568, Bremerhaven.....

E r k l ä r u n g

Hiermit versichere ich, dass ich

1. die Arbeit ohne unerlaubte fremde Hilfe angefertigt habe,
2. keine anderen als die von mir angegebenen Quellen und Hilfsmittel benutzt habe und
3. die den benutzten Werken wörtlich oder inhaltlich entnommenen Stellen als solche kenntlich gemacht habe.

_____, den

.....

(Unterschrift)

Abstract

Paleoclimate research and climate models demonstrate that the Arctic is very sensitive to climate change and also plays a key role in driving and amplifying global climate variability and sea-level change. Study of the late Quaternary paleoceanography in the Arctic Ocean is of great importance to understand the glacial-interglacial climate changes. As the sediment in the central Arctic Ocean is mostly transported by iceberg and sea-ice, provenance studies can be used to infer the ice-sheet history and the surface circulation pattern. Bulk mineral assemblages are one of the proxies that can be used to identify the source areas of the Arctic sediments. The main aim of this thesis is to study in detail the quantitative X-Ray Diffraction (qXRD) software package RockJock which is used to obtain the bulk mineral assemblages result and the comparison of the two qXRD software packages RockJock and QUAX.

In Chapter 4, three different sets of artificial mixtures are used to assess the accuracy of RockJock, and the possible sources of errors are proposed. The comparison of RockJock and QUAX is based on the surface sediment samples retrieved from the Siberian shelf seas as well as the central Arctic Ocean. Quartz, feldspars, calcite, dolomite, and the sum of clay minerals show fairly good correlations, while the differences of individual clay minerals are high.

In Chapter 5, surface sediment samples, which are used in Chapter 4, were analyzed using RockJock to test the possibility to use bulk mineral assemblages as provenance indicator. It shows that the combination of quartz, Qz/Fsp, dolomite and kaolinite can be used to identify source areas. Sediment input from the Canadian Arctic is generally characterized by high dolomite and Qz/Fsp values. Sediment input from the Eurasian Arctic shelf seas is generally characterized by low dolomite, Qz/Fsp, kaolinite values and high quartz values. Although the contents of amphibole are mostly too small to be quantified, the occurrence of amphibole might be an indicator of sediments from the Siberian shelf seas.

In Chapter 6, three sediment cores selected from a transect across the Mendeleev Ridge were used in this thesis to study the provenance of terrigenous sediments from the Central Arctic in order to study the ice sheet history. It shows that the provenance of sediments deposited on the Makarov Basin side of the Mendeleev Ridge is different from that deposited on the Canada Basin side of the Mendeleev Ridge. The IRD events of MIS16, 12, 10, 8 are characterized by high dolomite contents, high quartz/feldspar ratios and low plagioclase contents and may suggest IRD input from the Canadian Archipelago. The IRD events that occur in MIS6, are characterized by high quartz and low dolomite contents, which indicates IRD from the Eurasian sources.

Kurzfassung

Paläoklimatologischen Untersuchungen und Klimamodellierungen zufolge, reagiert die Arktis sehr sensibel auf Klimaschwankungen. Zudem spielt die Arktis eine Schlüsselrolle im Bezug auf das Auslösen und Verstärken von Klimaveränderungen und Meeresspiegelschwankungen. Das Erforschen der Paläoozeanographie des Arktischen Ozeans ist essentiell, um die Schwankungen zwischen Glazialen und Interglazialen während des späten Quartärs zu verstehen. Da Sedimente in der Zentralen Arktis größtenteils mit Hilfe von Eisbergen oder Meereis transportiert werden, eignen sich Provenienz Studien besonders gut, um die Geschichte der Eisschilde und die Struktur der Oberflächenzirkulation zu rekonstruieren. Die gesamte Mineralverteilung wird häufig angewandt, um die Quellregionen der Arktischen Sedimente zu bestimmen. Das Hauptforschungsziel dieser Doktorarbeit ist sowohl die detaillierte Anwendung und Evaluation der quantitativen Röntgen (X-Ray) Diffraktion (qXRD) Software RockJock, welche zur Bestimmung der gesamte Mineralverteilung genutzt wird als auch den Vergleich zwischen RockJock und einer weiteren qXRD-Software (QUAX) aufzustellen.

In Kapitel 4 werden drei verschiedene künstlich angesetzte Mineralzusammensetzungen genutzt, um die Messgenauigkeit sowie mögliche Fehlerquellen von RockJock zu bestimmen. Der Vergleich zwischen RockJock und QUAX basiert auf Oberflächensedimentproben, die aus Sibirischen Schelfmeeren und aus der Zentralen Arktis stammen. Quarz, Feldspat, Kalzit, Dolomit und die Summe der Tonminerale zeigen eine gute Korrelation, wohingegen die Abweichung innerhalb der einzelnen Tonminerale hoch ist.

In Kapitel 5 werden die Oberflächensedimente, welche auch in Kapitel 4 herangezogen wurden, mittels der RockJock Software analysiert, um die Anwendbarkeit von Bulk Mineral Verteilungen als Provenienz Indikator zu erproben. Dabei stellt sich heraus, dass sich die Kombination von Quarz, dem Verhältnis aus

Quarz und Feldspat (Qz/Fsp), Dolomit und Kaolinit als Indikator für Quellregionen eignen. Der Sedimenteintrag von der Kanadischen Arktis kann generell mit hohen Dolomit und Qz/Fsp Werten charakterisiert werden. Sedimenteintrag, stammend von den Eurasisch Arktischen Schelfmeeren, kennzeichnet sich durch niedrige Dolomit, Qz/Fsp und Kaolinit Werte und hohe Quarz Werte. Obwohl der Anteil der Amphibole für eine Quantifizierung größtenteils zu gering ist, könnte jedoch allein das Auftreten der Amphibole ein Indikator für Sedimente aus den Sibirischen Schelfmeeren sein.

In Kapitel 6 wird die Provenienz von terrigenen Sedimenten aus der Zentralen Arktis untersucht, um die Geschichte der Eisschilde zu erforschen. Dafür wurden drei Sedimentkerne, die auf einem Transekt entlang des Mendeleev Rückens positioniert sind, ausgewählt. Hierbei zeigt sich, dass die Provenienz von Sedimenten, abgelagert auf der Seite des Makarov Beckens des Mendeleev Rückens, sich von der Provenienz der auf der Seite des Kanadischen Beckens abgelagerten Sedimente unterscheidet. Die Ablagerungsereignisse von Meereis transportiertem Material (IRD- ice rafted debris) während der marinen Isotopenstadien (MIS) 16, 12, 10, 8 werden durch hohe Dolomit, hohe Qz/Fsp und niedrige Plagioklas Werte charakterisiert, welches auf einen IRD Eintrag vom Kanadischen Archipelago hindeutet. Die IRD Ereignisse während des MIS 6 weisen hohe Quarz und niedrige Dolomit Werte auf und deuten auf Eurasische Quellregionen hin.

Acknowledgements

Here I would like to sincerely thank the persons who help me a lot all these years throughout my PhD study at the Alfred Wegener Institute in Bremerhaven. First I would like to thank my supervisor Prof. Dr. Rüdiger Stein, who provided me the opportunity to do the PhD study in AWI. He helped me to adapt to the new environment when I first came to Germany. And he allowed me to participate in various scientific research activities, e.g. scientific cruises, conferences. More importantly he showed me with his passion how a scientist is dedicated to his beloved scientific researches, which may have significant impact on my future life. He also helped me through plenty of suggestions and comments on abstracts, presentations and especially thesis writing. Prof. Dr. Gerhard Bohrmann is thanked for reviewing my thesis.

I would also like to thank Dr. Petra Westhaus-Ekau, who provided me the information about the PhD Project supervised by Prof. Dr. Rüdiger Stein. Without her help, I may never have the chance to start my PhD study in AWI.

Dr. Christian März (Newcastle University), Dr. Jens Matthiessen (AWI), and Dr. Christoph Vogt (Bremen University) are thanked for being my PhD committee members and contributing various suggestions and discussions. Dr. Jens Matthiessen and Dr. Christoph Vogt are also thanked for their critical comments when helping me revising my thesis. Dr. Christoph Vogt also helped me a lot from the quantification using QUAX to the comparison on the QUAX and RockJock results, as well as intensive discussions on XRD measurement and quantification. Rita Fröhlking is thanked for the guide in the lab, especially for the instructions on the sample preparation and XRD measurement. Prof. Dr. Ralf Tiedemann and Aysel Sorensen are thanked for your helps for administration works.

I am very grateful to Evgenia Bazhenova. She started her PhD several months before

me and gave me all kinds of help after I came to AWI. She taught me to learn how to do my lab work and worked together with me to study how to use the XRD quantification program. She also discussed a lot with me on various problems.

Dr. Claudia Hanand, Dr. Claudia Sprengel and the Helmholtz Graduate School for Polar and Marine Research (POLMAR) are thanked for providing me the possibilities to take part in the courses, workshops, scientific cruises and conferences.

Andrea Bleyer is thanked for providing German classes to us none-German speaking students, which made my life in Germany easier. I appreciate greatly that she was always so kind and willing to help, no matter what kind of favor I asked.

Fellow PhD students are thanked for their help and company during all these years.

I would like to give special thanks to my dear friend Jian Ren and Shuang Gao. Jian started to help me even before I came to Germany. He is the first Chinese student I contacted and he answered all my questions regarding how to start the life and study in Germany. His kindness made me to feel that we are old friends at first sight. He was always there when I needed help, not to mention that he helped to revise my thesis draft even when he was quite busy. And if it was not for his constant encouragement, I would not be able to get through the tough time of my PhD study. Shuang also gave me great mental supports when I felt depressed sometimes during the last phase of thesis writing. I should also thank Shuang and Jian for the memorable time we had parties together.

Words cannot fully express my thanks to my parents. Thank you for motivating me to study abroad and see the wonderful world outside. Thank you for always be there supporting me. I love you!

Contents

Abstract	i
Kurzfassung	iii
Acknowledgements	v
Chapter 1: Introduction	1
1.1 General remarks	1
1.2 Provenance study and the quantitative X-Ray Diffraction (qXRD) method	3
1.3 Outlines and key objectives of the dissertation	4
Chapter 2: Regional settings	7
Chapter 3. Materials and Methods	15
3.1 Materials	15
3.2 Methods	16
3.3 The evaluation software RockJock	19
3.4 The evaluation software QUAX	24
3.5 Differences between RockJock and QUAX	25
Chapter 4. Comparison of RockJock and QUAX	27
4.1 Quantitative XRD methods	27
4.2 Assessing accuracy of RockJock	29
4.3 Possible error sources of RockJock	33
4.4 Standardless analysis in RockJock	36
4.5 Weight percentages vs. peak intensities	43
4.6 Comparison between RockJock and QUAX	45
4.7 Useful tips for the usage of RockJock	52
Chapter 5. Bulk mineral assemblages of surface sediments from the Siberian-Arctic shelf and the central Arctic	55
5.1 Different approaches for reconstruction of sediment sources	55
5.2 The distribution of surface minerals: Results from bulk mineral assemblages	64

5.3 Bulk mineral assemblages as provenance indicators	68
Chapter 6. Provenance study of late Quaternary sediments on a transect across the Mendeleev Ridge as derived from grain size and bulk mineral assemblages	83
6.1 Down-core grain size distributions and bulk mineral variations	84
6.2 Age model	87
6.3 The IRD events and their provenances	95
6.4 Implications for the ice-sheet history and paleoenvironment	100
Chapter 7. Conclusions and outlook	103
References	105

Chapter 1. Introduction

1.1 General remarks

Despite being the smallest among the world oceans, the Arctic Ocean plays an important role in global climate system. The Arctic Ocean influences the global climate mainly through the seasonal or permanent sea ice cover and the deep water formation controlling the oceanic thermohaline circulation (Stein, 2008 and references therein). The Arctic has undergone dramatic changes (Macdonald, 1996; Moritz et al., 2002; Serreze et al., 2000) over the past decades. The Arctic sea ice cover has declined continuously during past three decades (Serreze et al., 2007; Stroeve et al., 2007) and reached the lowest in the summer of 2007 (Comiso et al., 2008; Fig 1.1a; Stroeve et al., 2008; Stroeve et al., 2012) and even lower in the summer of 2012 (Parkinson and Comiso, 2013; Fig1.1b). The loss of sea ice has a significant impact on the oceanic thermohaline circulation (Clark et al., 2002; Mauritzen and Häkkinen, 1997), which in return increases the warming of the Arctic (Serreze et al., 2007). Because the warming of the Arctic is an amplified signal of global warming (Comiso, 2006; Pithan and Mauritsen, 2014; Fig 1.2; Screen and Simmonds, 2010; Serreze and Francis, 2006),

which drives a lot of concerns of scientists and policy maker, it's important to

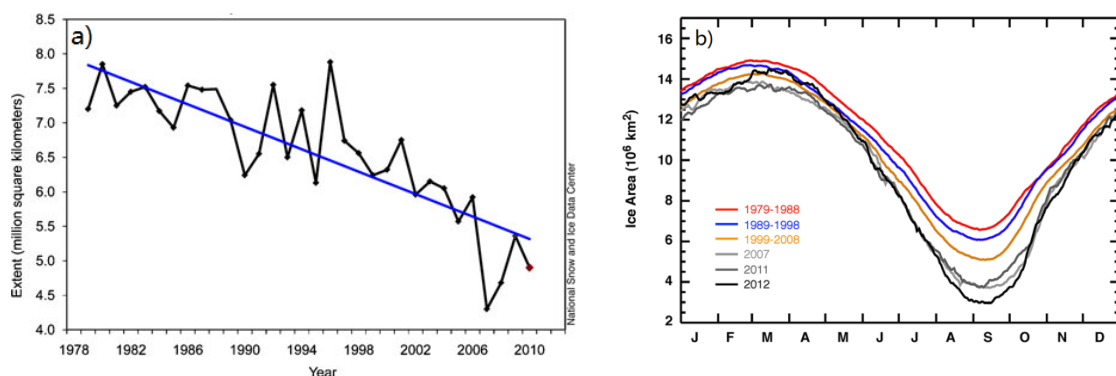


Fig 1.1 a) Time-series of monthly averaged September sea ice extent with linear trend line from 1979-2010 (Stroeve et al., 2012). b) Seasonal cycles of daily Arctic sea ice area for the decades 1979–1988, 1989–1998, and 1999–2008, and the individual years 2007 (which included the record minimum prior to 2012), 2011, and 2012 (Parkinson and Comiso, 2013).

understand the dynamics behind it in order to set up valid predictive climate models. To predict the future climate change, it is essential to study the paleoclimate and paleoceanography in the Arctic Ocean.

Paleoclimate researches can provide important information for understanding the mechanism of past climate change and thus predicting the future changes in the climate system. However, due to the limited accessibility to this permanently ice-covered region to recover undisturbed high-resolution sediment cores, the knowledge of the paleoceanography and paleoclimate of the Arctic Ocean is still limited. Multidisciplinary researches focus on very different topics, e.g. sea ice cover, primary production and permafrost. One of them is the study of sediment provenance, an approach that may allow people to obtain information about present and past environment conditions.

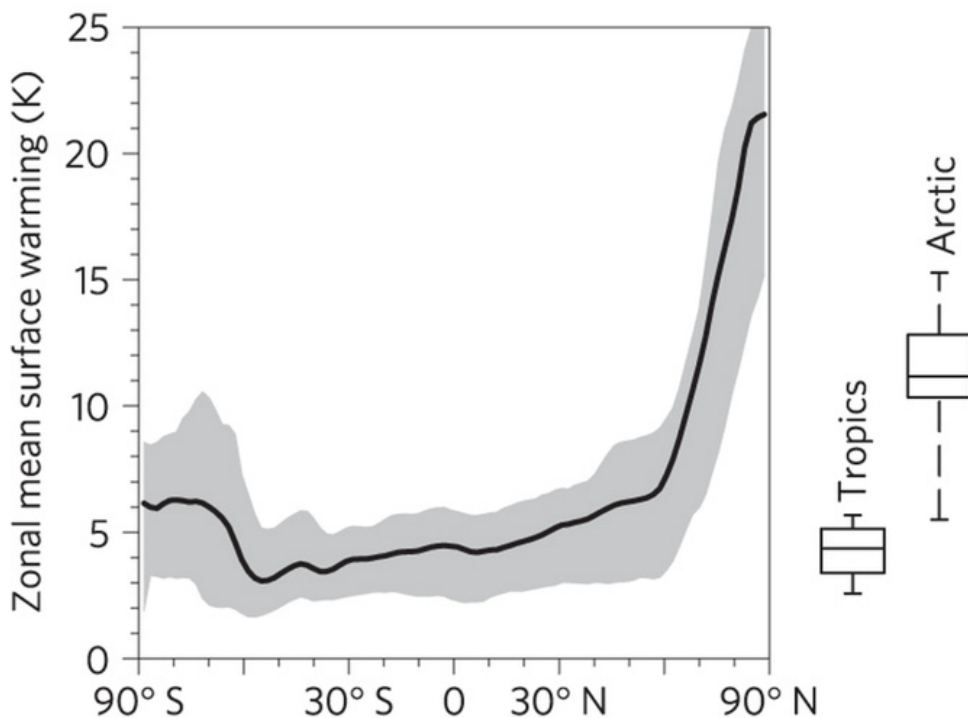


Fig 1.2 Zonal mean surface temperature change for the last 30 years of the CMIP5 $4 \times \text{CO}_2$ experiment compared with the last 30 years of the control run. Box and whisker plots show the median (lines), 25th to 75th percentiles (boxes) and full spread (whiskers) of temperature change averaged over the tropics ($30^\circ \text{S} - 30^\circ \text{N}$) and the Arctic ($60^\circ \text{N} - 90^\circ \text{N}$)

(Pithan and Mauritsen, 2014).

1.2 Provenance study and the quantitative X-Ray Diffraction (qXRD) method

Provenance studies can provide important information on the Late Quaternary history of circum-Arctic ice sheets and the paleoceanographic circulation patterns. Many provenance studies have been performed in the Arctic Ocean, using lithic fragments composition by microscopy (Bischof et al., 1996; Phillips and Grantz, 2001), Fe oxide grains (Bischof and Darby, 1997; Darby, 2003; Darby and Bischof, 1996, 2004; Darby et al., 2002; Darby et al., 2011), clay mineral assemblages (Naidu et al., 1982; Naidu and Mowatt, 1983; Wahsner et al., 1999), heavy mineral assemblages (Behrends et al., 1999; Krylov et al., 2008; Levitan et al., 1999), bulk mineral assemblages (Andrews et al., 2010a; Vogt, 1997), major, minor, and trace elements (März et al., 2011b; März et al., 2011a; Schoster et al., 2000; Viscosi-Shirley et al., 2003b) and radiogenic isotopes of Sr, Nd and Pb (Asahara et al., 2012; Fagel et al., 2014; Jang et al., 2013; Tütken et al., 2002).

The Arctic Ocean is characterized by permanent sea ice cover, which causes low biological production compared to other oceans. Thus, the sediment in the central Arctic and the shelf seas is mainly composed of terrigenous material from the surrounding land masses. Therefore, the study of mineral assemblages is very useful to identify source areas. The identification of source areas further gives important information on transport processes and pathways, and thus, the surface circulation patterns in the Arctic Ocean. Additionally, understanding modern sedimentary processes is vital for the reconstruction of paleoceanic circulation patterns. Numerous mineralogical studies have been performed to identify source areas (for reviews see Stein (2008)). Bulk mineral assemblages have own advantages over other mineral proxies. Clay minerals are very fine grained and thus are able to be transported over long distances by ocean currents. Heavy minerals in the fine sand fraction can only be

transported to sites far from the original sources by sea ice or icebergs. Ice-rafted debris (IRD) coarser than 250 μ m are usually believed to be transported only by icebergs (Darby et al., 2011). Bulk mineral analysis uses not only the coarse fraction transported by icebergs, but also the fine fractions transported by icebergs and sea ice. Thus bulk mineral assemblages may give more information on transporting agency over other proxies. Besides, other proxies are very time consuming, either in sample preparation or in data evaluation, and sometimes subjective. And because of the different methods and grain size they use, the results cannot be compared with each other. In this study, bulk mineral assemblages are studied using the quantitative X-Ray Diffraction (qXRD) and the raw data are converted to mineral percentages by RockJock (Eberl, 2003).

1.3 Outlines and key objectives of the dissertation

The first chapter is a general introduction to the Arctic and the proxy we used. Chapter 2 gives an overview on the regional settings. Chapter 3 shows the materials and methods we used. It explains in detail how to use the qXRD evaluation software package RockJock, and introduces in general the qXRD evaluation software package QUAX and the differences between them.

After these three introductory chapters, the main results of this research (Chapter 4-6) are presented. Chapter 4, the main part of this thesis, aims to study in detail the quantitative X-Ray Diffraction (qXRD) software package RockJock and the comparison of RockJock and QUAX. In Chapter 4, the following research questions are addressed:

1. What will be the error bar of RockJock and what are the possible causes of the errors?
2. How to diminish the errors?
3. What are the advantages and disadvantages of RockJock and QUAX?
4. Can the results of RockJock be compared with QUAX?

RockJock is applied for quantification of mineral contents in surface sediments from XRD data to identify sediment provenance (Chapter 5). In Chapter 5, the key questions are:

1. What are the characteristics of the bulk mineral assemblages in the specific source areas?
2. Is it possible to reconstruct modern transport pathways of terrigenous materials and, with this, modern oceanic circulation patterns?

In Chapter 6, RockJock results are used to study the temporal variability of mineral assemblages in cores across the Mendeleev Ridge to reconstruct the paleoenvironmental changes in the Arctic Ocean (Chapter 6). In Chapter 6, key questions are: How did the sediment provenance and the surface circulation patterns (the Beaufort Gyre and Transpolar Drift) change over the past ~600ka?

The conclusions and outlook are presented in Chapter 7.

Chapter 2. Regional settings

The Arctic Ocean is the smallest among the world's oceans with a surface area of $9.5 \times 10^6 \text{ km}^2$, which is about 2.6% of the total area of the world's oceans (Jakobsson, 2002). It is unique, compared to the other oceans, that the central Arctic Ocean is surrounded by vast areas of shallow continental shelves, which make up 52.7% of the Arctic Ocean surface area (Jakobsson et al., 2003). It is a landlocked ocean with only two passages connecting to other oceans. The Bering Strait connects the Arctic Ocean to the Pacific Ocean, with a depth of 50m. The Fram Strait is the only deep passage (2600m), which allows two-way deep water exchange between the Arctic Ocean and the Atlantic Ocean (Rudels, 2015).

The Arctic Ocean is divided into two basins, the Eurasian Basin and the Amerasian Basin, by the Lomonosov Ridge (Fig 2.1). The Eurasian Basin is bounded by the Lomonosov Ridge, the Laptev Sea, the Kara Sea, the Barents Sea, and northern Greenland. It is subdivided into the Amundsen Basin and the Nansen Basin by the Gakkel Ridge. The Amerasian Basin is bounded by the Lomonosov Ridge, the East Siberian Sea, the Chukchi Sea, the Beaufort Sea and the Canadian Arctic Archipelago. It is subdivided into the Canada Basin and the Makarov Basin by the Mendeleev Ridge and the Alpha Ridge.

The Arctic Ocean consists of three main water masses: the upper waters, the intermediate waters (Atlantic Layer), and the deep waters (Fig 2.2). The upper waters can be divided into the Polar Mixed Layer (PML) and the Arctic halocline (Fig 2.2). The PML is at the depth of 30-50m and is characterized by temperature close to the freezing point and very low salinity caused by river-runoff (Schlosser et al., 1995). Beneath the PML is the Arctic halocline (30 to 50 m to about 200 m depth), which is cold and salty and permanent over the deep basins as a barrier between the deeper ocean and the upper ocean (Macdonald and Bowers, 1996). The warm and salty Atlantic Layer is at the depth of ~200m to 800m and traditionally defined as the layer

between the 0°C isotherms. (Schlosser et al., 1995). The deep waters below the Atlantic Layer, representing ~60% of the total volume, are characterized by relatively high salinities (Schlosser et al., 1995).

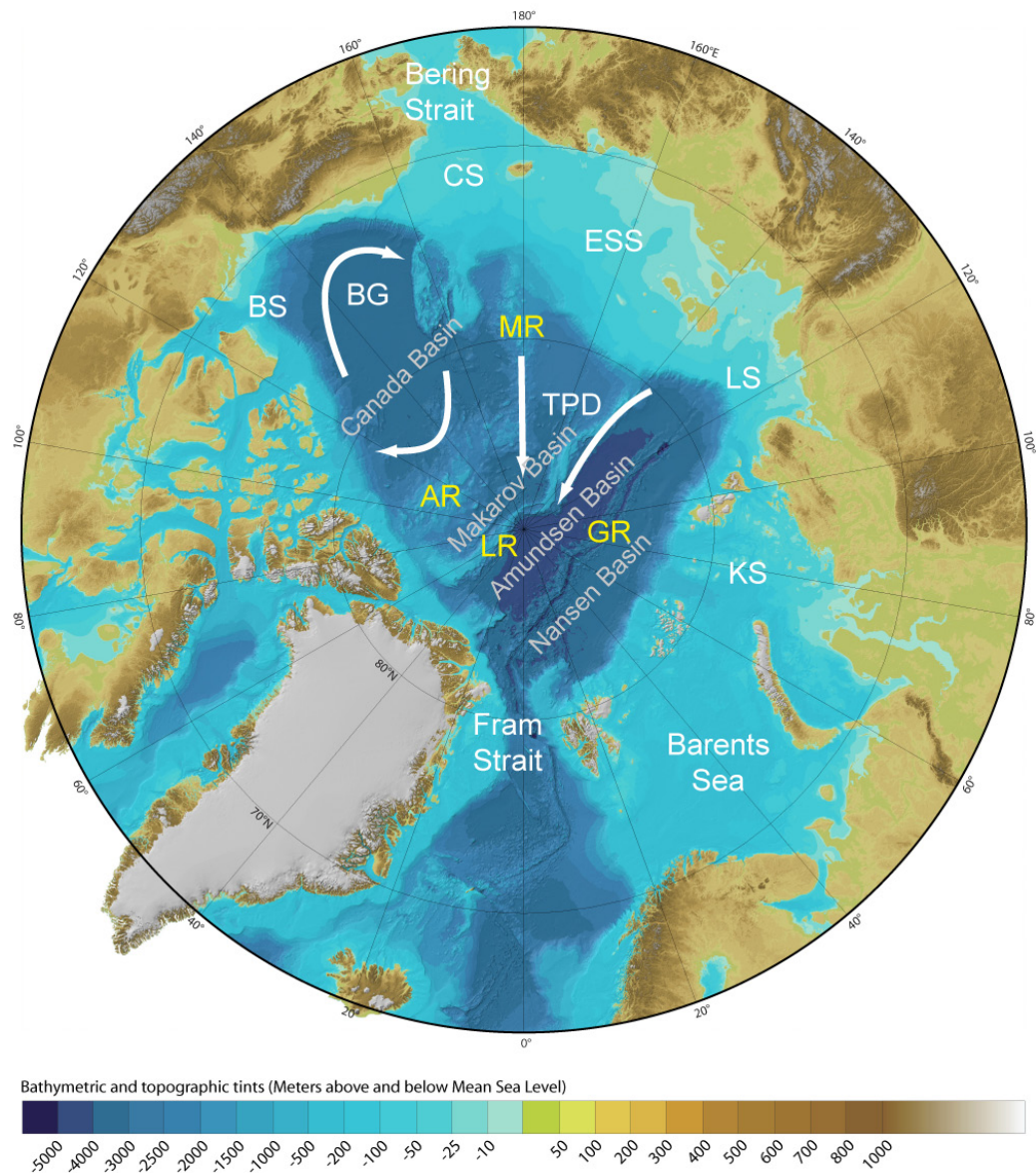


Fig 2.1 Physiography and surface circulations map of the Arctic Ocean. The base map is the Bathymetric map of the Arctic Ocean, IBCAO (Jakobsson et al., 2012). White arrows show the two main surface circulation patterns: BG – Beaufort Gyre, TPD – Transpolar Drift. Names of shelf seas are indicated in white colour: CS – Chukchi Sea, ESS – East Siberian Sea, LS – Laptev Sea, KS – Kara Sea, BS – Beaufort Sea. Major geomorphologic features are indicated in yellow font: MR – Mendeleev Ridge, AR – Alpha Ridge, LR – Lomonosov Ridge, GR – Gakkel Ridge. The basins are shown in grey font.

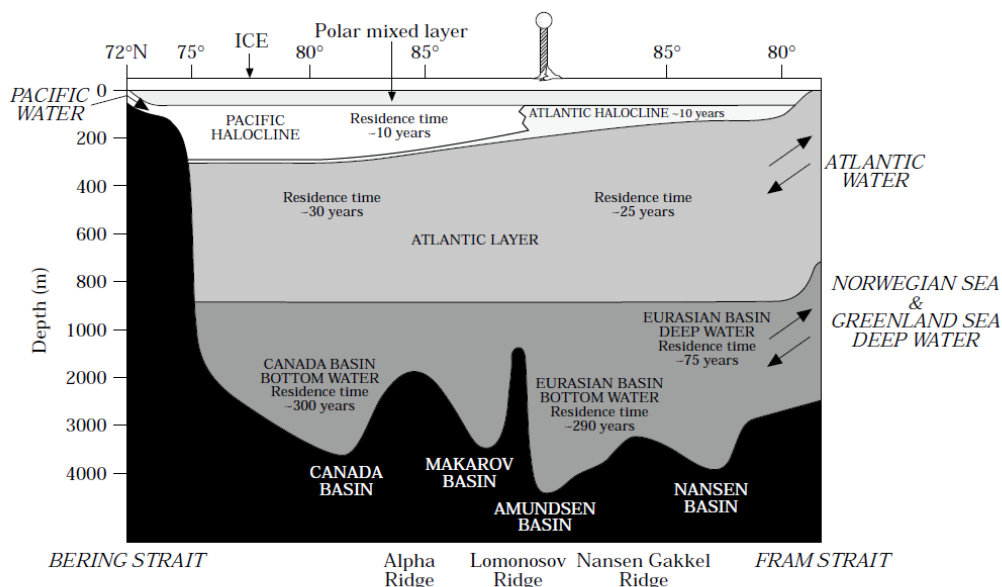


Fig 2.2 A schematic diagram showing the stratification of the Arctic Ocean (Macdonald and Bewers, 1996; Macdonald, 2004).

There are two main wind-driven surface circulations in the Arctic Ocean: the anti-cyclonic Beaufort Gyre (BG) centered in the Amerasian Basin, and the Transpolar Drift (TPD) in the Eurasian Basin (Fig 2.3). The TPD transports sea ice from the Siberian shelves towards the Fram Strait. The boundary between these two surface circulations is currently located on the Lomonosov Ridge. There are two main currents through Fram Strait: the cold East Greenland Current transporting sea ice out of the Arctic Ocean; and the eastern West Spitzbergen Current carrying warm and relatively salty water into the Arctic Ocean. Pacific water masses enter the Arctic Ocean via the Bering Strait and then penetrate into the Chukchi and Beaufort Seas. The Arctic Oscillation (AO) (Thompson and Wallace, 1998) is closely related with the wind patterns, and thus changes the location of the TPD (Darby and Bischof, 2004; Kwok et al., 2013; Mysak, 2001). During a positive AO phase, the TPD shifts towards North America and the BG is restricted. During a negative AO phase, the TPD is mainly in the Eurasian Basin and similar to today's location, and the BG dominates the Amerasian Basin (Fig 2.4).



Fig 2.3 Surface currents in the Arctic region (AMAP, 1998).

An important feature of the Arctic is its perennial sea-ice cover. Sea ice shows strong seasonal changes in the marginal seas. In winter the shelf seas are mostly covered by sea ice, while in summer they are almost ice free (Fig 2.5). Sea ice plays a key role in the Arctic climate system as it influences the albedo, the deep water formation and the productivity. The sea ice albedo is much higher than the open water, which is 0.6 to 0.8 compared to 0.1 (Barry, 1996). The high albedo makes sea ice to reflect more shortwave radiation in summer and thus lowers the surface temperature (Dieckmann and Hellmer, 2010). The seasonal melting of the sea ice helps to maintain the low salinity of the surface water and the brine rejection occurred during sea ice formation produces dense waters (Aagaard et al., 1981; Aagaard et al., 1985). This causes the stratification of the water column and restricts the lateral convections. The dense

water then flows from the shelf into the central Arctic, yielding a thicker and colder halocline (Aagaard et al., 1981). This thicker halocline prevents the warm Atlantic water from reaching the sea ice cover. Furthermore, the sea ice cover strongly influences the biological productivity, as the biological activities underneath the ice are restricted due to the insufficient light (Arrigo et al., 2011).

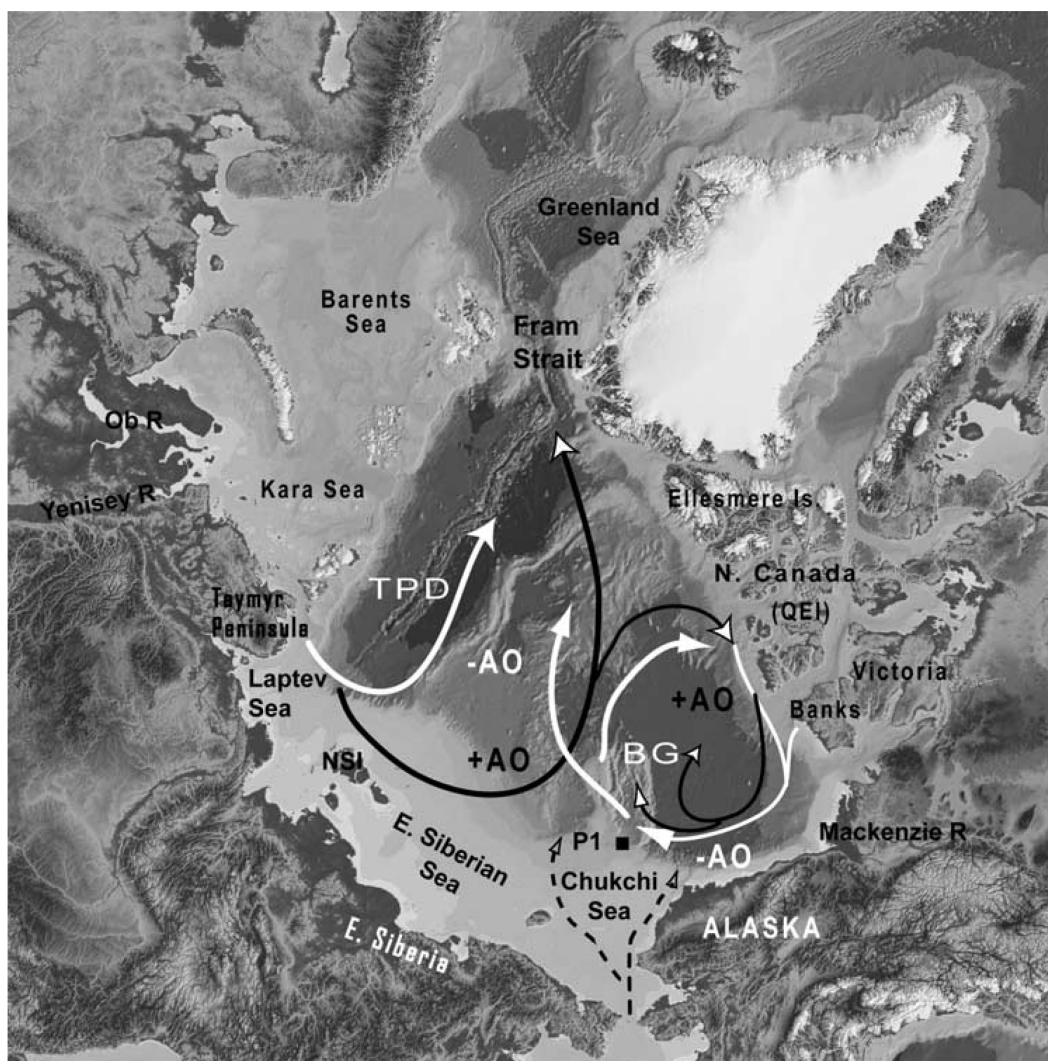


Fig 2.4 Map of the Arctic Ocean showing two sea-ice drift regimes (Darby and Bischof, 2004). The TPD and the Beaufort Gyre (BG) depict endmember extremes for both a strongly $-AO$ phase (white arrows) and a strongly $+AO$ (black arrows).

Factors controlling the terrigenous particles into the Arctic Ocean are river discharge, coastal erosion, sea ice and icebergs, ocean currents, gravity flows, and aeolian input (Fig 2.6). Of all the factors, aeolian input is of the minimum importance, as only $\sim 5.7 \times 10^6 \text{ ty}^{-1}$ of total material is transported into the marginal seas and the central Arctic Ocean (Shevchenko et al., 2004). In contrast to aeolian input, coastal erosion

supplies the most terrigenous material. As estimated by Grigoriev et al. (2004), the total sediment input by coastal erosion is $\sim 430 \times 10^6 \text{ ty}^{-1}$. Coastal erosion shows prominent regional differences. Compared to the Siberian shelf seas, Beaufort Sea receives much less sediment input from coastal erosion (Grigoriev et al., 2004 and references therein). The major rivers transport huge amount of fresh water as well as total suspended matters (TSM) into the Arctic Ocean. The total TSM flux of the entire Arctic Ocean is $227 \times 10^6 \text{ ty}^{-1}$ (Rachold et al., 2004). Note that not all the TSM measured are transported to the Arctic Ocean, as some may be trapped in the estuaries and deltas. Due to the distinct geology of the hinterland, the TSMs transported by different rivers are characterized by different mineralogical and geochemical tracers, such as clay minerals and heavy minerals as well as major, minor, and rare earth elements, which can be used as indicators for source areas (e.g. Behrends et al., 1999; Schoster et al., 2000; Wahsner et al., 1999).

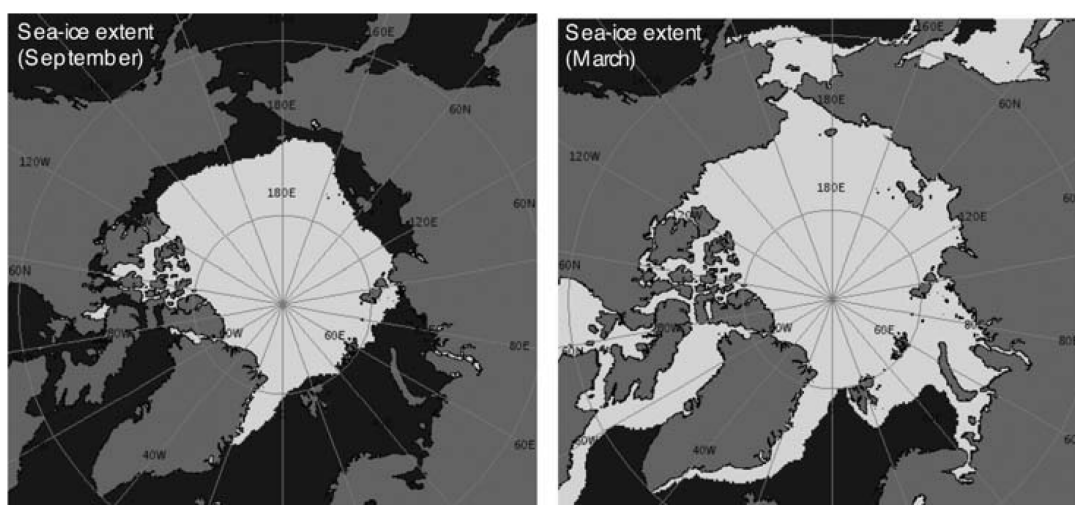


Fig 2.5 Map showing the average distribution of sea ice in the Arctic Ocean in September (1979-2004) and March (1979-2005); according to Maurer (2007; <http://nsidc.org/data/atlas/>)

Sea ice is one of the very important agents accounting for transporting sediment from the shallow marginal seas to the ridges and plateaus in the central Arctic (Bischof, 2000). Sediments entrainment into the sea ice takes places all over the Arctic Ocean and its marginal seas (Darby, 2003; Darby et al., 2011; Eicken et al., 2005; Eicken et al., 1997; Nürnberg et al., 1994; Pfirman et al., 1990; Reimnitz et al., 1993). There

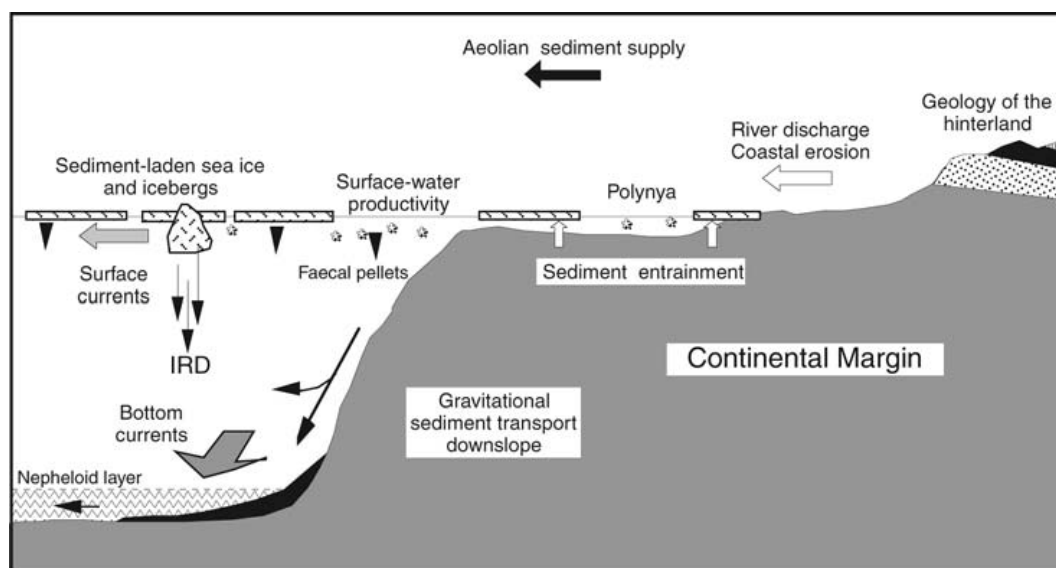


Fig 2.6 Processes controlling terrigenous sediment supply in the Arctic Ocean (Stein, 2008).

are two most important mechanisms for entraining sediment into sea ice: suspension freezing by frazil ice and anchor ice (Darby et al., 2011). The former mainly incorporates finer sediments less than 30-60 μm and the latter entrains theoretically whatever sediment on the seafloor, but usually less than 250 μm (Darby et al., 2011). Sea ice transports sediment from the marginal seas via the Transpolar Drift towards Fram Strait (Fig 2.7). However, the estimation of sea-ice sediment is difficult to make (Stein, 2008 and references therein). Another important agent for transporting sediment in the Arctic Ocean is icebergs. Although sediment transport by icebergs is less important than sea ice in the modern interglacial Arctic Ocean, it played a major role in glacial periods (Stein, 2008). The drift of iceberg is along the motion of sea ice via the wind driven surface circulations – the Beaufort Gyre and the Transpolar Drift. The mineralogy of sediment in sea ice and iceberg varies laterally and temporarily, and thus, can be used to identify source areas and reconstruct transporting pathways.

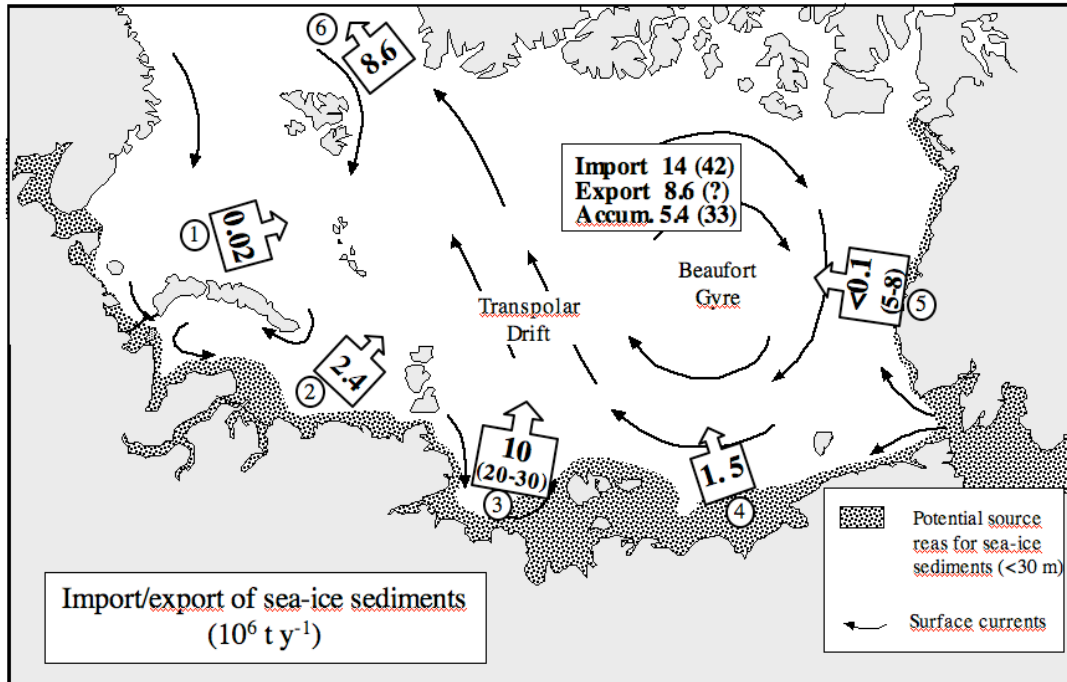


Fig 2.7 Import of sea-ice sediments from the marginal seas into the open Arctic Ocean and export from the Arctic Ocean into the North Atlantic Ocean (Stein, 2008).

Chapter 3. Materials and Methods

3.1 Materials

Three different sets of artificial mixtures are used to test the accuracy of RockJock, namely two-phase mixtures, six-phase mixtures and eleven-phase mixtures, respectively. Six two-phase mixtures consist of one to three minerals of commercially available pure phases. Eight six-phase mixtures are composed of quartz, plagioclase, k-feldspar, smectite, illite and kaolinite with different proportions. Ten eleven-phase mixtures contain various proportions of PFI-1, STx-1, Kga-1b, Nau-1, quartz, albite, microcline, biotite, muscovite, calcite and gypsum (Table 3.1).

Table 3.1 Compositions of three sets of artificial mixtures. The six two-phase mixtures are composed of one to three different minerals and the six-phase and eleven-phase mixtures are composed of same sets of minerals with different proportions. Pure mineral phases for the mixtures were provided by Dr. Christoph Vogt, Geosciences, University of Bremen). The two-phase mixtures were prepared by Bazhenova using the pure minerals. The eleven-phase mixtures were newly prepared while the six-phase mixtures of Vogt et al., (2002) have been re-measured.

	Mix 1	Mix2	Mix3	Mix4	Mix5	Mix6
Two-phase	Chlorite	Kaolinite	Quartz	Quartz	Quartz	Quartz
		Chlorite	Plagioclase	Kspar	Plagioclase	Smectite
					Chlorite	
Six-phase	Quartz	Plagioclase	Kspar	Smectite	Illite	Kaolinite
Eleven-phase	PFI-1	STx-1	Kga-1b	Nau-1	Quartz	Albite
	Microcline	Biotite	Muscovite	Calcite	Gypsum	

To compare RockJock with QUAX as well as to study the modern mineral distribution patterns, surface sediment samples from the Arctic Ocean retrieved from two Polarstern cruises ARK-XXIII/3 (Jokat, 2009) and ARK-XXVI/3 (Schauer, 2012) and two Russian cruises RUSALCA-2009 (Bakhmutov et al., 2009) and ISSS-2008 (Dudarev, 2008) were studied (see also in Bazhenova (2012)). For paleoceanographic research, samples from selected sediment cores (PS 72/396-5, PS 72/410-3, and PS 72/422-5) in central Arctic Ocean across Mendeleev Ridge are used, recovered during the Polarstern cruise ARK-XXIII/3 (Jokat, 2009). The locations of the surface

samples and the cores are shown in Fig 3.1 and the coordinate of the cores are shown in Table 3.2.

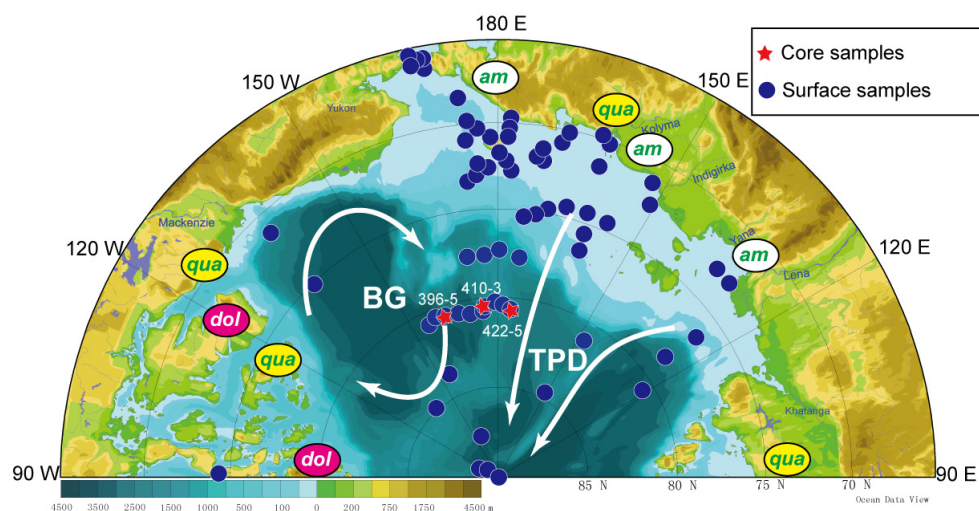


Fig 3.1 Locations of surface samples (blue dot) and core samples (red pentagram) from the Arctic Ocean. White arrows indicate the major surface circulation systems: Beaufort Gyre (BG) and Transpolar Drift (TPD). Bathymetry map is from IBCAO (Jakobsson et al., 2008). Main minerals source areas are indicated (Stein et al., 2010a).

Table 3.2 Coordinates of Polarstern ARK-XXIII/3 expedition cores used in this study.

Station	Latitude	Longitude	Water depth (m)
PS72/396-5	80°34.74'N	162°10.01'W	2722
PS72/410-3	80°31.29'N	175°43.49'W	1847
PS72/422-5	80°32.68'N	175°44.63'E	2536

3.2 Methods

3.2.1 Grain size analysis

All samples were freeze dried and subdivided into two parts. One part is for grain size analysis and the other one is for XRD measurement (Fig 3.2). About 10 g of sediment was taken for grain size analysis. It was suspended in de-ionized water and left overnight on a shaker-table at a speed of 180 r/min. The samples then went through wet sieving at 63 μ m and the coarse fraction (>63 μ m) was collected and oven-dried at 60°C before weighing. After weighing, the coarse fraction was dry sieved into

different fractions (63-125 μm , 125-250 μm , 250-500 μm , 500-2000 μm and >2mm). The different fractions were then weighed separately. The fine fraction (<63 μm) was left for settling and after one week the water was removed and the sediment was oven-dried and collected for weighing. As this study focuses mainly on the coarse fractions, the fine fraction was kept for future studies.

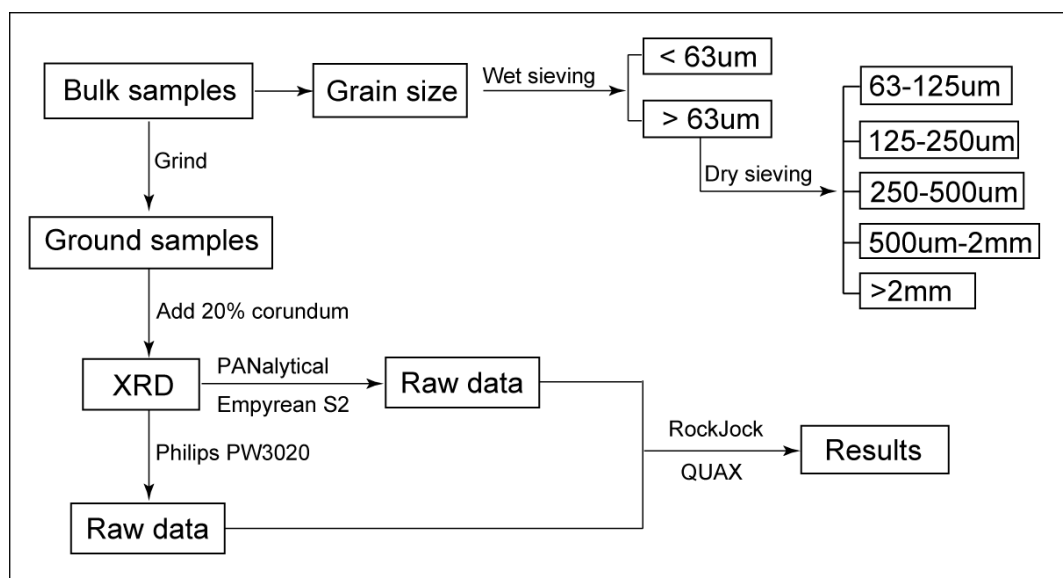


Fig 3.2 Flow chart showing the process of sample preparation and measurement.

3.2.2 XRD measurement

Randomly oriented samples of bulk fractions were prepared for X-ray diffraction (XRD). Samples were prepared following the preparation steps described in user's guide of RockJock (Eberl, 2003). The bulk samples were ground in the grinding machine "pulverisette 5" for two minutes with a rotation speed of 200r/min. 0.5g of the ground samples were carefully weighed and mixed with 0.125g corundum as internal standard, which equals 20% corundum in the sample. The mixed samples were then ground with pestle and mortar to homogenize them. After sieving them through a 500 μm sieve in order to delimit agglomerates of the sample after the homogenization, the samples were back loaded into sample holders. Then the samples were measured on a Philips PW 3020 diffractometer equipped with Co K-alpha radiation, graphite monochromator and automatic divergence slit at the Alfred Wegner

Institute (AWI, Bremerhaven). The samples were X-rayed from 5 to 80° 2 θ with a step size of 0.02° 2 θ and a counting time of 2 seconds per step. Because the raw data should be converted to Cu K-alpha radiation in order to do the calculation in the RockJock, the 2 θ range with Co K-alpha radiation is wider than the suggested 5 to 65° 2 θ with Cu K-alpha radiation. The 2 θ range used in RockJock may cause some problems for the recognition of mixed-layered clay minerals which might have significant peaks in the smaller than 5° range.

During the study, there was a replacement of the XRD machine in the laboratory of the AWI. Therefore some samples were measured in the new machine. Although it might affect the consistency of the result, it gave us the opportunity to compare the results from different XRD machines. The new machine is PANalytical Empyrean S2 with Cu K-alpha radiation, PIXcel – 3D detector and automatic anti-scatter slit. Samples were measured from 5 to 65° 2 θ with a step size of 0.013° 2 θ and a counting time of 24 seconds per step (40 kV, 40 mA). The settings differ remarkably from the ones used in developing the standards in RockJock and also from the PW3020 that was used before (Table 3.3). The new diffractometer has a smaller step size and thus a better resolution. The PIXcel – 3D detector is a multiline detector, which is different from the single line detector used in the old XRD machines. The single line detector receives the diffracted X-ray once a step. However, the PIXcel 3D detector has 191 lines for our measurement and the 191 lines receive the diffracted X-ray simultaneously, and thus every single line receives it 191 times. It takes 24 seconds to go through the 191 lines. This will greatly increase the counts, which are summed up, for each step, and thus can improve the resolution. The detailed comparison between two different machines is discussed in Chapter 4.

Table 3.3 Different parameters of different diffractometers: Philips PW 3020 – old diffractometer used in this study; PANalytical Empyrean S2 – new diffractometer used in this study; Siemens D500 – diffractometer used to develop reference minerals in RockJock.

Diffractometer	Anode	Divergence	Step size	Counting time
Philips PW 3020	Co	Automatic	0.02°	2 seconds
PANalytical Empyrean S2	Cu	Automatic	0.013°	24 seconds
Siemens D500	Cu	Fixed	0.02°	2 seconds

3.3 The evaluation software RockJock

3.3.1 Theory

Raw XRD data were then converted to minerals weight percentages using RockJock (Eberl, 2003). Before the RockJock calculation, the intensities from 5 to 65° were copied and pasted into RockJock. Minerals that are likely to be present in the samples were chosen in the list of standards. Some mineral groups, such as feldspar, illite, smectite, kaolinite and chlorite, contain several minerals with different compositions and structures. In this case, if it's not for sure which one(s) is/are present in the sample, all the minerals within the same group should be selected. After the first calculation, those that are less than 1 percent should not be chosen for the final calculation (Eberl, 2003). Because the diffractometer used in this study is different from which RockJock standards' patterns were developed from, the Auto Background correction should be turned on in order to include the background into the Solver solution (the purple line in Fig 3.5 shows the background line calculated by the Auto Background). Then the calculation starts and RockJock begins to calculate the sum of stored XRD patterns of the chosen reference minerals (calculated pattern) and to fit it to the measured pattern using the Excel Solver tool (the fitting is usually done in the range of 19.0 to 64.5 degrees two-theta, which might cause difficulties for calculating minerals with major peaks smaller than 19 degree). In order to get the best fit, the Solver minimizes the Degree of

fit (DOF) by varying the proportion of each mineral standard pattern. DOF is determined by the R factor outlined by Smith et al. (1987),

$$R = \frac{\sum |I_M(2\theta) - I_C(2\theta)|}{\sum I_M(2\theta)}$$

where $I_M(2\theta)$ and $I_C(2\theta)$ are the measured and calculated intensities of a single 2θ step respectively. According to Smith et al. (1987), R values should be less than 0.20 and preferably less than 0.10. However, because $\sum I_M(2\theta)$ contains background when the Auto Background option was turned on, the R value will be reduced remarkably while using a diffractometer which produces quite high background, which is the case of PANalytical Empyrean S2 in this study. When the Solver finds the best fit, the proportion of each reference mineral pattern is determined. It is then multiplied by the integrated intensity of the pure reference mineral, which is already measured and stored in RockJock, to get the integrated intensity for each phase in the sample. The weight percentage of each phase is calculated by the equation according to Chung (1974a):

$$X_i = \frac{X_c}{RIR} \times \frac{I_i}{I_c} = \frac{X_c}{RIR} \times \frac{I'_i}{I'_c} \times \frac{\omega_i}{\omega_c}$$

where:

X_i = Weight percentage of phase i in the sample

X_c = Weight percentage of internal standard (corundum) in the sample

I_i = Integrated intensity of phase i in the sample

I_c = Integrated intensity of internal standard (corundum) in the sample

I'_i = Integrated intensity of pure reference mineral i

I'_c = Integrated intensity of pure standard (corundum)

ω_i = Weight fraction of phase i in the sample

ω_c = Weight fraction of internal standard (corundum) in the sample

RIR = Reference intensity ratio (Snyder and Bish, 1989).

3.3.2 Running RockJock

The installation of RockJock might be tricky. The most important thing is to make sure that the analysis tool Solver has been installed in Microsoft Excel 2007. After opening the workbook RkJock11, which is used in this study, go to the *Full Pattern* sheet and open and close the Solver in order to make sure Solver is installed and activated. The program should be ready to use now. If one wants to use the quick version of RockJock, repeat opening and closing Solver in the *SolverStart* sheet of the *StartRkJock11* workbook. Then go to the *InputStart* sheet and follow the instructions there to install the proper path. Note that if the program would have been moved to somewhere else, the path should be installed again. For details of the installation, see the User's Guide (Eberl, 2003).

After the installation, paste a XRD pattern (5 to 65 degrees two-theta with 0.02 steps) into column D. The file name should be in cell D1 and the pattern start from cell D2. Set cell B15 to 1 if background correction is necessary and B21 to 2 if internal standard was used (Fig 3.3). Raw XRD data can be converted to steps size of 0.02° with Cu k-alpha radiation and fixed slit divergence mode in the computer program MacDiff 4.2.6 (Petschick, 2002; Petschick et al., 1996). After the conversion, the data were saved as txt files, in order to be used in RockJock.

	A	B	C	D
1	MANUAL RESULTS:	INPUTS Paste intensities starting in D2:	MANUAL SETTINGS:	B 1B 01
2		SAMPLE NAME (Automatically entered from Cell D1)	START ANGLE (19 for std)	1804.28
3	PEAK MAX (TWO-THETA & d)	ARA2B_1B_015_GM	5	1792.06
4		START ANGLE FOR ALL INTENSITIES (Use max of 5 degrees; enter 5)	END ANGLE (64.5 for std)	1781.03
5		5	65	1776.74
6	ANAL_RANGE (TWO-THETA)	STEP SIZE (deg 2-theta; limited to 3400 steps; Enter 0.02)	AUTO PICK L_BG? (1 = yes)	1773.89
7		0.02	0	1770.47
8		QUIT EXCEL AT END OF CALCULATION? (1 = yes; enter 1 if program often crashes after calculation)	AUTO PICK R_BG? (1 = yes)	1773.69
9	MAX INTENSITY OF PEAK	AUTO ANALYSIS? (0 = no; or give number of patterns to be analyzed in Auto XRD sheet)	0	1791.22
10		0	BG COR? (0 = no; 1 = left; 2 = right; 3 = line; 4 = 6-64° min)	1794.81
11	ANGLES FOR TAIL MINS	USE AUTOSHIFT? (Do not use with FastRjl; 0 = no; 1 = yes; choose minerals to shift in column I)	0	1782.05
12		0	RUN FAST ROCKJOCK? (1 = yes)	1770.76
13		0	0	1768.39
14	INTEGRATED INTENSITY	AUTO BACKGROUND CORRECTION? (0 = no; 1 = yes; Enter 1)	0	1754.48
15		1	SOLVER CONVERGENCE (Enter 3)	1734.29
16	INTEGRAL PEAK BREADTH	COLLECT RESULTS (Enter 1); RESET DEFAULTS (2); INPUT FROM MIN INDEX (3); Usually enter 0	[1 = low (0.001); 2 = medium (0.0001); 3 = high (0.00001)]	1719.48
17		0	3	1706.6
18	NUMBER OF MINERALS CHOSEN	TYPE OF ANALYSIS (Usually enter 2)	3	1688.03
19		[0 = Plot measured pattern with no shift; 1 = Plot pattern with shift; 2 = Solve with corundum standard; 3 = Standardless analysis (set Shifter to qtz)]	Std/sample ratio	1681.75
20	DATE AND TIME		[Normally enter 0.25 (20% corundum)]	1691.9
21	2014/11/22 0:36		0.25	1696.22
22		2		1702.57
23	Reference:			1710.37
24	Eberl, D.D. (2003) User's guide to	START ROCKJOCK	RockJock11 version 11/24/09	1737.89
25	RockJock--A program for determining quantitative mineralogy	[Slower]	Contact: ddeberl@usgs.gov	1740.58
26	from powder X-ray diffraction data. Revised 11/24/09.	U.S. Geological Survey		1713.09
27	U.S. Geological Survey Open File Report 03-78, 48 p.			1707.29

Fig 3.3 Part of the Input sheet of RockJock where the XRD patterns are inputted before running RockJock.

Select the possibly present minerals in the “Column H” in the *Input* sheet by entering 1 (Fig 3.4). It can also be entered in the *Mineral Index* sheet. Note that corundum as an internal standard should not be selected as present, because the weight percentages of corundum should be excluded from the results. Press the START ROCKJOCK button to start the calculation. The program can also be started from the *Input* sheet of StartRkJock11 workbook, if faster calculation to be expected. After several minutes or one hour (depending on the number of minerals chosen), the weight percentages will be shown in the *Result* sheet. Because each mineral is analyzed separately, the total abundance might differ a little from 100%. This is an independent check if the calculation is reliable. To further check the quality of the result, go to the *Full Pattern* sheet and check the goodness of fit from the graphs (Fig 3.5). The red curve should match the blue curve. Otherwise, there might be some minerals missing or mistakenly chosen.

F	G	H	I	J	K
		Present?	AutoShift?	Report as:	The usual
No.	Mineral	(1 = yes)	(1 = Yes)	(1 = No report; 2 = Non-Clay; 3 = Clay)	suspects (1 = yes)
1	Quartz	1	0	2	1
2	Kspar (ordered Microcline)	1	0	2	1
3	Kspar (intermediate microcline)	1	0	2	1
4	Kspar (sanidine)	1	0	2	1
5	Kspar (orthoclase)	1	0	2	1
6	Kspar (anorthoclase)	0	0	2	0
7	Plagioclase (albite, var. cleavelandite)	1	0	2	1
8	Plagioclase (oligoclase; NC)	0	0	2	1
9	Plagioclase (oligoclase; Norway)	1	0	2	0
10	Plagioclase (andesine)	1	0	2	1
11	Plagioclase (labradorite)	1	1	2	1
12	Plagioclase (bytownite)	0	0	2	0
13	Plagioclase (anorthite)	0	0	2	0
14	Calcite	1	0	2	1
15	Calcite (Mg-rich)	0	0	2	0
16	Aragonite	1	0	2	0
17	Dolomite	1	0	2	1
18	Dolomite (Fe-rich)	0	0	2	0
19	Ankerite	0	0	2	0
20	Magnesite	0	0	2	0
21	Siderite	0	0	2	0
22	Halite	1	0	2	0
23	Halloysite	0	0	3	0
24	Kaolinite (disordered)	1	0	3	1
25	Kaolinite (ordered)	0	0	3	0
26	Kaolinite (Dry Branch)	0	0	3	0
27	Dickite	0	0	3	0
28	Smectite (Na-Kinney montmorillonite)	1	0	3	1
29	Smectite (Ca-Kinney montmorillonite)	1	0	3	1
30	Smectite (Saponite)	0	0	3	0
31	Smectite (hectorite)	0	0	3	0
32	Smectite (ferruginous)	1	0	3	1
33	Illite (1Md)	1	0	3	1
34	Illite (1M; R>3; 95%)	0	0	3	0
35	Illite (R>1, 70-80%)	1	0	3	1
36	Illite (1M; RM30)	0	0	3	0

Fig 3.4 Part of the mineral standards listed in the Input sheet of RockJock where the minerals supposed to be present in the sample that could be selected.

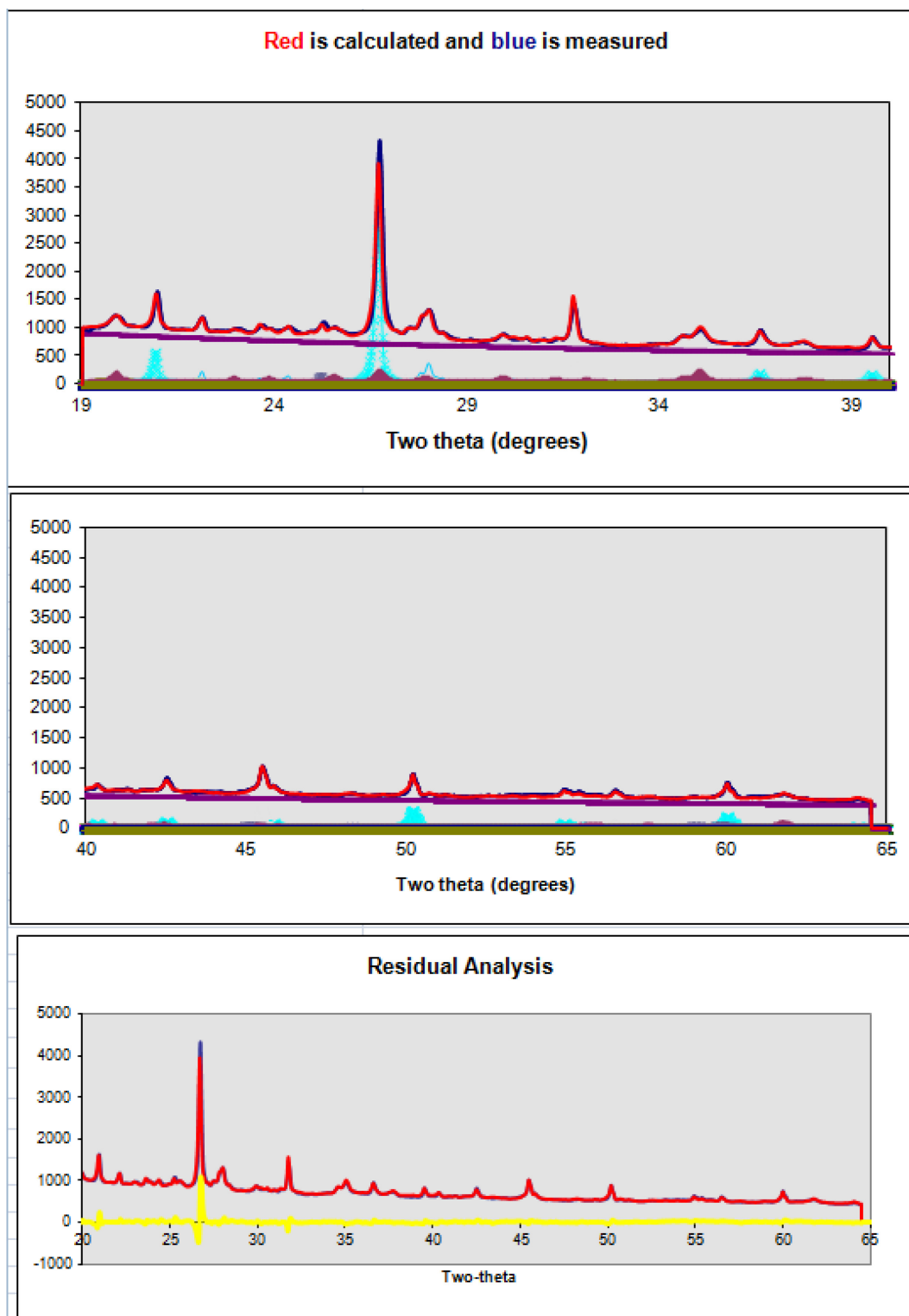


Fig 3.5 Charts from the FullPattern sheet of RockJock showing the fitness of the measured pattern (blue) and the calculated pattern (red) and the differences between the two patterns (yellow curve). The purple curve is the automatic background line.

3.4 The evaluation software QUAX

Quantification was also carried out using the QUAX (Quantitative Phase-Analysis with X-ray Powder Diffraction) software package (Emmermann and Lauterjung, 1990) by Dr. Christoph Vogt (Crystallography, Geosciences, University Bremen), in order to compare the two software packages. QUAX also uses the whole pattern fitting method to run quantitative phase analysis. The working scheme of QUAX is shown in Fig 3.6. The software packages consist of two parts: the qualitative phase analysis module PROFIL and the quantitative analysis module QUALITY. Before a quantitative analysis, a qualitative phase analysis is done automatically. Peaks are recognized and characterized by the module PROFIL. The peak intensities and peak areas are calculated. A binary file is then generated and will be used in the quantitative evaluation QUALITY (Vogt, 1997). In the module QUALITY, it compares the sample diagram with reference minerals already stored and a list of all possible minerals is established. Then the software uses a statistic method to determine the probability of presences. The minerals combination with the highest probability is used to calculate an XRD pattern to fit the measured pattern. This calculated pattern is subtracted from the measured pattern and the residual intensities are used for the second search and fitting iteration (Vogt, 1997). As Vogt et al. (2002) showed the use of pure mineral phase measurements and the grouping of these in reference database are highly important for the outcome of the Quantitative Phase Analysis. After several iterations, all the possible present minerals are recognized and the scale factor of each mineral is calculated. The weight fractions then are calculated by:

$$X_i = a_i \cdot \mu_s / \mu_i$$

X_i = weight fraction of the phase i

a_i = scale factor of phase i

μ_s = mass attenuation coefficient of the sample

μ_i = mass attenuation coefficient of phase i

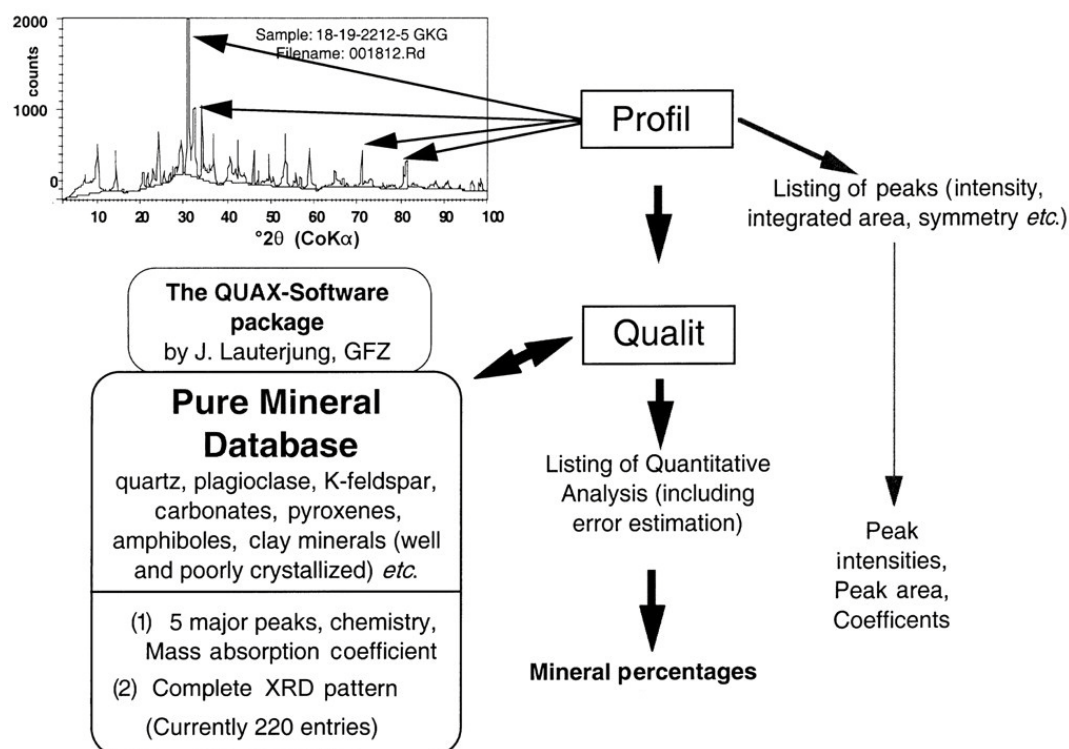


Fig 3.6 Structure and working scheme of QUAX (from (Vogt et al., 2002)).

3.5 Differences between RockJock and QUAX

Between RockJock and QUAX five important basic differences exist, which may cause different results calculated from these two software packages (see details in Chapter 4).

(1) The reference minerals are different, which will surely cause differences on the results. Eberl (2003) established the reference minerals data set for RockJock and documented their patterns in RockJock spreadsheet as raw measurement. In the version we used in our study (RockJock 11), there are 166 of them. QUAX was first applied to the determination of mineralogical and chemical composition of cuttings and rock flour from the drilling fluid for the German Continental Deep Drilling Program (KTB) (Emmermann and Lauterjung, 1990) and it contained 280 reference mineral patterns. Vogt (1997) established his own database of reference minerals measured with the AWI PW3020 diffractometer for the study on Arctic Ocean

sediments and new data were continuously entered into the database (Vogt et al., 2002), especially from clay and feldspar groups. Currently there are approximately 250 reference minerals in the database.

(2) The methods both packages use to calculate the weight percentage are different. RockJock uses matrix-flashing method (Chung, 1974a) to avoid using of calibration curves and flashes the mass absorption coefficient out. It uses internal standard and RIR to convert intensities to weight percentages. While for QUAX, it is critical to use mass attenuation coefficients to calculate the weight percentages. It should be measured for the reference minerals instead of citing from the textbook, which is calculated from the general chemical composition. As the unknown μ_s can only be correctly calculated if all the mineral percentages sum to 100% (Emmermann and Lauterjung, 1990), the phase identification becomes quite important for QUAX.

(3) RockJock uses an internal standard of corundum while QUAX can be run with or without an internal standard. The adding of internal standard dilutes the mineral contents, thus increases the detection limit of minor minerals and may cause some minor minerals being undetected. On the other hand, adding internal standard makes weight percentage of each mineral be calculated individually (if every mineral phase in the sample has an equivalent with RIR in the RockJock database), therefore failing to identify one mineral will not influence other minerals' calculation.

(4) For the Arctic sediments, it is common that the whole pattern fitting process goes from 19 to 64.5° 2θ for RockJock and 2 to 85° 2θ for QUAX (Vogt et al., 2002). The wider range of QUAX makes it possible to better analyze minerals that have prominent peaks in the lower and/or the higher angle.

(5) RockJock uses the Cu radiation and radiations other than Cu should be converted to Cu wavelength in the program, while the AWI-Vogt-QUAX database uses Co wavelength.

Chapter 4. Comparison of RockJock and QUAX

4.1 Quantitative XRD methods

Quantitative x-ray powder diffraction (QXRD) was suggested firstly by Hull (1919). Clark & Reynolds (1936) then proposed an internal-standard method, to which Alexander & Klug (1948) provided a theoretical foundation. But as it needs to construct a calibration curve for each component, it is rather complicated.

The much simpler but equally reliable Reference Intensity Ratio (RIR) method has been developed by Chung (1974a, 1974b) and Hubbard et al. (1976) and became one of the most popular methods for QXRD (Bish and Chipera, 1988, 1995; Chipera and Bish, 1995; Pawloski, 1985; Snyder and Bish, 1989). The RIR is defined as intensity ratios of one or several strongest peaks of a phase and a standard in a 50:50 mixture. Once the RIRs for all the phases are known, their abundances in a sample can be calculated. It gives a simple relationship between intensity and concentration and flushes out the absorption factors. It can even determine the total amount of amorphous component by the difference from 100%. But it is impossible to calculate the abundances of each amorphous component if several phases exist. In addition, as it only uses one or several peak height intensities, it will be difficult to apply when dealing with disordered phases or phases with variable chemistry or preferred orientation. The reference intensities should be determined using the same diffractometer under the same instrumental conditions (Chung, 1974a).

Another very popular method, the Rietveld method (Rietveld, 1969), was modified for QXRD analysis in the 1980s (Bish and Howard, 1988; Hill and Howard, 1987). The Rietveld method fits an observed pattern with a calculated pattern using a crystal structure model, minimizing the differences by varying parameters in the model. It provides not only phase abundances but also something like unit-cell parameters, atomic occupancies, and information on crystallite size. The method uses all the

intensities of the pattern instead of just the strongest one(s) and thus minimizes the effect of preferred orientation. It used to have difficulties to be applied to disordered materials due to the difficulty in describing refineable structures (Bish and Post, 1993). Models have been developed to describe disorder (Bergmann and Kleeberg, 1998; Ufer and Kleeberg, 2015; Ufer et al., 2012a, b). If understood well and run properly Rietveld quantifications are by all means the best way to quantify multi-phase analysis even for clay mineral rich samples (Omotoso et al., 2006).

A whole-pattern fitting method was developed by Smith et al. (1987) using the observed pattern to fit the measured pattern and was widely used thereafter with some kind of modification (Batchelder and Cressey, 1998; Chipera and Bish, 2002; Cressey and Schofield, 1996). It combines the advantages of the RIR and Rietveld methods. By using the whole diffraction pattern instead of individual peak(s), including the background, it allows for the identification of amorphous or disordered phases such as glasses and some clay minerals.

RockJock is based on this kind of whole-pattern fitting method and was widely used in quantitative phase analysis of marine sediment (Andrews et al., 2012; Andrews and Eberl, 2007; Andrews et al., 2010b; Darby et al., 2011; Eberl, 2004; Ortiz et al., 2009; Polyak et al., 2009). Although it has been proved that the error is around $\pm 4\%$ at 95% confidence level, it's better to run artificial mixtures to test it before apply it to sediment samples. In this study, three sets of artificial mixtures are used to access the accuracy.

QUAX (Quantitative Phase-Analysis with X-ray Powder Diffraction) is also a whole-pattern fitting method and is used initially at the KTB site (German Continental Deep Drilling) to determine mineral phases (Emmermann and Lauterjung, 1990). Vogt (1997) has used it in the mineralogical study of the Arctic Ocean and further improved the reference minerals as well as added new mineral standards (Vogt, 1996; Vogt et al., 2001). As a lot of data has been produced by both methods, it is necessary

to study if the data produced by the two methods can be comparable. Comparison between RockJock and QUAX has been done by Bazhenova (2012) and Andrews and Vogt (2014b). In this study, a more detailed comparison is done and the possible reasons for the differences of results produced by the two methods are discussed.

4.2 Assessing accuracy of RockJock

Accuracy assessment is quite important before deploying RockJock for quantitative XRD analysis, and has been checked for accuracy using artificial mixtures and generally gives results that are within 1 or 2 wt% of actual values (Eberl, 2003). Using minerals identical to the reference minerals and proper preparation methods, the results are quite satisfying, with relative errors for kaolinite or quartz of approximately $\pm 4\%$ at the 95% confidence level. However, as minerals in most samples will not be exactly the same as the reference minerals, it is necessary to test with artificial mixtures which have minerals different from the reference minerals. In this case, three sets of artificial mixtures with different mineral phases are used for the assessment. The data are calculated from measurements on the old diffractometer PW3020. Bias, defined as the absolute difference between the RockJock results and the true abundance, is used to assess the accuracy.

Two-phase mixtures

The RockJock quantitative analysis results of the six two-phase artificial mixtures compared to the true abundances are shown in Table 4.1 and Fig 4.1. Here both the actual results calculated by RockJock and the normalized ones are listed. Except for Mix1 and Mix6, the totals are close to 100%, which indicates a good quality of the analysis. Mix1 is composed of pure chlorite and is used to check its difference from the reference chlorite. Despite the relatively large bias of 14.6% for chlorite in Mix1, good results can be derived from Mix2 and Mix5, with biases of 4.6% and 0.3% respectively. For quartz and plagioclase, the results are not good in Mix3 and Mix5. However, an approximate 1:2 ratio can be seen in both mixtures. The 1:1 mixed quartz and K-feldspar of Mix4 shows a quite good result, with a bias of 1% for each.

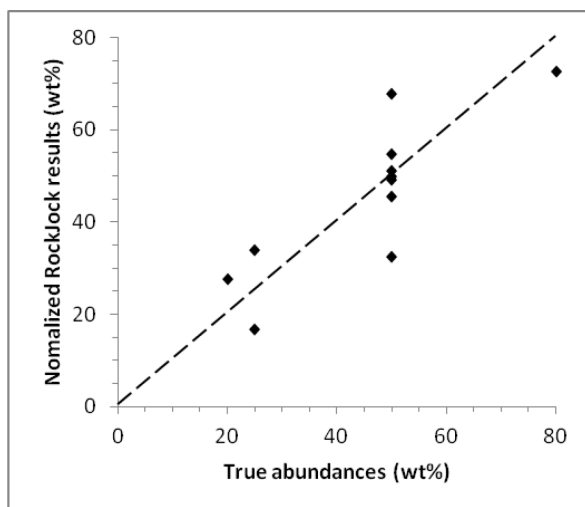


Fig 4.1 True abundances versus normalized RockJock results for two-phase mixtures listed in Table 4.1. The dashed line is the one-to-one correlation line. The standard deviation is $\pm 8.77\%$.

Table 4.1 RockJock results for two-phase mixtures (wt%).

	True	RockJock	RockJock (normalized)
Mix1			
Chlorite	100	85.4	100
Mix2			
Kaolinite	50	57	54.6
Chlorite	50	47.4	45.4
Total		104.4	100
Mix3			
Quartz	50	32.7	32.4
Plagioclase	50	68.3	67.6
Total		101	100
Mix4			
Quartz	50	47.6	49
Kspar	50	49.6	51
Total		97.2	100
Mix5			
Quartz	25	17.1	16.5
Plagioclase	25	35.1	33.8
Chlorite	50	51.6	49.7
Total		103.8	100

Table 4.1 (continued)

Mix6			
Quartz	20	21	27.4
Smectite	80	55.6	72.6
Total		76.6	100

Six-phase mixtures

The six-phase mixtures are composed of quartz, k-feldspar, plagioclase, kaolinite, smectite and illite with various abundances (see Table 3.1). Fig 4.2 shows the quality of fit of all these minerals. For quartz, k-feldspar and kaolinite, the solid line lies above the dashed line, indicating that the RockJock result is higher than the true abundance. For plagioclase, smectite and illite, the solid line lies below the dashed line, indicating that the RockJock result is lower than the true abundance. Most of them, except for k-feldspar and smectite, have a high coefficient of determination ($R^2 > 0.9$) and the trend lines are parallel to the 1:1 correlation lines, indicating that calibrations can be easily made between RockJock results and true abundances.

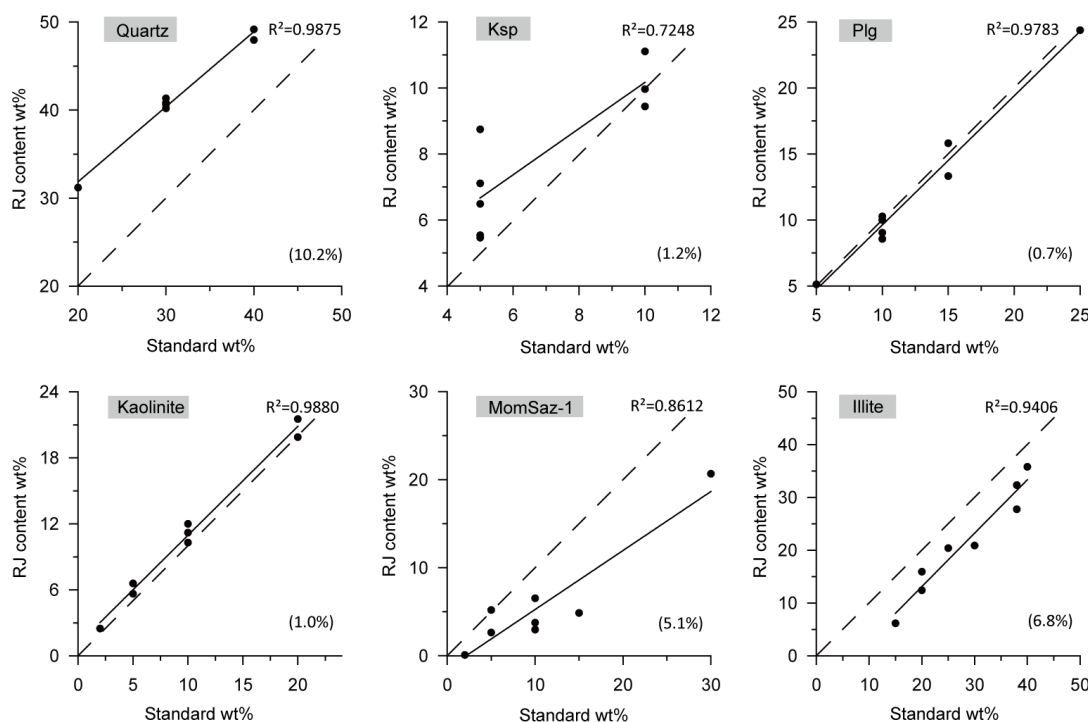


Fig 4.2 True abundances versus normalized RockJock results for six-phase mixtures. The solid line is the linear regression line and the dashed line is the one-to-to correlation line.

Plagioclase and kaolinite show very minor differences between RockJock results and true abundances, with average bias of 0.7% and 1% respectively. However, quartz and illite show relatively high average bias of 10.2% and 6.8% respectively.

Eleven-phase mixtures

There are in total ten eleven-phase mixtures, consisting of quartz, k-feldspar, plagioclase, calcite, gypsum, kaolinite, smectite, biotite, muscovite, palygorskite and nontronite (see Table 3.1). Fig 4.3 shows that, for clay minerals, RockJock results are very poor. As there is no nontronite in the reference minerals in RockJock, it cannot be recognized. Biotite in all the samples and muscovite and smectite in most samples are not recognized at all (with zero abundances). Only kaolinite and palygorskite give relatively good results. The average bias of kaolinite is large (8%), but the coefficient of determination is very good ($R^2=0.9853$), which means that it can be calibrated to the true abundance using a linear function at a high confidence level. The coefficient of determination of palygorskite is not that good (only 0.8413), but the best fit line is very close to the 1:1 correlation line and the average bias is small (2.6%). The RockJock results for non-clay minerals, compared to clay minerals, are much better. Most of the non-clay minerals have a very small average bias (0.5% to 2.9%), with the exception for quartz (15.1%). In this case, the sum of the clay minerals can also be well determined.

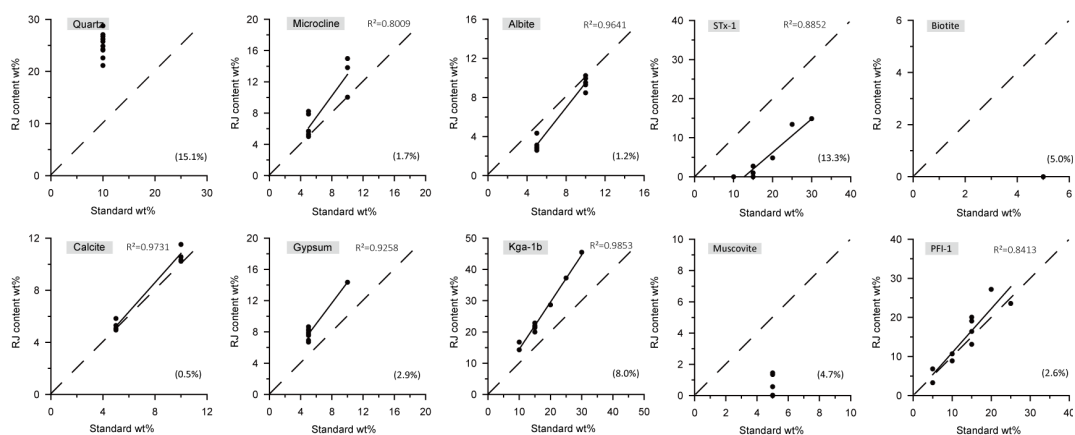


Fig 4.3 True abundances versus normalized RockJock results for eleven-phase mixtures. The solid line is the linear regression line and the dashed line is the one-to-to correlation line.

4.3 Possible error sources of RockJock

RockJock, a rather sophisticated computer program developed for quantitative X-ray diffraction, has been checked for accuracy using artificial mixtures. Whereas Eberl (2003) gives an accuracy of 1-2 wt%, the error bars are clearly larger when applied to the artificial mixtures in this study. So it has to be figured out what are the possible sources of the error.

Preferred Orientation

Preferred orientation can cause significant intensity variations in an XRD pattern, and thus introduces systematic errors into the quantification. However, the preparation of completely random samples is almost impossible. A lot of efforts have been put to produce random powders (Bish and Reynolds, 1989). Among these, the spray drying method is considered to be the most effective one (Hillier, 1999; Hughes and Bohor, 1970; Jonas and Kuykendall, 1966; Kleeberg et al., 2008; Smith et al., 1979a, b). But this method is not widely used possibly because of the lack of equipment and the need of relatively large amount of samples (Bish and Reynolds, 1989). A new method (Omotoso and Eberl, 2009) modified from that reported in Środoń and others (Środoń et al., 2001) has been used for achieving almost perfectly random sample orientation, which is convenient to the spray drying method. Due to the different equipment, the sample filling method of back loading instead of side loading is used in this study. Back loading is proved to be an effective method to minimize preferred orientation (Chao et al., 1996; da Silva et al., 2011). Fig 4.4a and 4.4b show that the measured pattern differs greatly from the calculated pattern, which suggests some degrees of preferred orientation. However, Table 4.1 indicates that the bias for chlorite in Mix 1 and Mix 2 is acceptable. When mixed with non-clay minerals (Quartz and Plagioclase) in Mix 4, the bias is even smaller. It comes to the conclusion that, to some extent, the whole pattern fitting process in RockJock can decrease the effect of preferred orientation on quantification. And with the increase of mineral phases in the sample, the effect of preferred orientation on quantification is even smaller.

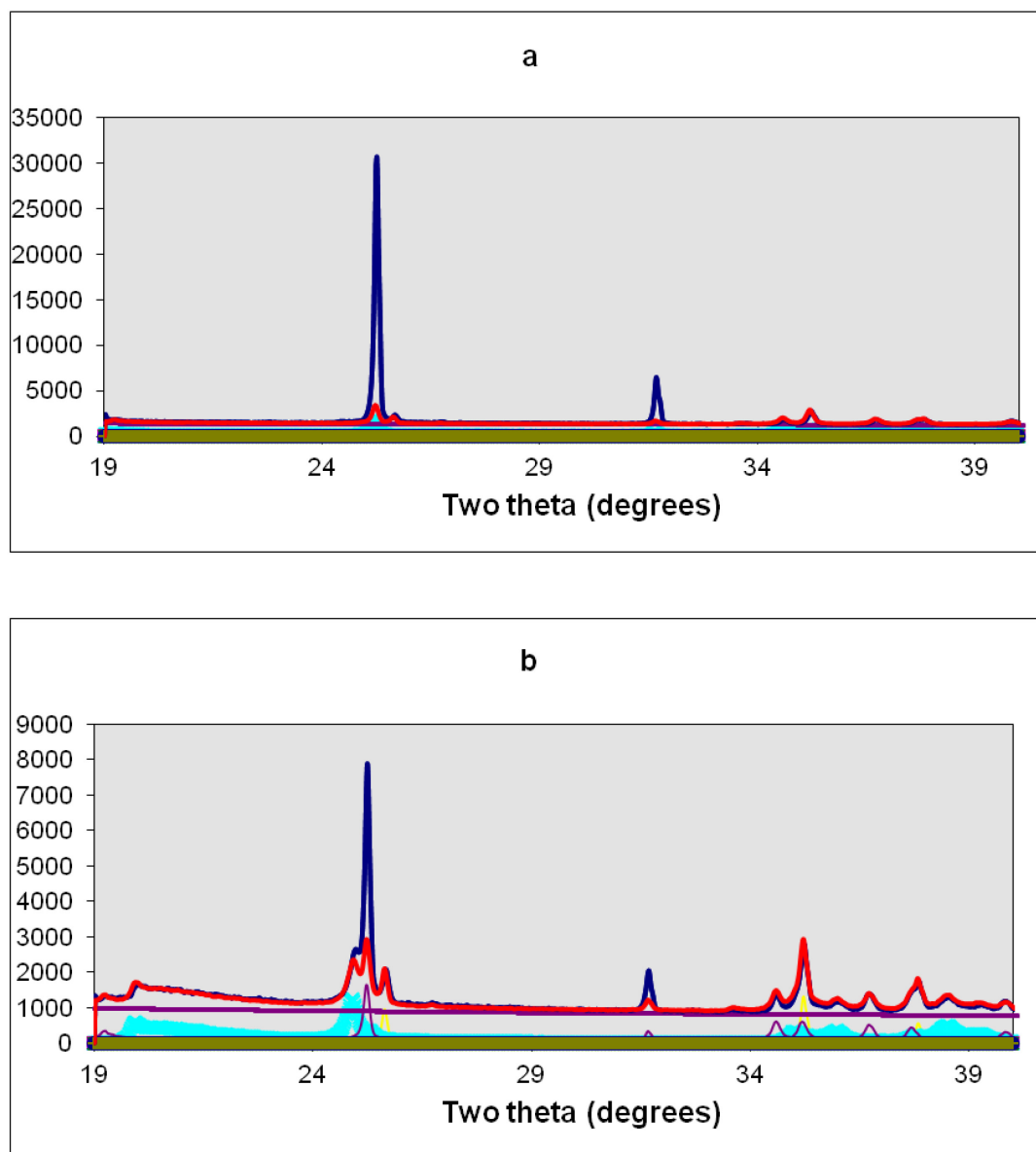


Fig 4.4 XRD pattern of a) Mix 1 with 100% chlorite and b) Mix 2 with 50% chlorite and 50% kaolinite in RockJock. Red is calculated and blue is measured.

Different diffractometers

Ideally samples should be measured on the same machine as the reference minerals, which should give the best results. But in reality different laboratories usually have different diffractometers. This would be an important error source, because the configuration might be totally different (e.g. different tubes, divergences, detectors etc.). It has been tested based on limited data by Eberl (2003) that results are acceptable when analyzing samples measured on different machines. Andrews has done a lot of studies on the mineralogy of glacial sediments using RockJock on a

different diffractometer from the one on which the reference minerals were measured and fairly good results have been obtained (Andrews et al., 2012; Andrews et al., 2010a; Andrews and Eberl, 2007; Andrews et al., 2010b). Andrews and Vogt (Andrews and Vogt, 2014b) also showed comparisons of same samples on different machines.

During this study, there was a replacement of diffractometers in our laboratory, which gave us the opportunity to test the influences of different diffractometers on the results. For two-phase mixtures, the comparison between wt% known and wt% found analyzed by two different diffractometers and the absolute errors are given in Table 4.2 and the comparison between two diffractometers are plotted in Fig 4.5a. Although the absolute errors for most samples are larger than what is so called ‘highly accurate’ of 3 wt% absolute defined by Calvert et al (1989), the correlation between the two different diffractometers is very good, which means that good results can be obtained using different diffractometers in this case. What if the number of mineral phases increases? The analyzing results of eleven-phase mixtures can be seen in Table 4.3 and comparisons between two diffractometers are plotted in Fig 4.5b and 4.5c. It shows that the correlation between the two diffractometers is not as good as that of the two-phase mixtures. But for most mineral phases the new machine has smaller absolute errors.

Reference minerals

RockJock is a whole-pattern fitting method by which a measured pattern is fitted by summing patterns of previously measured reference minerals from 19 to 64.5 degrees two-theta. So the database of the reference minerals is very important to the quantification. The best results will be obtained when minerals in samples are identical to the reference minerals. However, minerals like feldspars and various clay minerals have extremely variable structures and/or chemical composition, it is virtually impossible to include all possible patterns in the database. This could be an important error source from two aspects. The first is that there is a reference mineral

similar to the one identified in samples, but with different structures. The second is that the mineral phases in the sample are not included in the reference minerals database. The first situation is quite common. It is suggested that reference minerals in the current RockJock program give good results for most purposes (Eberl, 2003). And good results have been obtained when RockJock was applied in Arctic Ocean sediments (Darby et al., 2011; Myers and Darby, 2015; Ortiz et al., 2009) and sediments near Greenland (Andrews et al., 2010a; Andrews et al., 2014; Andrews et al., 2010b; Andrews and Vogt, 2014b). The users can develop their own references if the most accurate quantification is to be made. The second situation happens when the eleven-phase mixtures are tested. Nontronite (Nau-1) cannot be found in the references. Both situations of reference minerals should be accounted partly for the large error bars of the eleven-phase mixtures.

4.4 Standardless analysis in RockJock

Standardless analysis can be done in RockJock, which means that samples can be run without an internal corundum standard (Eberl, 2003). It should give similar results as the internal standard analysis. However, there is no much data support. Here a standardless analysis using 15 samples is presented to study whether it gives good results as internal standard analysis (Wassmuth, 2014). Although it is written that samples can be run without an internal standard (standardless analysis) (Eberl, 2003), and the Reynolds Cup patterns stored in the program that should be run using standardless analysis can be run successfully in this study, unexpected difficulties existed when running the samples. Firstly, it seems that the RockJock cannot work properly with a German version of Excel. It always ran normally at first and went totally wrong at some point. Different results were got when doing repeated analysis using the same sample. There is a detailed instruction to show how to run RockJock under non-English versions of Excel. But it doesn't work after going through all the steps. However, it has been proved that it can be run successfully with a Chinese version of Excel (the RockJock data obtained in this thesis were run with a Chinese

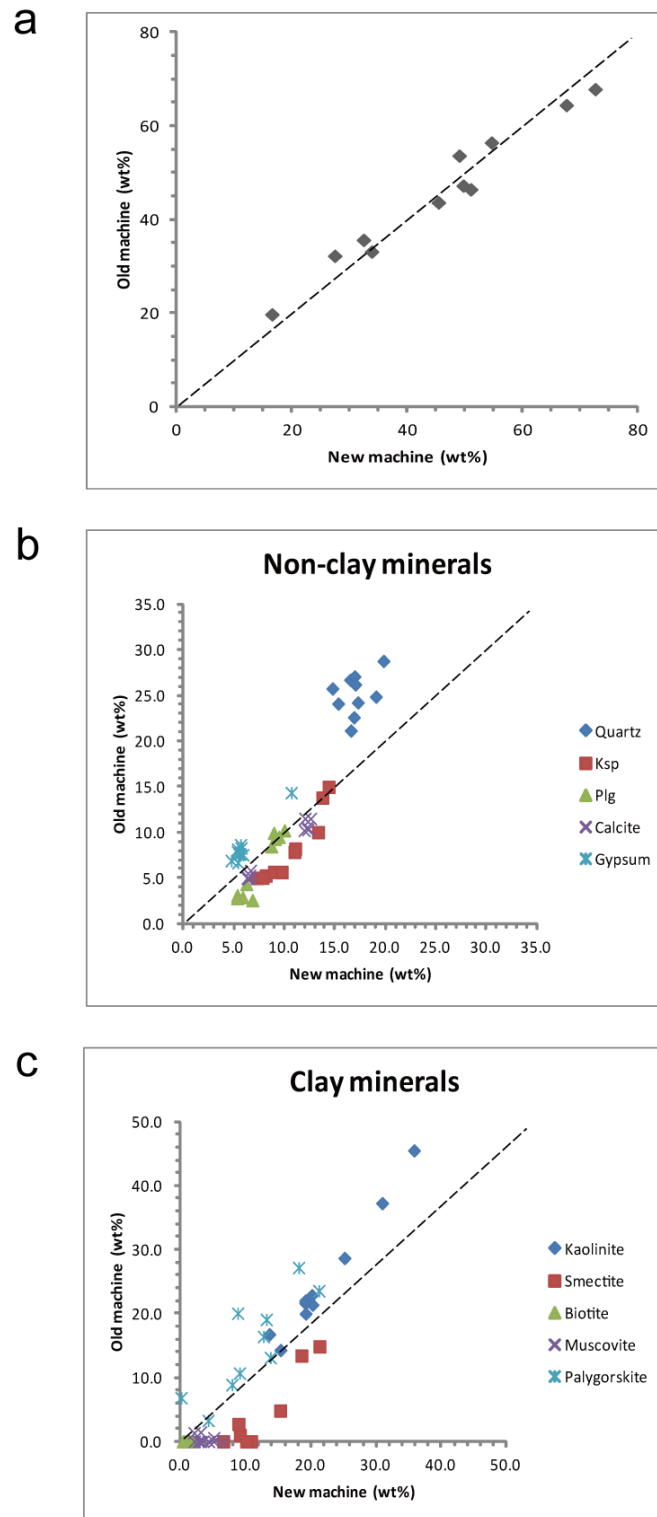


Fig 4.5 x-y plot of comparisons between the new machine and old machine. (a) two-phase mixtures (b) eleven-phase mixtures – non clay minerals (c) eleven-phase mixtures – clay minerals.

Table 4.3 Comparison between wt% known and wt% found for the eleven phase mixtures analyzed by two different diffractometers.

	Old machine			New machine	
	%known	%found	abs.error	%found	abs.error
Mix26					
Quartz	10	24.9	14.9	19.1	9.1
Kspar	10	15.0	5.0	14.4	4.4
Plagioclase	10	9.9	-0.1	8.9	-1.1
Calcite	10	10.2	0.2	12.0	2.0
Gypsum	10	14.4	4.4	10.7	0.7
Kaolinite	10	16.8	6.8	13.6	3.6
Smectite	10	0.0	-10.0	10.3	0.3
Biotite	5	0.0	-5.0	0.3	-4.7
Muscovite	5	0.0	-5.0	3.0	-2.0
Palygorskite	10	8.9	-1.1	7.8	-2.2
Mix27					
Quartz	10	26.7	16.7	16.5	6.5
Kspar	5	8.2	3.2	11.1	6.1
Plagioclase	10	9.5	-0.5	9.4	-0.6
Calcite	10	11.5	1.5	12.0	2.0
Gypsum	5	7.9	2.9	5.3	0.3
Kaolinite	15	22.0	7.0	19.1	4.1
Smectite	15	1.0	-14.0	9.1	-5.9
Biotite	5	0.0	-5.0	0.3	-4.7
Muscovite	5	0.0	-5.0	3.4	-1.6
Palygorskite	15	13.1	-1.9	13.7	-1.3
Mix28					
Quartz	10	22.6	12.6	16.9	6.9
Kspar	5	5.3	0.3	8.1	3.1
Plagioclase	5	3.1	-1.9	5.3	0.3
Calcite	10	10.6	0.6	12.2	2.2
Gypsum	5	8.2	3.2	5.3	0.3
Kaolinite	15	21.6	6.6	19.1	4.1
Smectite	15	0.0	-15.0	10.8	-4.2
Biotite	5	0.0	-5.0	1.1	-3.9
Muscovite	5	1.5	-3.5	3.0	-2.0
Palygorskite	20	27.2	7.2	18.1	-1.9
Mix29					
Quartz	10	24.2	14.2	17.3	7.3
Kspar	5	5.0	0.0	7.3	2.3

Table 4.3 (continued)

Plagioclase	5	4.3	-0.7	6.2	1.2
Calcite	10	11.5	1.5	12.6	2.6
Gypsum	5	8.7	3.7	5.6	0.6
Kaolinite	15	21.4	6.4	20.2	5.2
Smectite	20	4.8	-15.2	15.3	-4.7
Biotite	5	0.0	-5.0	1.8	-3.2
Muscovite	5	0.0	-5.0	5.0	0.0
Palygorskite	15	20.0	5.0	8.7	-6.3
Mix30					
Quartz	10	27.1	17.1	16.9	6.9
Kspar	5	5.0	0.0	7.8	2.8
Plagioclase	5	2.9	-2.1	5.8	0.8
Calcite	10	10.3	0.3	12.3	2.3
Gypsum	5	6.9	1.9	4.7	-0.3
Kaolinite	20	28.7	8.7	25.1	5.1
Smectite	15	0.0	-15.0	10.2	-4.8
Biotite	5	0.0	-5.0	1.9	-3.1
Muscovite	5	0.0	-5.0	2.1	-2.9
Palygorskite	15	19.1	4.1	13.1	-1.9
Mix31					
Quartz	10	25.7	15.7	14.7	4.7
Kspar	5	7.9	2.9	11.0	6.0
Plagioclase	10	9.3	-0.7	9.0	-1.0
Calcite	5	5.3	0.3	6.6	1.6
Gypsum	5	7.7	2.7	5.5	0.5
Kaolinite	15	20.0	5.0	19.2	4.2
Smectite	10	0.0	-10.0	6.5	-3.5
Biotite	5	0.0	-5.0	1.3	-3.7
Muscovite	5	0.6	-4.4	5.1	0.1
Palygorskite	25	23.6	-1.4	21.2	-3.8
Mix32					
Quartz	10	24.1	14.1	15.3	5.3
Kspar	10	13.8	3.8	13.8	3.8
Plagioclase	10	10.2	0.2	10.0	0.0
Calcite	5	5.8	0.8	6.6	1.6
Gypsum	5	7.6	2.6	5.6	0.6
Kaolinite	10	14.3	4.3	15.3	5.3
Smectite	25	13.4	-11.6	18.5	-6.5

Table 4.3 (continued)

Biotite	5	0.0	-5.0	1.7	-3.3
Muscovite	5	0.0	-5.0	4.3	-0.7
Palygorskite	10	10.7	0.7	9.0	-1.0
Mix33					
Quartz	10	26.2	16.2	17.0	7.0
Kspar	5	5.7	0.7	9.0	4.0
Plagioclase	5	2.8	-2.2	5.3	0.3
Calcite	5	5.0	0.0	6.5	1.5
Gypsum	5	6.7	1.7	5.4	0.4
Kaolinite	25	37.3	12.3	30.9	5.9
Smectite	15	0.0	-15.0	10.1	-4.9
Biotite	5	0.0	-5.0	0.6	-4.4
Muscovite	5	0.0	-5.0	2.7	-2.3
Palygorskite	15	16.4	1.4	12.7	-2.3
Mix34					
Quartz	10	28.8	18.8	19.8	9.8
Kspar	5	5.7	0.7	9.7	4.7
Plagioclase	10	8.5	-1.5	8.7	-1.3
Calcite	5	5.0	0.0	6.3	1.3
Gypsum	5	7.6	2.6	5.9	0.9
Kaolinite	15	22.9	7.9	20.1	5.1
Smectite	30	14.9	-15.1	21.3	-8.7
Biotite	5	0.0	-5.0	1.6	-3.4
Muscovite	5	0.0	-5.0	6.5	1.5
Palygorskite	5	6.8	1.8	0.0	-5.0
Mix35					
Quartz	10	21.1	11.1	16.6	6.6
Kspar	10	10.0	0.0	13.3	3.3
Plagioclase	5	2.6	-2.4	6.8	1.8
Calcite	5	5.1	0.1	6.4	1.4
Gypsum	5	8.3	3.3	5.7	0.7
Kaolinite	30	45.5	15.5	35.8	5.8
Smectite	15	2.7	-12.3	8.8	-6.2
Biotite	5	0.0	-5.0	0.3	-4.7
Muscovite	5	1.3	-3.7	2.0	-3.0
Palygorskite	5	3.3	-1.7	4.2	-0.8

version of Excel). Even if running with a Chinese version, the program often crashed. The same happened when running with an English version (Wassmuth, 2014). This is not the case when running it with an internal standard. Thus the results should be treated with care. One criteria is to see the degree of fit, which should be <0.100 (Eberl, 2003). Of the fifteen samples run for comparison, only three of them are usable as the degree of fit in these samples is <0.100 in all three runs (Table 4.4). The three samples shows a good reproducibility and can be compared to the samples measured with internal standard (Fig 4.6), however, the degrees of fit of other samples are too arbitrary. Thus the results of the standardless analysis should be treated with care.

Table 4.4 Three runs of the 15 samples (without standard). Only samples with a depth of 10, 40 and 70 cm (gray bar) are usable for comparison eith the standard samples, as the degree of fit in these depths is in the defined range < 0.1 . The data are from Wassmuth (2014).

Depth(cm)	Degree of fit		
	Run 1	Run 2	Run 3
0	0.738	0.733	0.026
5	0.264	0.264	0.025
10	0.031	0.031	0.031
15	0.767	0.028	0.028
20	0.023	0.757	0.023
25	0.747	0.272	0.030
30	0.269	0.032	0.032
35	0.232	0.024	0.024
40	0.027	0.027	0.027
45	0.769	0.761	0.030
50	0.266	0.269	0.030
55	0.033	0.275	0.034
60	0.764	0.027	0.027
65	0.269	0.027	0.027
70	0.030	0.030	0.030

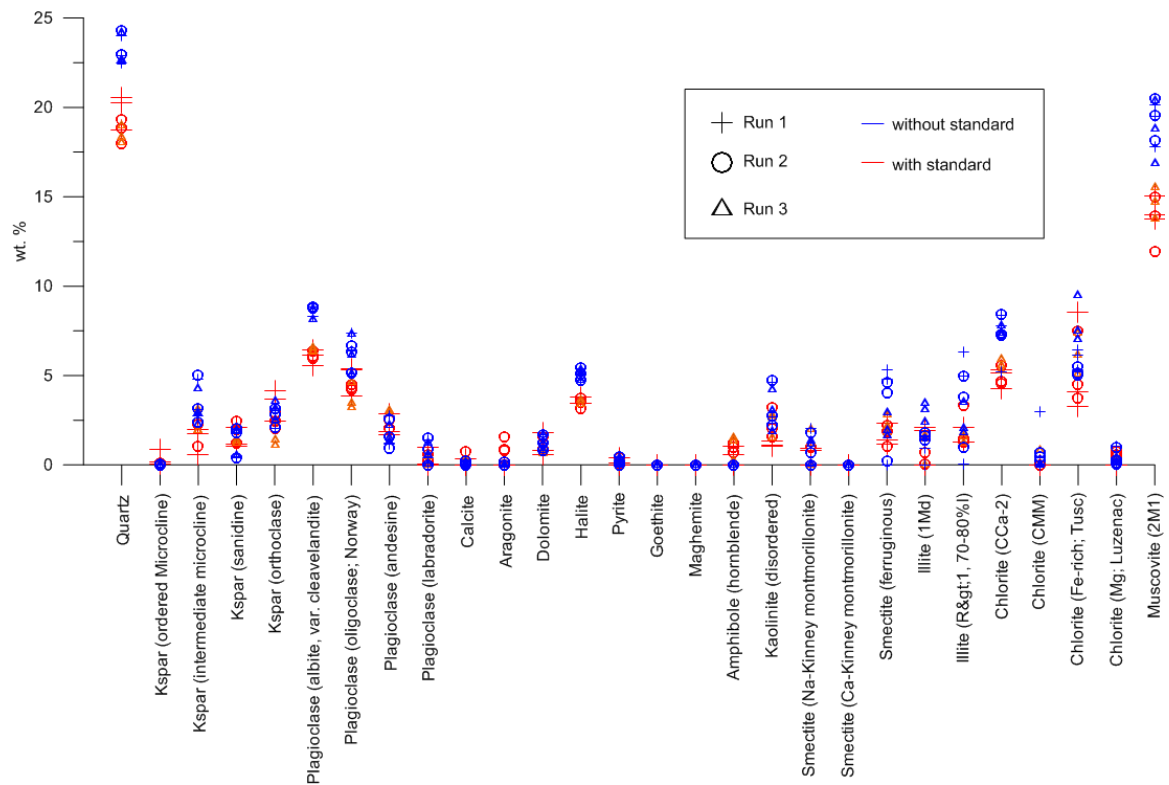


Fig 4.6 Comparison of the reproducibility of samples measured with internal standard (red) and without internal standard (blue) (Wassmuth, 2014).

4.5 Weight percentages vs. peak intensities

Beside the weight percentages obtained by qXRD, relative abundances of major minerals can also be estimated by single peak intensities, i.e., peak heights (Stein et al., 2010b). The peak intensity is directly proportional to the concentration of the component producing it (Klug and Alexander, 1954). And Chung (1974a, 1974b) developed a Reference Intensity Ratio (RIR) method giving a simple relationship between intensity and concentration. Therefore, using the single peak intensities may be a simple alternative to the qXRD results, when only the down-core variations of the minerals are studied. Note that the grinding should be thorough enough to ensure optimum particle size and sample homogeneity, and the loading of samples should be done properly to avoid preferred orientation (Chung, 1974a). Integrated intensities (peak area) is preferred to peak heights as it eliminates the effects of mineral structure variability (Kahle et al., 2002).

Single peak intensities were calculated using the MacDiff program (Petschick, 2002). The major peak heights of quartz (3.34 Å, 4.26 Å), K-feldspar (3.24 Å), plagioclase (3.18 Å), calcite (3.04 Å), and dolomite (2.89 Å), were measured. Because the strongest 3.34 Å quartz peak overlaps with other peaks (e.g. illite), the second strong peak of 4.26 Å was used. The weight percentages calculated by RockJock and the single peak intensities calculated by MacDiff of core PS72/396-5, PS72/410-3 and PS72/422-5 are plotted in Fig 4.7 (Schulte-Loh, 2009). While other minerals show fairly good correlations, K-feldspar shows no correlation between weight percentages and single peak intensities. The possible reasons why K-feldspar shows no correlation might be that 1) the 3.24 Å K-feldspar peak interferes with peaks of other minerals (e.g. plagioclase); 2) the K-feldspar group contains several different feldspars (ordered microcline, intermediate microcline, orthoclase, and anorthoclase recognized in RockJock), and they do not necessarily all have the 3.24 Å peak (Fig 4.7). Note that there are several points located on the X axis, which means that the peak intensities of

these points are zero while the weight percentages are not. This may well support the second reason.

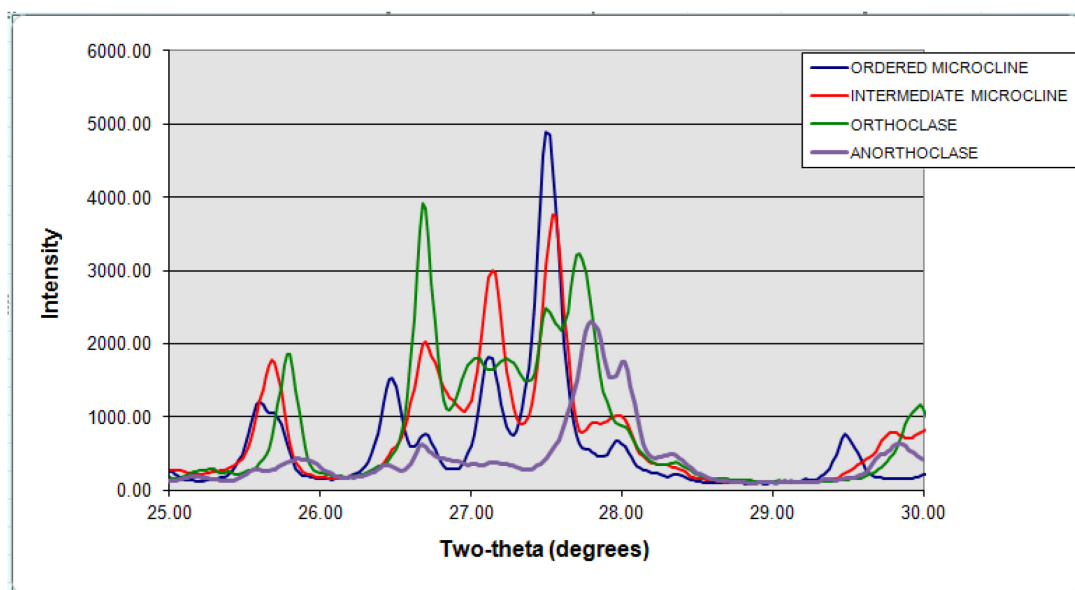


Fig 4.7 Plotted patterns of different k-feldspars stored in the RockJock. The anorthoclase doesn't have the 3.24 Å (27.53 degrees two-theta) peak.

Fig 4.8 shows the comparison between down-core variations of peak intensities and weight percentages of the three cores. For calcite and dolomite, the correlations in Fig 4.8 are very good ($r^2 > 0.8$) and down-core variations of peak intensities and weight percentages in Fig 4.9 correspond extremely well with each other. For quartz and plagioclase, the correlations in Fig 4.8 are not as good as calcite and dolomite. But peak intensities and weight percentages still show good peak to peak correlations. This indicates that although the amplitude of peak intensities and weight percentages may not be the same, it does not alter the trend of their down-core variations. For K-feldspar, there are almost no correlations between down-core variations of peak intensities and weight percentages, as also shown in Fig 4.9.

In summary, if only an estimate of relative abundances of major minerals (quartz, plagioclase, calcite and dolomite) of the sediment is needed, and sample homogenizing and preparation of sample in the back loading system has been done properly, the simple and time saving single peak intensities method can be a convincing alternative to the more time consuming qXRD method.

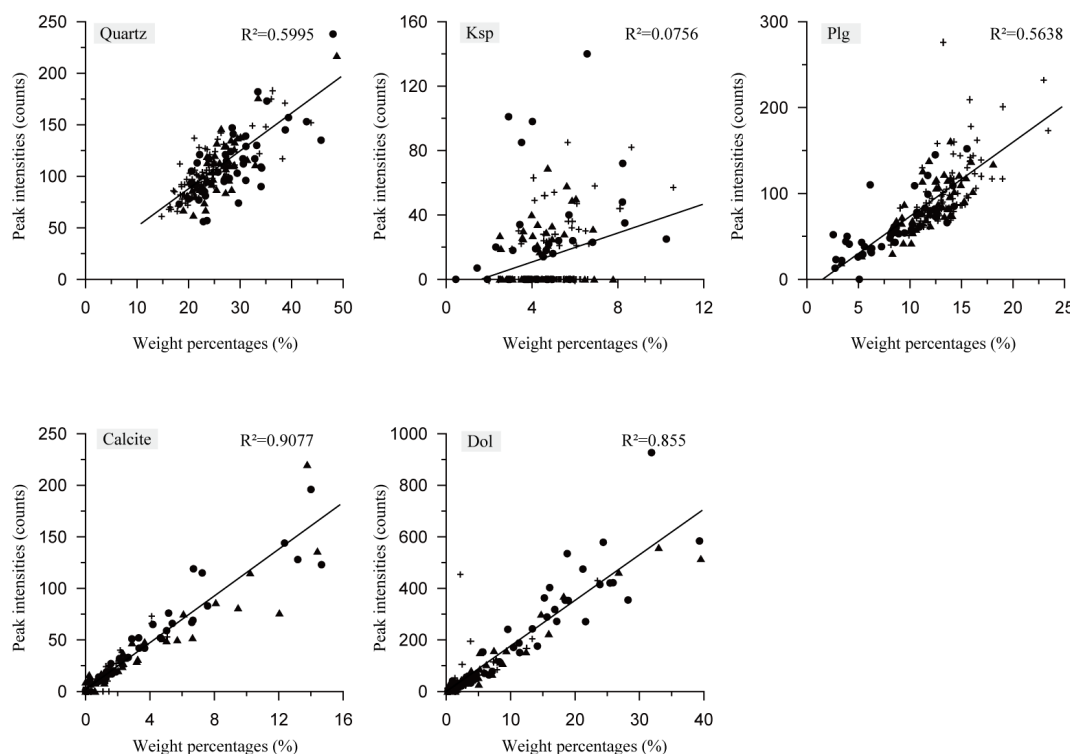


Fig 4.8 Weight percentages vs. peak intensity of core PS72/396-5, PS72/410-3 and PS72/422-5. Circles represent samples from core PS72/396-5. Triangles represent samples from core PS72/410-3. Crosses represent samples from core PS72/422-5. Peak intensities data are from Schulte-Loh (2009).

4.6 Comparison between RockJock and QUAX

In RockJock the identification of mineral phases shows that the major non-clay minerals are quartz, plagioclase, k-feldspar, calcite and dolomite in the surface samples. The main clay minerals are illite, smectite, kaolinite, chlorite and micas. During the calculation, it is found that it was not easy to distinguish smectite with illite as has been written by Eberl (2003), so the weight percentages of the two minerals should be added together when reported (see also in Bazhenova, 2012). This is an disadvantage for the Arctic Ocean sediment study as smectite is a key provenance indicator (Wahsner et al., 1999). There are also some minor minerals such as pyroxenes, amphiboles, garnet, rutile, magnetite and epidote that can be identified. But the amount is so low that it is within the error bar. Therefore their existences can only be used qualitatively to identify the provinces of the surface sediment. Comparison between RockJock and QUAX results is shown in Fig 4.10. Three

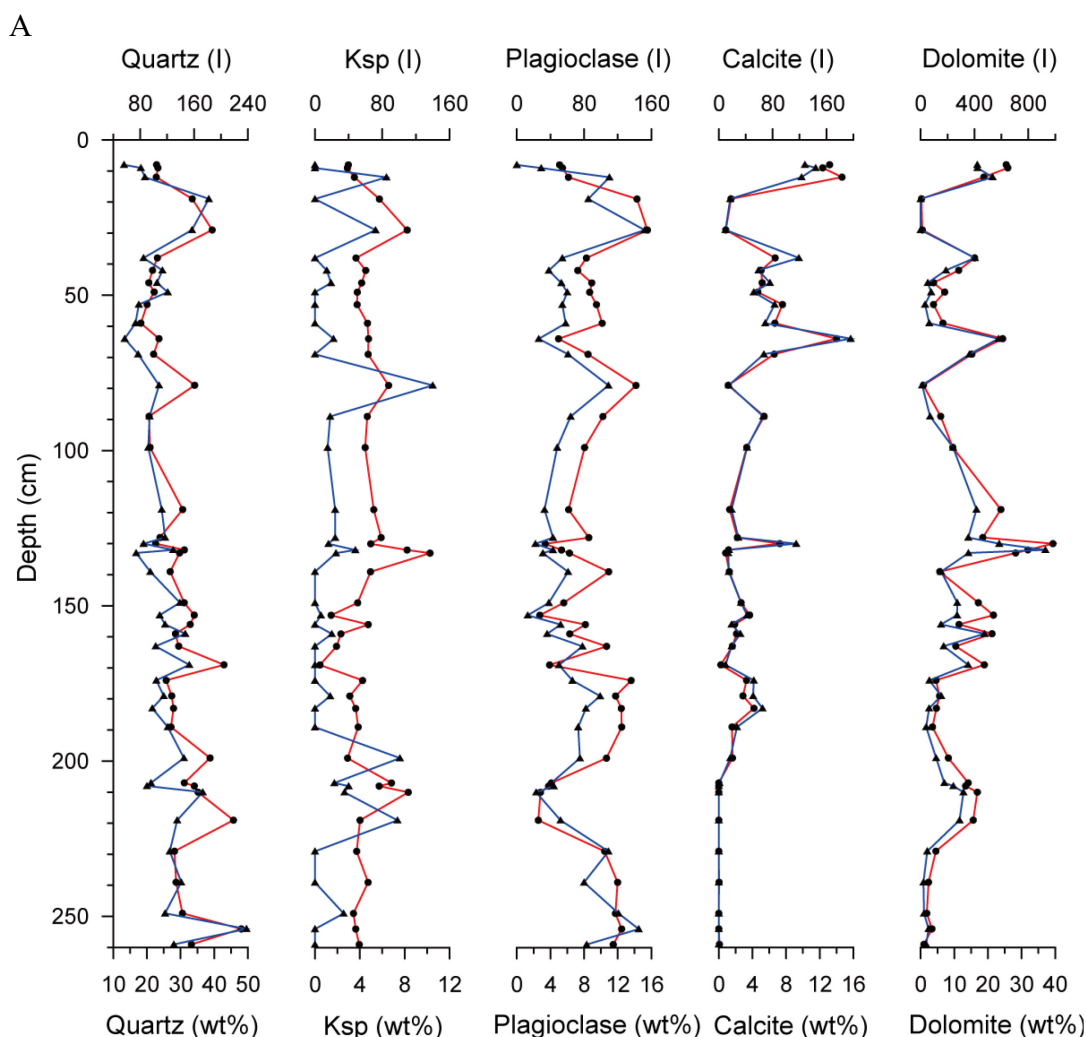


Fig 4.9 Comparison of downcore variations between weight percentages and peak intensities. A core PS72/396-5. B core PS72/410-3. C core PS72/422-5. Red curves are weight percentage variations and blue curves are peak intensity variations. Data are from Schulte-Loh (2009).

different correlation groups can be distinguished. Calcite and dolomite are the first group, which shows very good correlation between RockJock and QUAX results. The second group includes quartz, plagioclase, k-feldspar and micas, which shows intermediate correlations. The third group of kaolinite and chlorite shows no correlation. As already shown by Bazhenova (2012), in general fairly good correlations are observed for non-clay minerals and the sum of clay minerals, while the differences in the individual clay mineral group are high. Andrews and Vogt (2014b) also showed similar comparison patterns. Compared to QUAX, the quartz

contents are mostly underestimated and the phyllosilicate are overestimated in RockJock for surface sediment samples of which the true compositions are unknown.

B

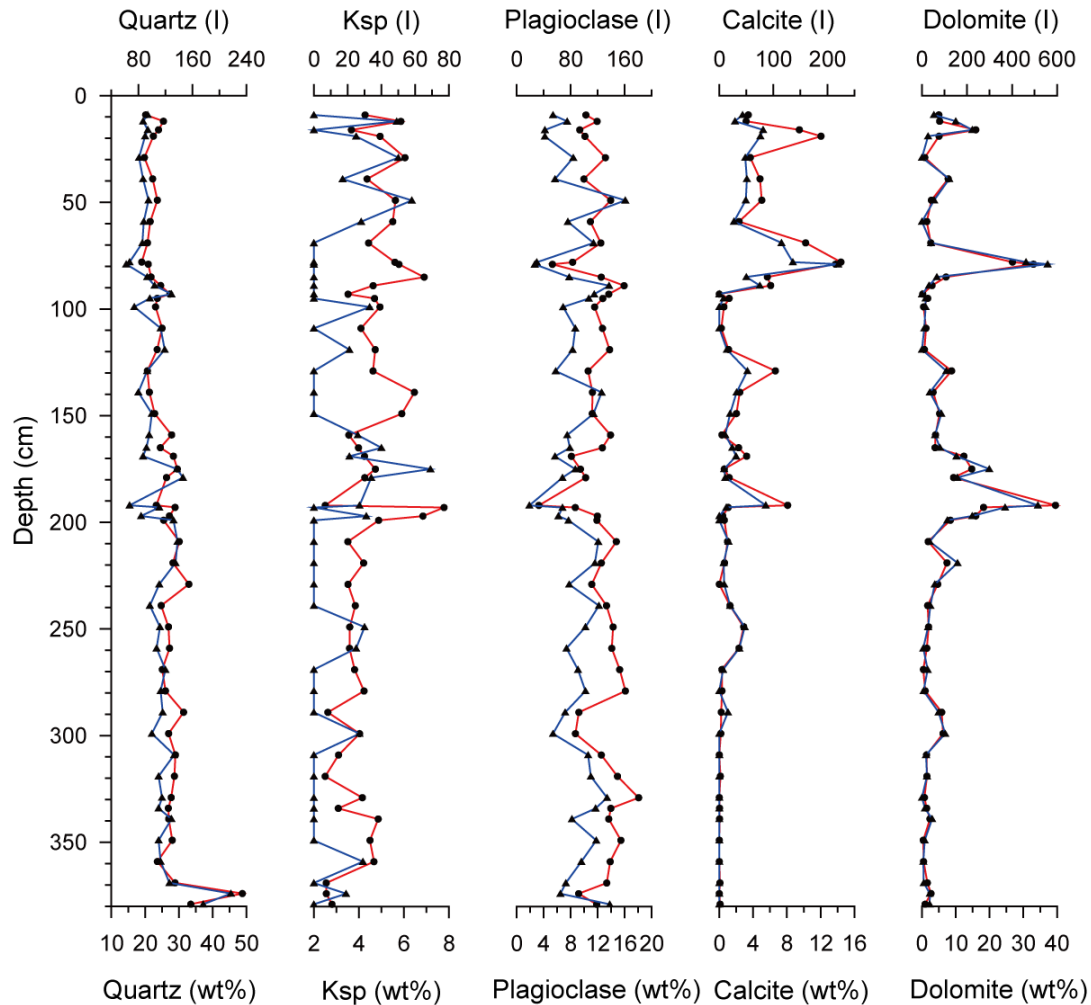


Fig 4.9 (continued)

Fig 4.11 is the distribution map of differences between RockJock and QUAX results. It can be seen that there are little variations on plagioclase and dolomite, while the variations on quartz and phyllosilicate are bigger. For quartz, samples from Central Arctic and East Siberian Sea show low differences, while samples from Laptev Sea and Chukchi Sea show medium differences. High differences occur near the Wrangel Island. For phyllosilicate, the differences are bigger than other minerals – most of the differences are medium to high. Low differences mainly located on the Southern

Mendelev Ridge. High differences are mostly seen in the Chukchi Sea and the Bering Strait.

C

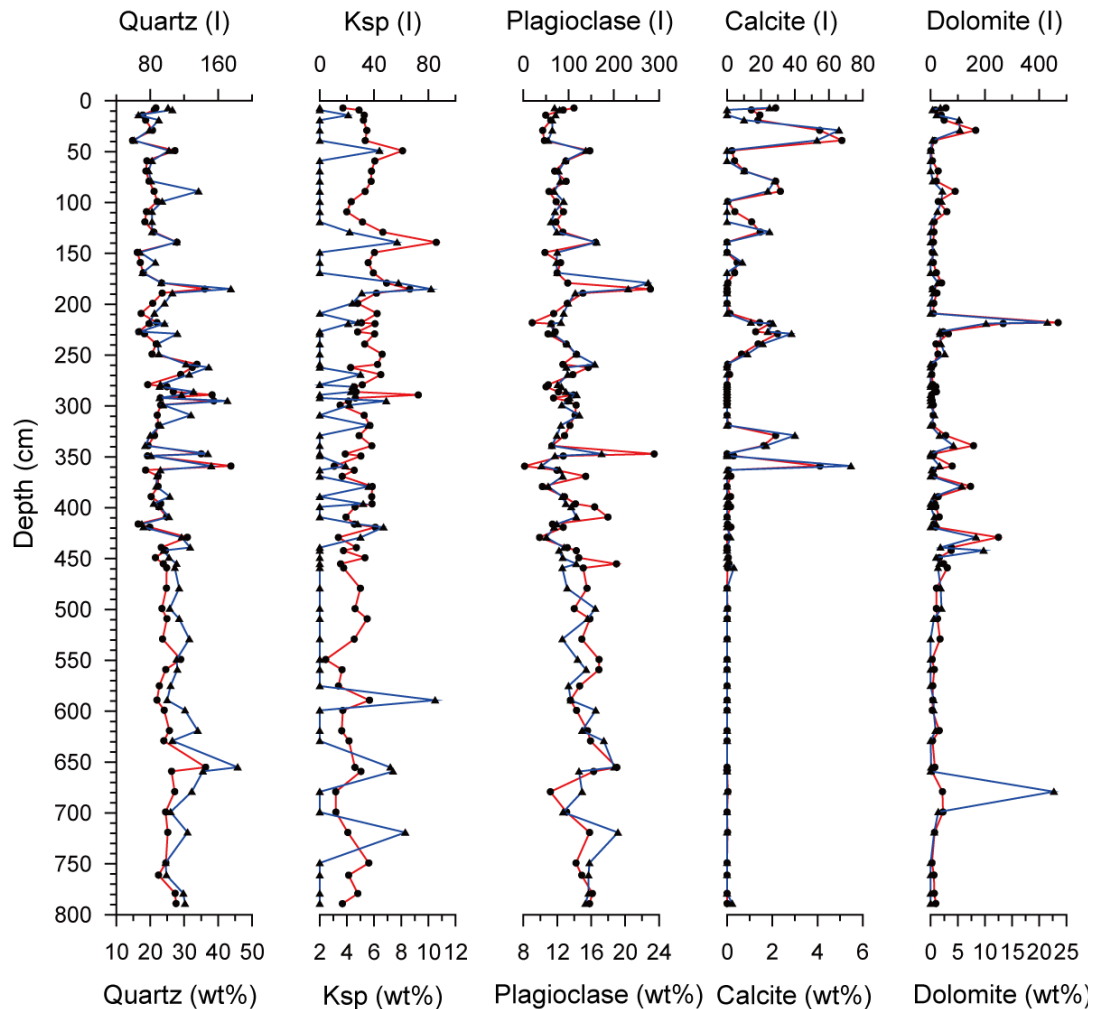


Fig 4.9 (continued)

Calcite and dolomite show the best correlations among all the minerals. Compared to other minerals (except for quartz), they have the advantage of relatively stable chemical composition, which will decrease the calculation error. Mg can substitute for Ca in calcite, however, the amount of calcite (Mg rich) is less than 1% in this study. Similarly dolomite (Fe rich) is also a trace mineral. This will not alter the peak position very much, thus, can decrease the error. Besides, the major peaks of dolomite (2.89 Å) and calcite (3.04 Å) have not many line interferences. These might be the reasons why the correlations are quite good.

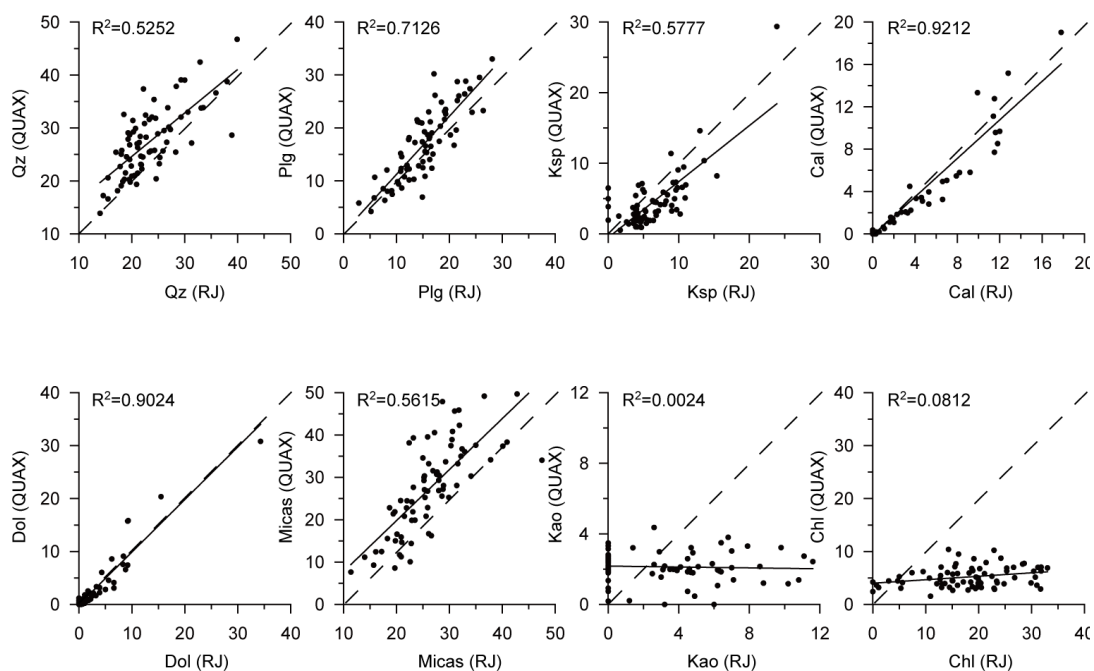


Fig 4.10 Plots showing the bivariate relationship between normalized mineral contents obtained using the RockJock and QUAX software. Note that here contents of micas include illite and smectite (see text for details). Dashed lines show the one-to-one correlation.

Similar to calcite and dolomite, the chemical composition and crystal structure of quartz does not vary much, which insures that the peak position does not move much and the XRD pattern of the quartz in the sample is quite similar to the reference mineral pattern. The degree of preferred orientation is also not as much as the clay minerals. However, the correlation of quartz is not as good as calcite and dolomite (Fig 4.10). The major peak of quartz (3.34 Å) may also belong to other minerals such as illite (Moore and Reynolds Jr, 1997; Stein et al., 2010b). When the content of one mineral is underestimated, the other one may be overestimated. In RockJock, quartz contents sometimes are underestimated as the calculated quartz peaks are often lower than the measured ones (Fig 4.12). In RockJock, to get the best results, the degree of fit should be the minimum (see details in Chapter 3). If the calculated quartz peaks are fit to the measured ones, the degree of fit might not be the minimum. Therefore, it's not possible to calibrate the quartz contents. This can also be explained by the closed sum issue (Aitchison, 1986) as the XRD results are normalized to 100%. Quartz and illite are the most abundant non-clay mineral and clay mineral respectively. Therefore, the closed sum issue might be more prominent than other minerals. It can be seen

clearly in Fig 4.8 that compared to QUAX, quartz contents are underestimated in RockJock, and the case of micas (mainly illite) is just the opposite. This can also be seen in the RockJock and QUAX comparison in Andrews and Vogt (2014b). Similar to this study, quartz contents are also underestimated in RockJock compared to QUAX (Fig 4.13). However, quartz contents are not always underestimated in RockJock. As can be seen in the artificial mixtures, quartz contents are often overestimated compared to the true abundances (Table 4.1, Fig 4.2 and 4.3). It seems that the calculation of quartz depends greatly on the mineral composition of the sample and the identification of minerals that are present in the sample. Therefore, the interpretation of quartz should be with caution.

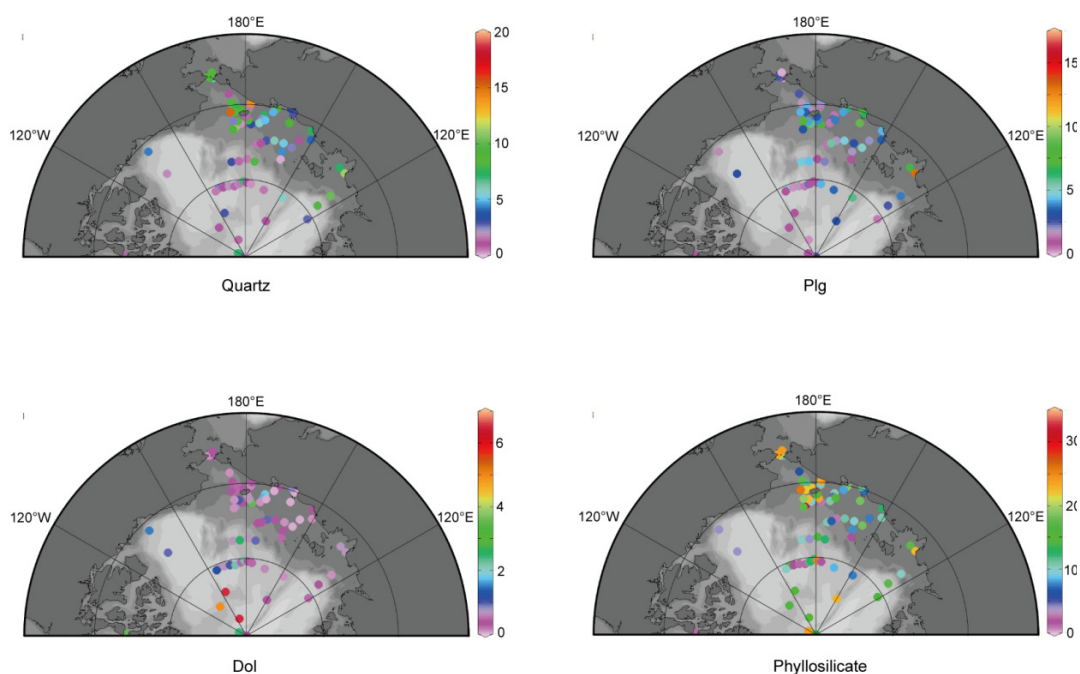


Fig 4.11 Geographical distribution of the differences between RockJock and QUAX results.

Similar to quartz, the correlations of k-feldspar, plagioclase and micas are also not as good as calcite and dolomite (Fig 4.10). But the reasons for that may not be the same as quartz. The most prominent characteristic of these minerals is that they are all groups of minerals with complicated chemical compositions. As the reference minerals in RockJock and QUAX are not the same, they are grouped together for comparison. Especially the micas group, it includes mineral groups of illite, smectite, and mix-layer minerals, as well as biotite and muscovite. The cumulative errors are

perhaps large. The differences of reference minerals in between RockJock and QUAX make the errors even larger (see Chapter 3). Similar intermediate correlation can also be seen in Andrews and Vogt (2014b) (Fig 4.13).

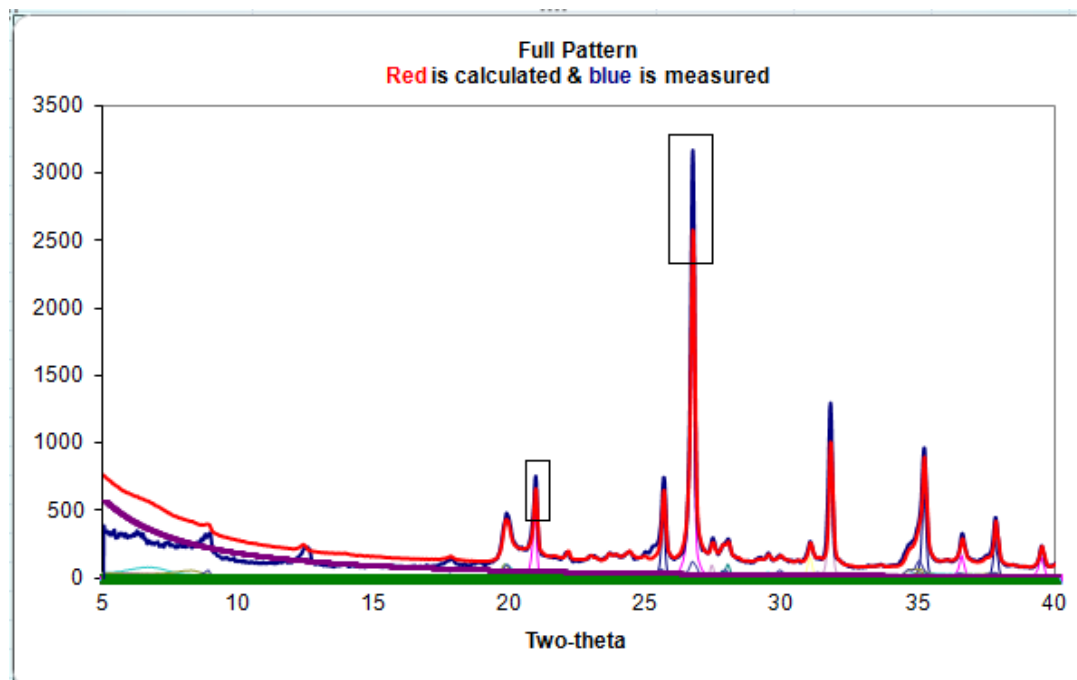


Fig 4.12 A Plot from the Full Pattern sheet of the RockJock11 program showing the measured (blue) and calculated (red) XRD pattern. The underestimations of quartz are marked with the rectangles.

Kaolinite and chlorite show no correlations at all in this study (Fig 4.10). This has also been recorded in the study of Andrews and Vogt (2014b) (Fig 4.13). It has already been shown in previous sub-chapter that RockJock can sometimes determine kaolinite and chlorite accurately (Table 4.1 and Fig 4.2). Villaseñor and Jaeger (2014) also showed that the accuracy for chlorite can be relatively good (6%). This might imply that the determination of kaolinite and chlorite depends greatly on the reference minerals. When the chemical compositions and structures of the reference minerals are similar to the minerals present in the samples, high accuracy can be obtained. In the eleven-phase mixtures, the absence of nontronite in the reference minerals may be the cause of the low accuracy for all the minerals. This may indicate that the selection of possibly present minerals when running RockJock is quite important for the result.

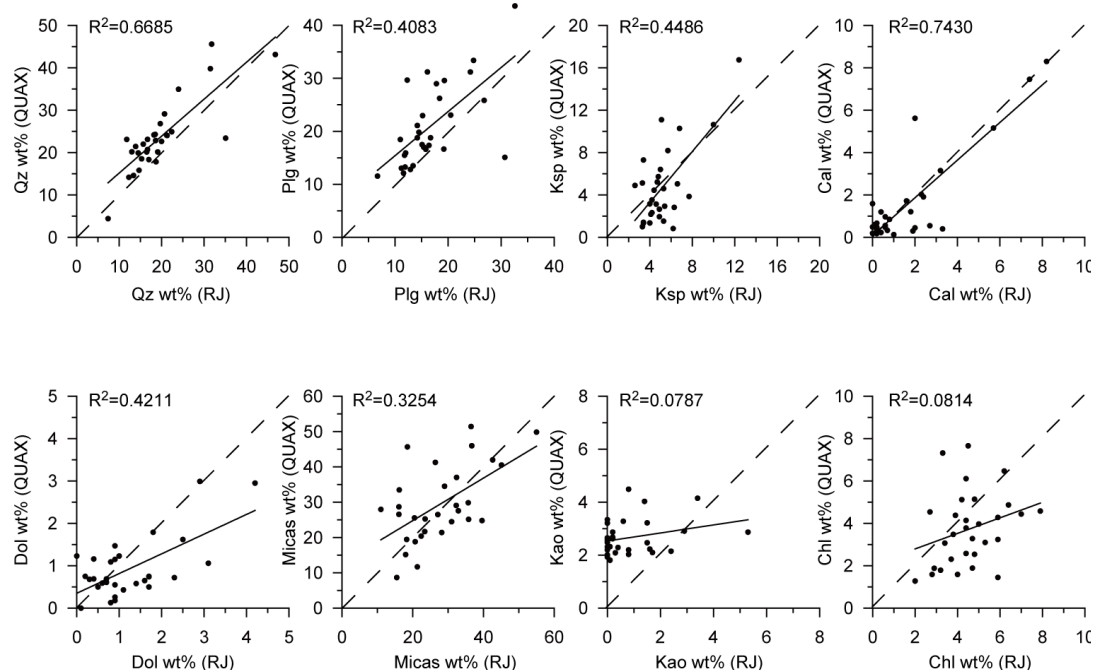


Fig 4.13 Comparison between RockJock and QUAX (data are extracted from Andrews and Vogt (2014a)). The solid line is the linear regression line and the dashed line is the one-to-to correlation line.

4.7 Useful tips for the usage of RockJock

RockJock is coded into Microsoft Excel and can be easily used on any computer on which Excel is installed. The installation and the use of it, however, can be tricky. During this study, a lot of time was spent on how to run it properly. There is already a very detailed user's guide (Eberl, 2003) that one should read carefully before starting working with RockJock. In addition to that, some additional tips that might be helpful for new users are listed below.

The most important point is to install the program carefully following the instruction (Eberl, 2003), but this will only guarantee a good start. After newly installed it, there are 8 XRD patterns for artificial mixtures stored in the *Synthetic mixtures* sheet, which we should run to test if the installation is right. And these patterns are also important to test if RockJock runs properly later, as will be mentioned below.

During this study, it is found out that if RockJock is run on different computers, different results might be expected, even if the Excel versions and all the settings are the same. The reason for that remains unknown, but it is important to run it on the same computer during one study. Note that sometimes different computer systems have different digits which may cause problems during the calculating.

After running RockJock for some time, the results might be very tricky. For example, different runs of the same sample might get different results. In this situation, it's better to run the 8 stored artificial mixtures and see if the results are good. If not, one should delete the current program and reinstall it.

Sometimes the background correction becomes very strange. In this study, the background value is sometimes minus or the background curve is far away from the base of the pattern towards the high angle. When this happens, it may be not easy to find out only by looking at the result. So always check the background line and column GH for the background values in the *Full pattern* sheet.

When running RockJock, do not open another Excel file because it simply cannot work. And better to run RockJock on a separate computer, because it may have some influence on the program when copy and paste things during running. When copying and pasting during the running, the data that is run in RockJock will sometimes be pasted out instead of what has been copying.

RockJock can be applied successfully to quantitative mineral analysis. It was ranked 3rd in the first Reynolds Cup competition (McCarty, 2002), which is an international quantitative analysis competition using complex artificial mineral mixtures. It has also won the third and the second places in the fourth and fifth Reynolds Cup respectively. But much laboratory efforts like separation of grain size fraction, X-ray fluorescence (XRF) and FTIR, extra adding of reference minerals should be done to accurately identify the mineral phases. The efforts put to improve the accuracy of RockJock to

win the Reynolds Cup can be seen in
<http://www.clays.org/SOCIETY%20AWARDS/5thRCresults.html>.

Chapter 5. Bulk mineral assemblages of surface sediments from the Siberian-Arctic shelf and the central Arctic

The work for this part is in close cooperation with Bazhenova (2012). In her thesis she mainly focused on the distribution patterns of dolomite, kaolinite and amphibole and their implications for the provenance study. In this thesis these researches are further extended in two aspects. Firstly the distribution patterns of other minerals (quartz, feldspars and quartz/feldspars) are shown. Then the bulk mineral assemblage patterns and their implications to the provenance study are discussed.

5.1 Different approaches for reconstruction of sediment sources

Terrigenous sediments are transported by sea ice and icebergs in the Arctic Ocean. Thus, identification of source areas of terrigenous sediments gives important information on the transporting pathways and the surface circulation patterns. As the landmasses surrounding the Arctic Ocean are composed of different geological terrains, the mineralogical and geochemical signals are distinct. Various mineralogical and geochemical proxies are used to identify source areas. Here, an overview of reconstructions of sediment sources based on clay mineralogy, heavy mineralogy, lithic and Fe oxide grains, major and minor elements, and Nd and Pb isotope are given in order to do a comparison with the provenance reconstruction based on bulk mineral assemblages in this study.

5.1.1 Clay mineralogy

The clay fraction is separated by Atterberg method and measured using XRD method. The clay minerals are grouped into illite, chlorite, kaolinite and smectite groups. Semi-quantitative calculation is made using the integrated peak areas, weighed by different empirical factors (e.g. Biscaye, 1965). In the Arctic most studies used the clay fraction of $<2\mu\text{m}$, while many Russian studies used the $<1\mu\text{m}$ fraction, which may cause difficulties in comparing the data from different studies as smectite is very sensitive to the grain-size fraction.

Illite is a common mineral in the plutonic and metamorphic rocks and is typically found in the cold region. It is the dominant clay mineral in the Arctic Ocean. Sediments from the East Siberian Sea, the eastern Laptev Sea, the north of Svalbard, the Morris Jesup Rise and along the Arctic coast of Alaska are enriched in illite (Fig 5.1a). The decrease of illite in the Kara Sea and the western Laptev Sea is caused by dilution due to high riverine input of smectite.

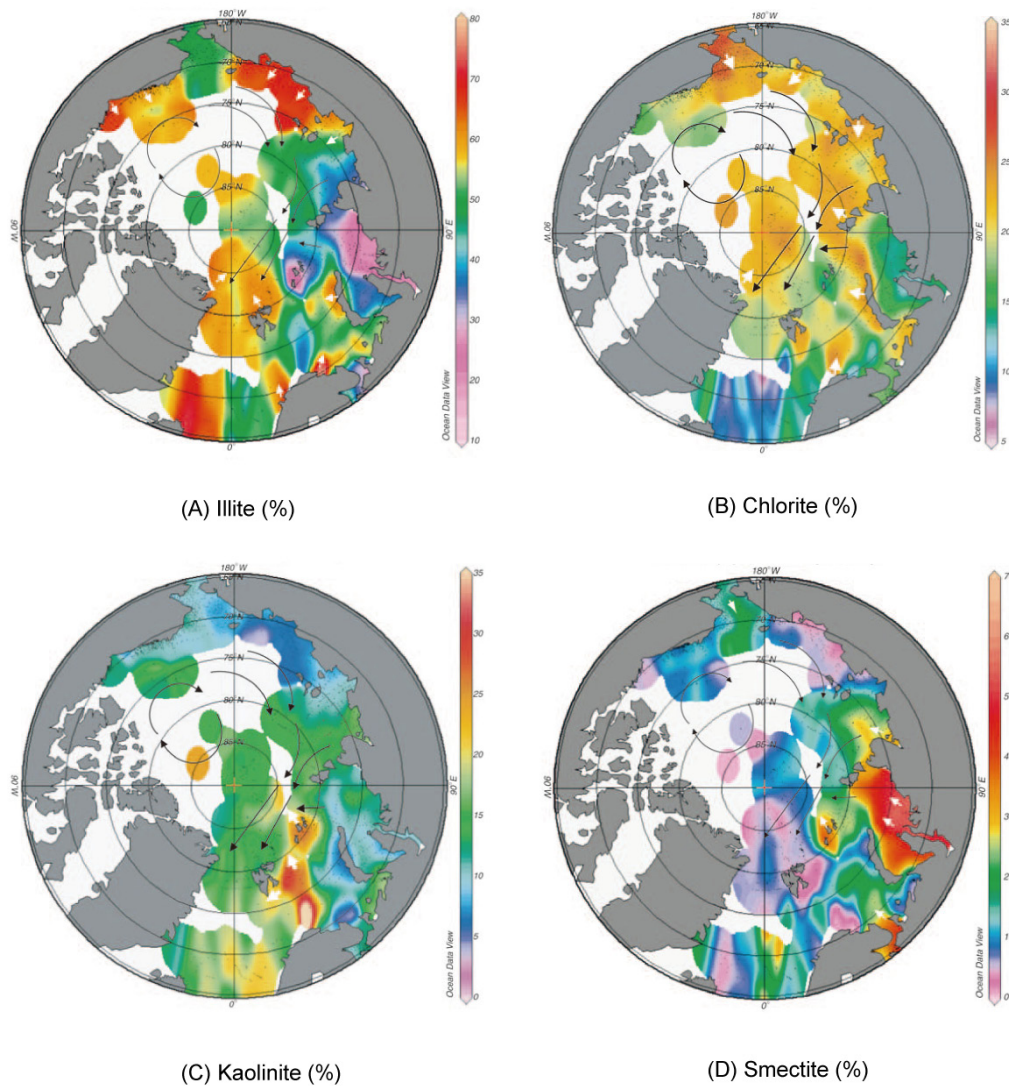


Fig 5.1 Clay-mineral distribution in Arctic Ocean surface sediments (from Stein (2008) and references therein). (A) Illite, (B) Chlorite, (C) Kaolinite, and (D) Smectite. Surface-water circulation patterns (i.e. mainly the Beaufort Gyre and the Transpolar Drift) are shown by black arrows, main input areas by white arrows.

Chlorite is the second abundant clay mineral in the Arctic Ocean. It is also a common mineral in the plutonic and metamorphic rocks. The distribution of chlorite in the Arctic Ocean is rather homogenous (Fig 5.1b). The potential source areas of chlorite in the Arctic are the Novaya Zemlya Island (Nürnberg et al., 1995), the rivers Lena and Yana (Rossak et al., 1999), along the Canadian Continental Rise and along the American coast (Clark et al., 1980). Chlorite in the Arctic Ocean surface sediment can also be possibly transported through the Bering Strait, as it is dominant in the northern Pacific (Naidu and Mowatt, 1983; Ortiz et al., 2009).

Kaolinite is a clay mineral formed under hot and humid conditions and is typically found in the tropics. In the Arctic Ocean, minor amount of kaolinite can be found. The potential source areas for kaolinite are very limited. Triassic and Jurassic rocks south of Svalbard, as well as Mesozoic rocks on Franz Josef Land, are the main source of kaolinite in the Eurasian Basin (Fig 1c, Nürnberg et al., 1995). Mesozoic and Cenozoic beds in northern Alaska and the Canadian Arctic contain high amount of kaolinite (Dalrymple and Maass, 1987; Darby, 1975; Naidu and Mowatt, 1983). Elevated amount of kaolinite is found around Ellef Ringnes Island (Darby et al., 2011).

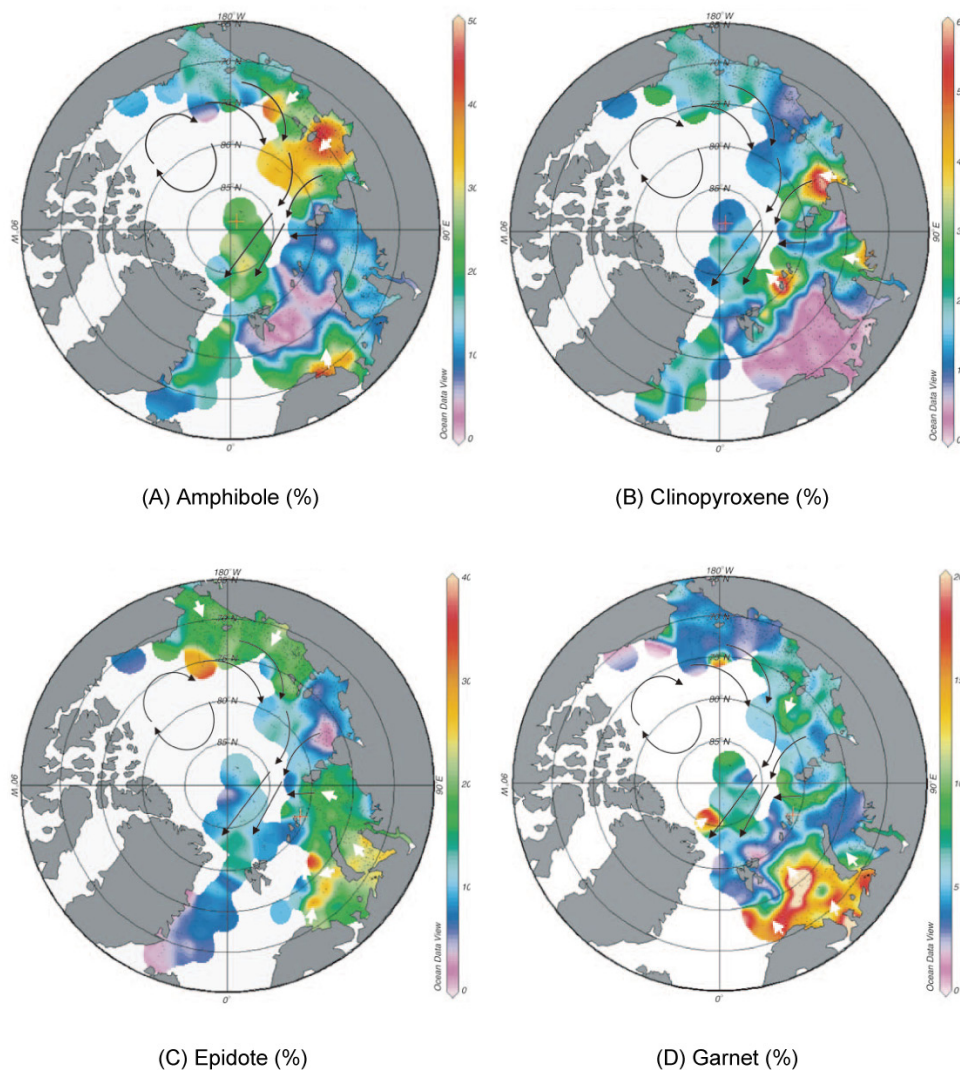
Smectite plays an important role in indicating source areas in the Arctic (Nürnberg et al., 1994; Wahsner et al., 1999). The main sources areas for smectite are the Kara Sea (from Ob and Yenisei rivers) and western Laptev Sea (from Khatanga River) (Fig 5.1d). Permian and Triassic basalts of the Putorana Plateau are the main sources (Stein et al., 2004; Vogt and Knies, 2008; Wahsner et al., 1999). Relatively high amount of smectite is also found in the Chukchi Sea (Naidu and Mowatt, 1983; Viscosi-Shirley et al., 2003a) and in some North American sites (Darby et al., 2011).

5.1.2 Heavy minerals

Heavy minerals are determined under light microscope using the fraction of 32-63 μ m and/or 63-125 μ m (references). Bulk sediment is separated to the needed fraction by

sieve and then separated into heavy minerals and light minerals using sodium metatungstate with a density of 2.83 g cm^{-3} or bromoform with a density of 2.89 g cm^{-3} . The study of Behrends (1999) shows that although different fractions are used for heavy mineral studies, the dataset are comparable. The main heavy minerals that can be used as source indicators are amphibole, clinopyroxene, epidote and garnet (Behrends et al., 1999; Lapina, 1965; Levitan et al., 1996; Naugler et al., 1974).

The main source areas for amphibole in the Arctic are the eastern Laptev Sea and the western East Siberia Sea (Fig 2a, Behrends et al., 1999; Naugler et al., 1974). Elevated amount of amphibole is also found in the southern Barents Sea. The amphibole is transported by the rivers (e.g. Lena), as the highest contents occurs in



the river mouth (Behrends et al., 1999). The amphibole originates from the sedimentary and metamorphic rocks of the Anabar massif and the Vekhyansk-Chukchee orogen (Krylov et al., 2008).

Clinopyroxene is the dominate pyroxene in the Arctic Ocean. The main source areas for clinopyroxene are the western Laptev Sea, the southeastern Kara Sea, and the area around Franz Josef Land (Fig 5.2b). The clinopyroxene originates from the Putoran Massif and is distributed to the Arctic Ocean via rivers.

High amount of epidote occurs in the eastern Barents Sea, southwestern Kara Sea, East Siberian Sea and Chukchi Sea (Fig 5.2c). The main source areas for garnet in the Arctic are the Barents Sea and north of northern Greenland (Fig 5.2d).

5.1.3 Lithic and Fe oxide grains

Darby & Bischof (1996) introduced a statistic method to determine source areas using lithic and Fe oxide grains. More than 300 samples from potential circum-Arctic source areas were taken and sieved into $>250\mu\text{m}$ and $45\text{-}250\mu\text{m}$ for lithic composition and Fe oxide grains analysis respectively. The lithic grains were studied under microscope. More than 300 types of grains were identified and grouped into 80 variables for cluster analysis. Samples that had less than 0.5 distances were grouped into one source group. Then the validity of source groups was tested by stepwise discriminant function analysis (DFA). Then the core data were matched to the source area data by DFA. Fe oxide grains were extracted from the $45\text{-}250\mu\text{m}$ fraction and nine different Fe minerals (fresh ilmenite, altered ilmenite, magnetite, magnetite with other phases, haematite, ferric-ilmenite, titano-haematite, titanomagnetite, and

Fig 5.2 Heavy-mineral distribution in Arctic Ocean surface sediments (from Stein (2008) and references therein). (A) amphibole, (B) clinopyroxene, (C) epidote, and (D) garnet. Surface-water circulation patterns (i.e., mainly the Beaufort Gyre and the Transpolar Drift) are shown by black arrows, main input areas by white arrows.

chromite) were identified. Twelve elements (TiO_2 , FeO , MnO , MgO , SiO_2 , Al_2O_3 , Cr_2O_3 , V_2O_3 , CaO , ZnO , Nb_2O_5 , and TaO) in each grain were analyzed using electronic microprobe. Similar statistical procedures were used to match each grain from the core sample to the source groups. Compared to other provenance proxies, this method has the advantage of being able to determine more precise source areas, as 41 potential source areas have been suggested (Fig 5.3; Darby, 2003). Darby et al. (2011) used this method to determine the sources of the sediments from dirty sea-ice samples obtained during the HOTRAX (2005) and the LOMROG (2007) expedition (Fig 5.4). The two samples from the Beaufort Sea (H1-6 and H1-7) suggest a Bering Strait source. Samples from the central Arctic mostly match to the sources of the northern Canadian Islands (Banks Island and/or Ellesmere Island), while H3-9 indicates a single source match to the Russian side (Yenisey River) and H3-5 and L4 indicates a secondary match to the Yenisey River.

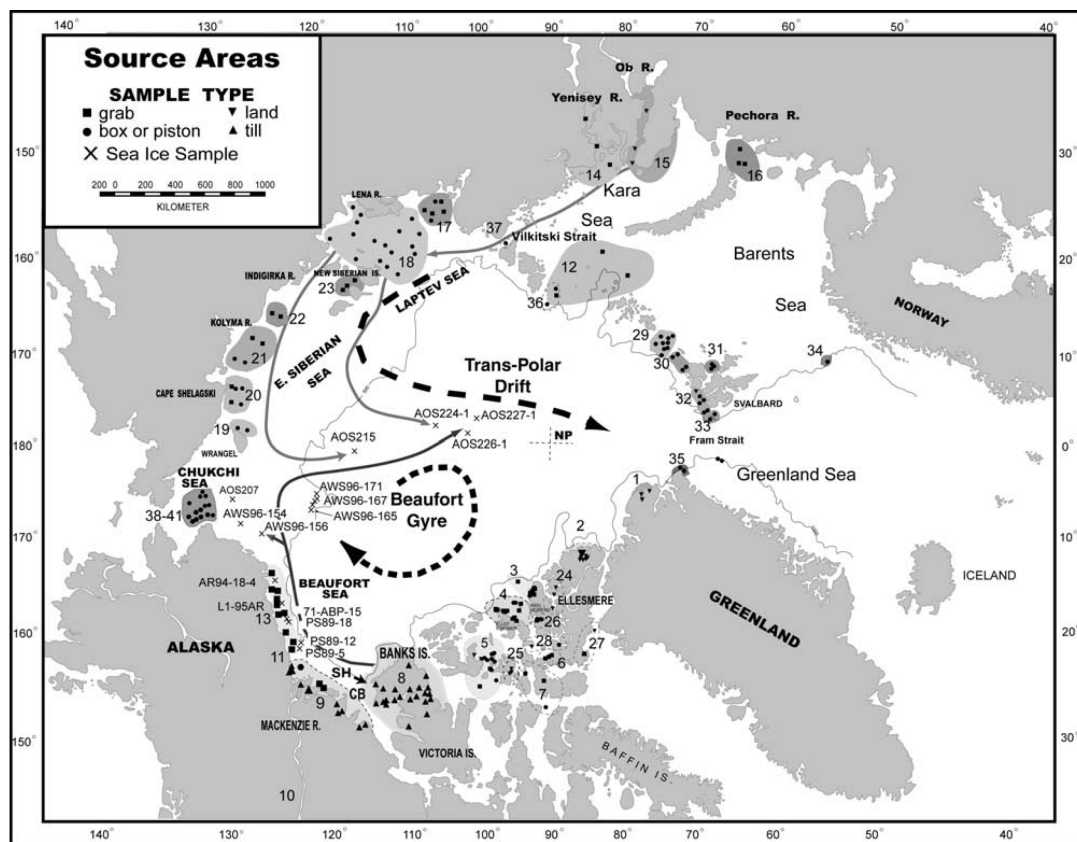


Fig 5.3 The 41 potential circum-Arctic source areas identified using Fe grains fingerprint (From Darby, 2003).

This method was later widely used and further developed by Darby and co-worker (Bischof and Darby, 1997; Darby, 2003; Darby and Bischof, 2004; Darby et al., 2002; Darby et al., 2011) in studying sediment sources. An improvement was made with less time and less error of misidentification by Darby et al (2015). The old method uses DFA to match Fe grains to the potential sources. This requires the source samples be grouped by composition by cluster analysis and repeated test and refinement using DFA to test the uniqueness of each grouping. The new method matches each element in each Fe grain to the same element of every grain of the same mineral in the entire source area database. The average standard deviation for each element of the source grain on replicate analyses was calculated and summed up. The difference between each of the 14 elements in the source grain and the grain to be matched was also calculated and summed up. Only when the latter value is less than the former one, the match is done. The new method is proved to have similar results as the old one, but with the advantages of less time consuming and being able to proportionally match a grain to multiple source areas (for more details see Darby et al (2015)).

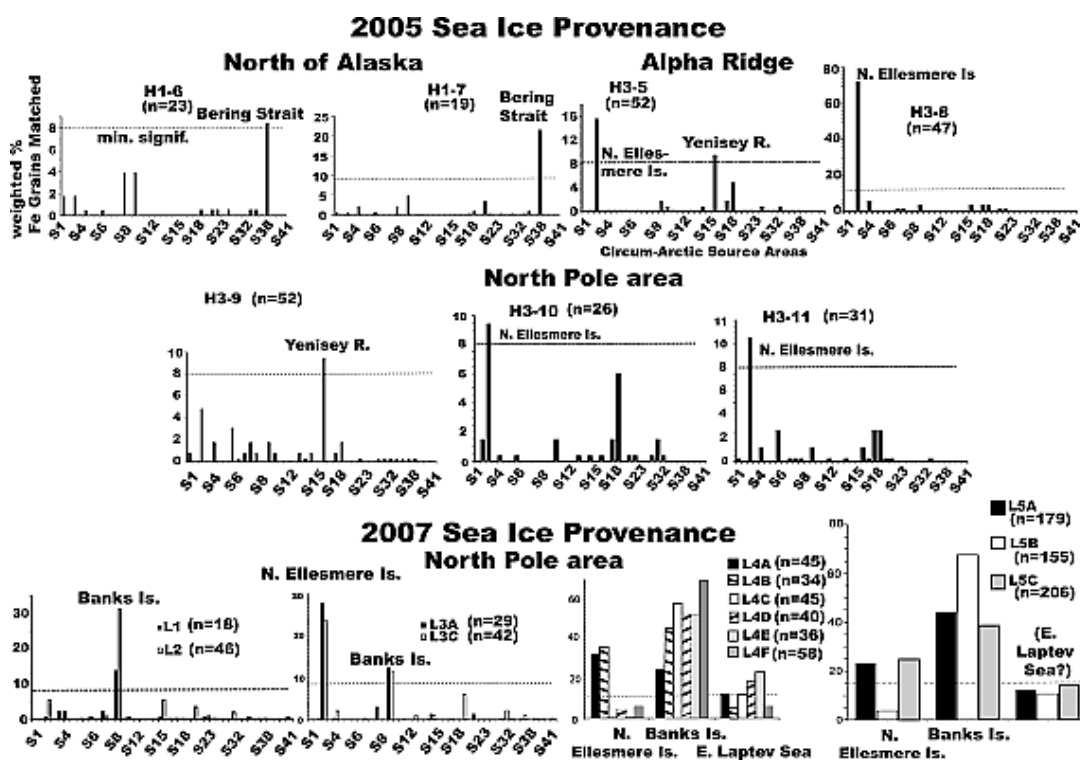


Fig 5.4 Sources for dirty ice samples based on Fe grain chemical matches to the circum-Arctic source database (from Darby et al., 2011). S1 to S41 are designated source areas (Darby, 2003). Significant sources are labeled. N is the total number of Fe grains matched to all sources in each sample. Multiple sub - samples are shown in L3, L4, and L5. All sub - samples were collected from the same floe but several meters distance from each other and as such were treated as separate samples but show essentially the same sources for each floe. Only the three sources of the six subsamples in L4 with at least one subsample above the minimum significance level are shown. The same for L5 but the E. Laptev Sea source contribution is shown because it is close to the number of matched Fe grains required for minimal significance for this source. The minimum significance level is determined from tests discussed previously (Darby, 2003) and essentially these are 8-10% of the total grains matched for any particular sample; thus this minimum can vary slightly with the total number of grains matched but is generally between 8 and 15 weighted percent, only exceeding 10 weighted percent for grain numbers above 100 (dashed lines).

5.1.4 Major and Minor Elements

While the mineralogical proxies can be used as indicators to trace sediment sources in the Arctic, multi-element chemistry has also been proved as a useful proxy as provenance indicator (Rachold, 1999; Schoster, 2005; Schoster et al., 2000; Viscosi-Shirley et al., 2003a; Viscosi-Shirley et al., 2003b). For example, Viscosi-Shirley et al. (2003a) studied the major and minor elements (Si, Al, K, Mg, Sr, La, Ce, Nd) of 81 Siberian shelf surface sediment samples. The major element data are plotted in a Si/Al vs. Mg/K scatter plot (Fig 5.5a). Four endmembers can be identified: (1) eastern Laptev and East Siberian Seas, (2) Chukchi Sea, (3) Wrangel Island region, and (4) western Laptev Sea and New Siberian Island region. The minor element scatter plot further proves these four endmembers (Fig 5.5b and 5.5c; Viscosi-Shirley et al., 2003a). The eastern Laptev and East Siberian Seas are characterized by Low Si/Al and Mg/K ratios and high Ce concentrations. Chukchi sediments have elevated Mg/K ratios and low Ce concentrations. Compared to the western Laptev Sea and New Siberian Island region, sediments from the Wrangel Island region has relatively high Si/Al and low Sr value. The study further shows that these four endmembers are likely to be derived from four source rocks: shale, basalt, mature sandstone and immature sandstone.

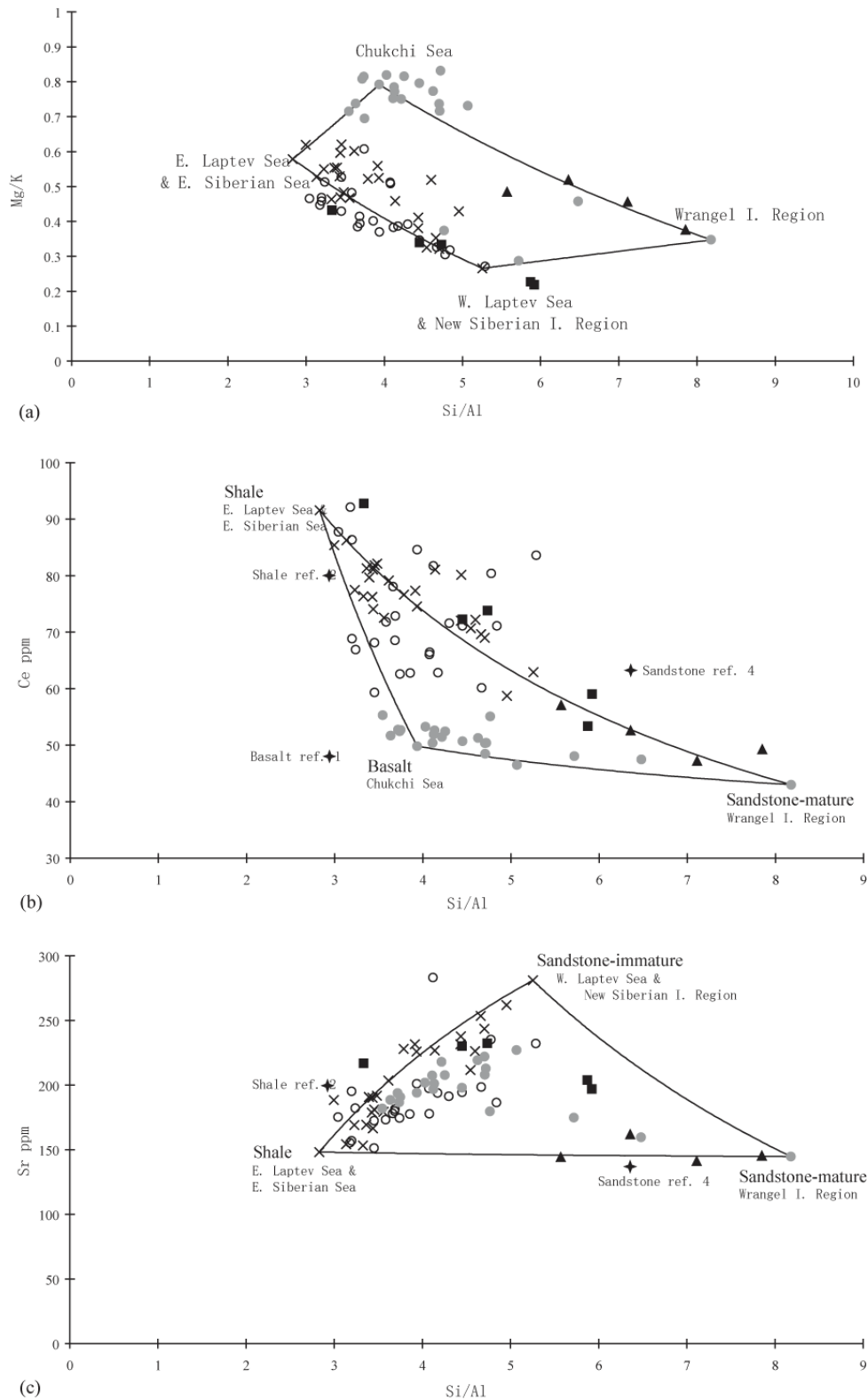


Fig 5.5 Siberian-shelf surface-sediment (a) major element data plotted as Si/Al vs. Mg/K (b) Si/Al ratios vs. Ce concentrations, and (c) Si/Al ratios vs. Sr concentrations (from Viscosi et al., 2003a). (Chukchi Sea, filled circles; East Siberian Sea, open circles; Laptev Sea, crosses; Wrangel Isl. region, triangles; New Siberian Isl. region, squares).

5.1.5 Nd and Pb isotope

Although mineralogical proxies are widely used to study the sediment provenances in the Arctic, sedimentary isotopes can be used to better constrain it (Fagel et al., 2014). Neodymium (Nd) and lead (Pb) isotopes have been used as tracers for provenance (Asahara et al., 2012; Fagel et al., 2014; Haley et al., 2008; Haley and Polyak, 2013; Jang et al., 2013; Tütken et al., 2002). For example, Fagel (2014) used Nd and Pb isotope signatures together with mineral assemblage and trace element content of sediment record from Northwind Ridge in the Arctic Ocean to identify sediment provenance. Trace element and isotope composition are measured on the $<20\mu\text{m}$ fraction in order to minimize the effect of winnowing. But the use of fine fraction will underestimate the contribution of glacial materials as well as the flux of coarse materials such as IRD and overestimate the sedimentary pulse signature such as meltwater events (Fagel et al., 2014). Therefore interpreting these data should be with caution. In a $^{207}\text{Pb}/^{206}\text{Pb}$ vs. $^{208}\text{Pb}/^{206}\text{Pb}$ diagram (Fig 5.6a), data points show a linear trend suggesting the potential two end members of Mackenzie and Lena SPM, which is consistent with mineralogical evidences. In a ϵNd vs. $^{207}\text{Pb}/^{206}\text{Pb}$ diagram (Fig 5.6b), the data points show less negative ϵNd values than the Mackenzie and Lena SPM, indicating the presence of a new end member. Combining the trace elements data (REE spidergram) and mineralogical data (amphibole and smectite), other potential sources (e.g. the Siberian traps, Eolian supply from the Kamchatka and the Aleutian Arc) can be excluded, leaving the Okhotsh-Chukotka the most possible candidate. After the three end-members are identified, the source strength can be estimated based on the mean $[\text{Nd}]$, $[\text{Pb}]$, ϵNd and $^{207}\text{Pb}/^{206}\text{Pb}$ ratios of the three end-members (Fig 5.6c).

5.2 The distribution of surface minerals: Results from bulk mineral assemblages

Bulk mineral assemblages are a mineralogical proxy that can be used as provenance indicator in the Arctic (Andrews and Vogt, 2014b; Darby et al., 2011; Eberl, 2004;

Nørgaard-Pedersen et al., 2007; Ortiz et al., 2009; Vogt, 1997; Vogt et al., 2001). Bulk mineral assemblages are determined by quantitative XRD technique using the ground bulk sediment sample (Vogt, 1997) or sediment samples from specific fraction (e.g. <2mm in (Andrews and Vogt, 2014b) and <45 μ m in (Darby et al., 2011)). In this chapter, bulk mineral assemblages determined by the qXRD software packages RockJock are presented.

Fig 5.6 (a) Biplot $^{207}\text{Pb}/^{206}\text{Pb}$ versus $^{208}\text{Pb}/^{206}\text{Pb}$ measured on fine <20 μ m calcite-free sedimentary fraction of 12MC core by MC-ICP-MS. All samples define a linear trend (0.88 in silicate layers < r^2 < 0.99 in carbonate layers). (b) Biplot ϵNd versus $^{207}\text{Pb}/^{206}\text{Pb}$ ratios measured on fine <20 μ m calcite-free sedimentary fraction of 12MC core by MC-ICP-MS. (c) Ten % - increment mixing grid (plain line) used to estimate the relative contribution of the three end-members in each MC12 samples. A mixing grid taking into account the Siberian craton (data from GEOROC, 2003 database) rather than the Lena SPM is shown for comparison (dashed line) (from Fagel et al., 2014).

The surface samples used in this study were retrieved mainly from Laptev Sea, East Siberian Sea, Chukchi Sea and Central Arctic during two Polarstern expeditions and

two Russian cruises (sample locations see Fig 5.7). XRD results show that the most abundant non-clay minerals are quartz, plagioclase, K-feldspar, calcite and dolomite. Main clay minerals are illite, chlorite, kaolinite, smectite and muscovite. Because sometimes illite is difficult to distinguish from smectite in RockJock (Eberl, 2003) and it is found that, during the calculation, muscovite is also difficult to distinguish from illite, they are added together and names as micas. Some accessory minerals, such as amphiboles, pyroxenes, garnet, epidote, rutile and magnetite, can also be observed. However, the amounts of them are usually below the detection limit (<2%) and cannot be quantified. The distributions of major non-clay minerals and clay minerals are shown in Fig 5.8.

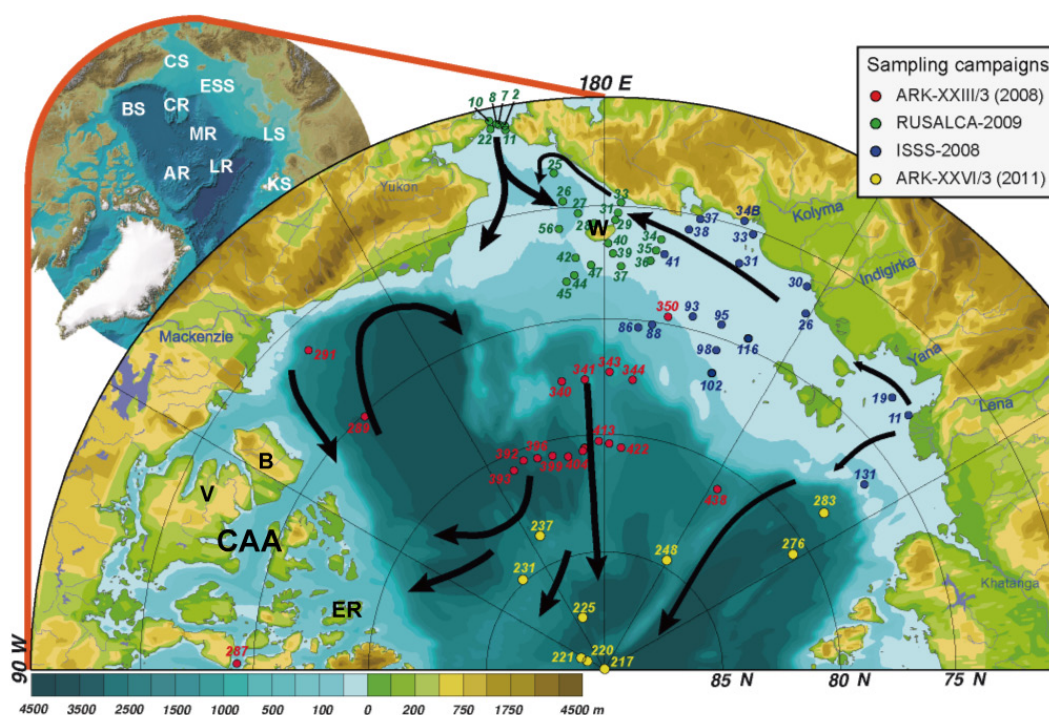


Fig 5.7 Locations of surfaces samples from the Arctic Ocean marked according to the different cruises specified in the legend. Black arrows mark the directions of major surface current systems: BG – Beaufort Gyre, TD – Transpolar Drift, ACC – Arctic Coastal Current (for details see text). Bathymetry and the circum-polar inlay map are from IBCAO (Jakobsson et al., 2008). CS – Chukchi Sea, ESS – East Siberian Sea, LS – Laptev Sea, KS – Kara Sea, BS – Beaufort Sea, CR – Chukchi Rise, MR – Mendeleev Ridge, AR – Alpha Ridge, LR – Lomonosov Ridge, B – Banks Island, V – Victoria Island, ER – Ellef Ringnes Island, W – Wangel Island, CAA – Canadian Arctic Archipelago. (Modified from Bazhenova 2012)

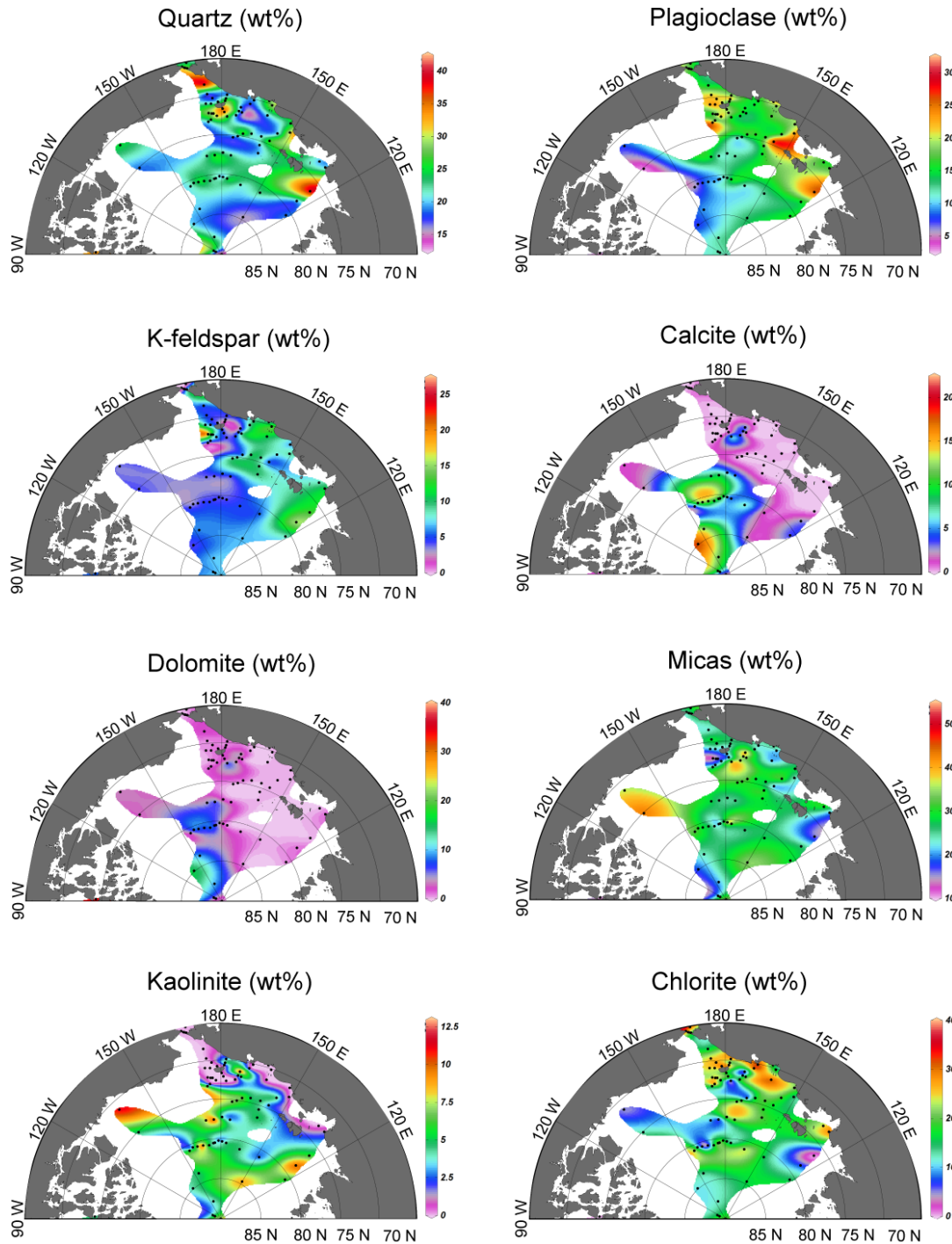


Fig 5.8 Bulk minerals distribution map in the Arctic Ocean surface sediments.

Quartz concentrations range from 14% near the North Pole, to 39.9% in the Bering Strait. The highest concentrations occur in the Chukchi Sea, around the Wrangel Island, in the Laptev Sea and it decreases to intermediate values towards the Mendeleev Ridge and further decreases to lowest values towards the North Pole.

Feldspar is the second most abundant non-clay minerals, among which plagioclase is the dominant group. Plagioclase percentages vary between 2.9% and 28.1%. It shows a clear pattern of decreasing from the East Siberian Shelf seas to the Eurasian Basin and further to the Amerasian Basin. K-feldspar values are relatively low (0-23.9%) and show no significant differences in the Central Arctic (mostly below 5%). The highest values occur in the Chukchi Sea, northwest of the Wrangel Island.

The highest dolomite contents of 34.3% are measured at the Canadian Arctic Archipelago station (PS72/287-1). High amount of dolomite (3%-15.5%) only appears in the Amerasian Basin and northeast of the Wrangel Island in the East Siberian Sea. Dolomite contents in all other samples are below 3%. Calcite values range from 0 to 17.8%, with highest values on the Alpha Ridge and the northern Mendeleev Ridge. In the Eurasian Basin and the East Siberian Shelf seas, calcite contents are mostly below 5%.

Micas with percentages from 11.4% to 47.5% are the most abundant clay minerals. The higher values occur in the Beaufort Sea and the eastern East Siberian Sea. Chlorite concentrations vary between 0 to 33%, with higher values in coastal areas and in the Bering Strait. Kaolinite shows a somewhat opposite distribution pattern as Chlorite, with the lower values in coastal areas and in the Bering Strait.

5.3 Bulk mineral assemblages as provenance indicator

Bulk mineral assemblages data can be obtained by microscopic analysis (Bischof, 2000; Bischof et al., 1996; Nørgaard-Pedersen et al., 2003; Nørgaard-Pedersen et al., 1998; Phillips and Grantz, 2001) or by X-ray diffraction analysis (Darby et al., 2011; Nørgaard-Pedersen et al., 2007; Ortiz et al., 2009; Vogt, 1997; Vogt et al., 2001). Vogt (1997) did a very comprehensive X-ray diffraction study on sediments taken from the Eurasian Basin and the adjacent slopes of Barents, Kara and Laptev Seas. Darby (2011) has expanded the X-ray diffraction analysis to many circum-Arctic source area samples in order to study the source of the dirty ice samples. However, the data

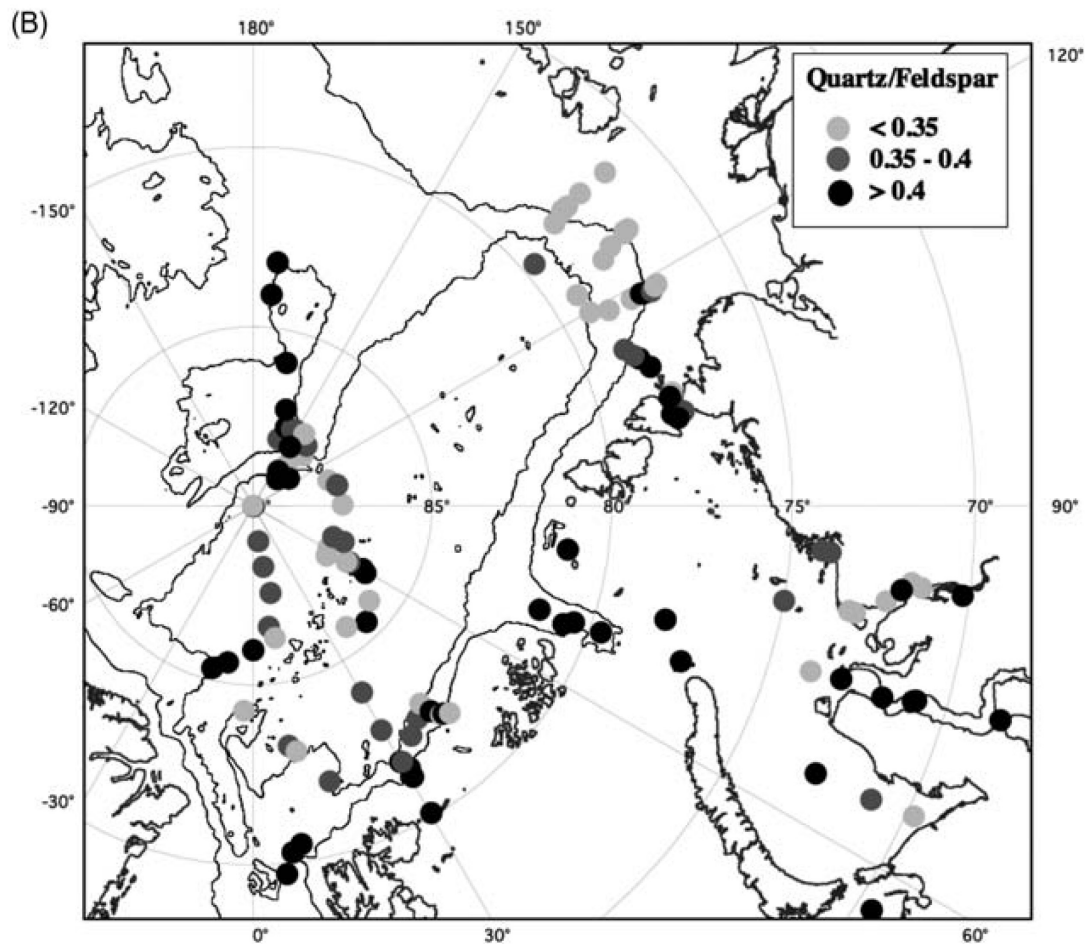
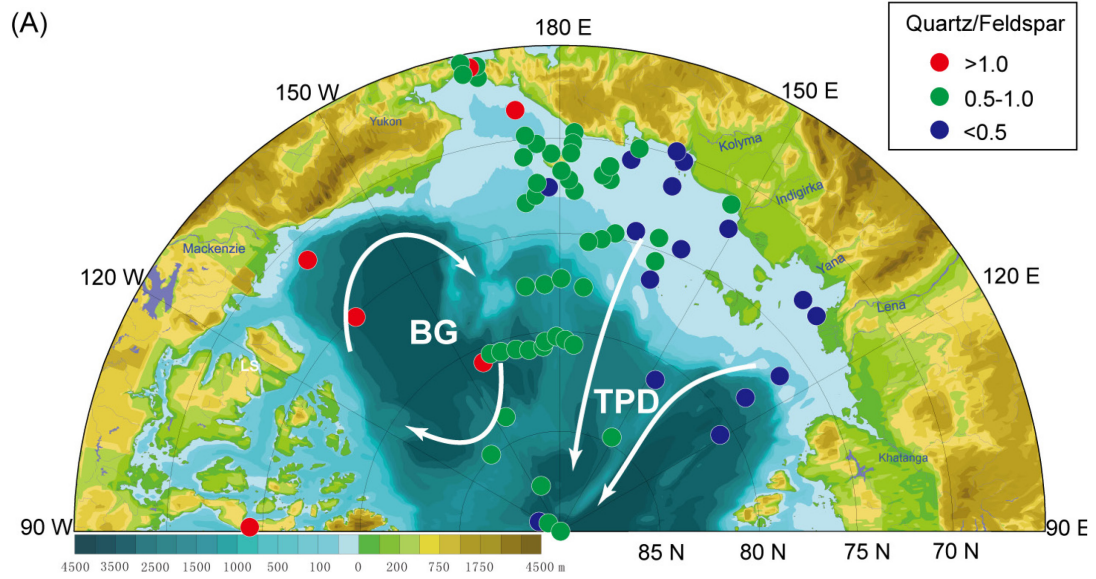
obtained by X-ray diffraction analysis of Arctic Ocean sediments are still limited. In this study, we supplemented the bulk mineral XRD study with surface sediments mainly taken from the East Siberian Sea, the Chukchi Sea and the Central Arctic Ocean.

5.3.1 Bulk minerals distribution patterns

Bedrocks that can produce abundant quartz are probably sandstones, quartzite, or conglomerates from the western Queen Elizabeth Islands, the northeastern District of Mackenzie and the northern Banks Island (Bischof et al., 1996) in the Canadian Arctic. In the Eurasian shelf seas, high amounts of quartz can be found on the outer Barents Sea shelf and near the Severnaya Zemlya in the Western Laptev Sea (Vogt, 1996, 1997). It was found that quartz shows a decreasing trend from the shelf to the basin on the Laptev Sea slope (Vogt, 1997), which agrees with our result.

Quartz is ubiquitous in the Arctic and therefore it is not qualified for provenance indicator. But when combining with feldspar, it may give important information on source areas and transport pathways (e.g. Moros et al., 2004; Ruddiman and Bowles, 1976; Vogt, 1997; Vogt et al., 2001). It was shown by Bischof (1996) that the western Arctic Ocean IRD is characterized by more quartz than feldspar, which is high Qz/Fsp (quartz to feldspar ratio). This can be further supported by Darby (2011) (Fig 5.9C). The high Qz/Fsp in the samples from the Canadian Archipelago and the Beaufort Sea in this study also agrees with it (Fig 5.9A). In the Eurasian shelf seas, the Qz/Fsp is quite low (0.3-0.5) in the Laptev Sea and the Barents Sea slope while sediments in the Kara Sea have relatively high Qz/Fsp (0.4-2) (Fig 5.9B). The data from this study indicate that sediments from the Laptev Sea and the East Siberian Sea have low Qz/Fsp, except for the samples adjacent to the Wrangle Island (Fig 5.9A). If recalculate the Qz/Fsp value using peak intensity ratio and plot it with the data from Vogt (1997) in the Ksp/Plg versus Qz/Fsp diagram (Fig 5.10), it can be seen that sediments from Laptev Sea can be distinguished clearly with sediments from the Canadian Archipelago, the Chukchi Sea and the Kara Sea by much lower Qz/Fsp

values.



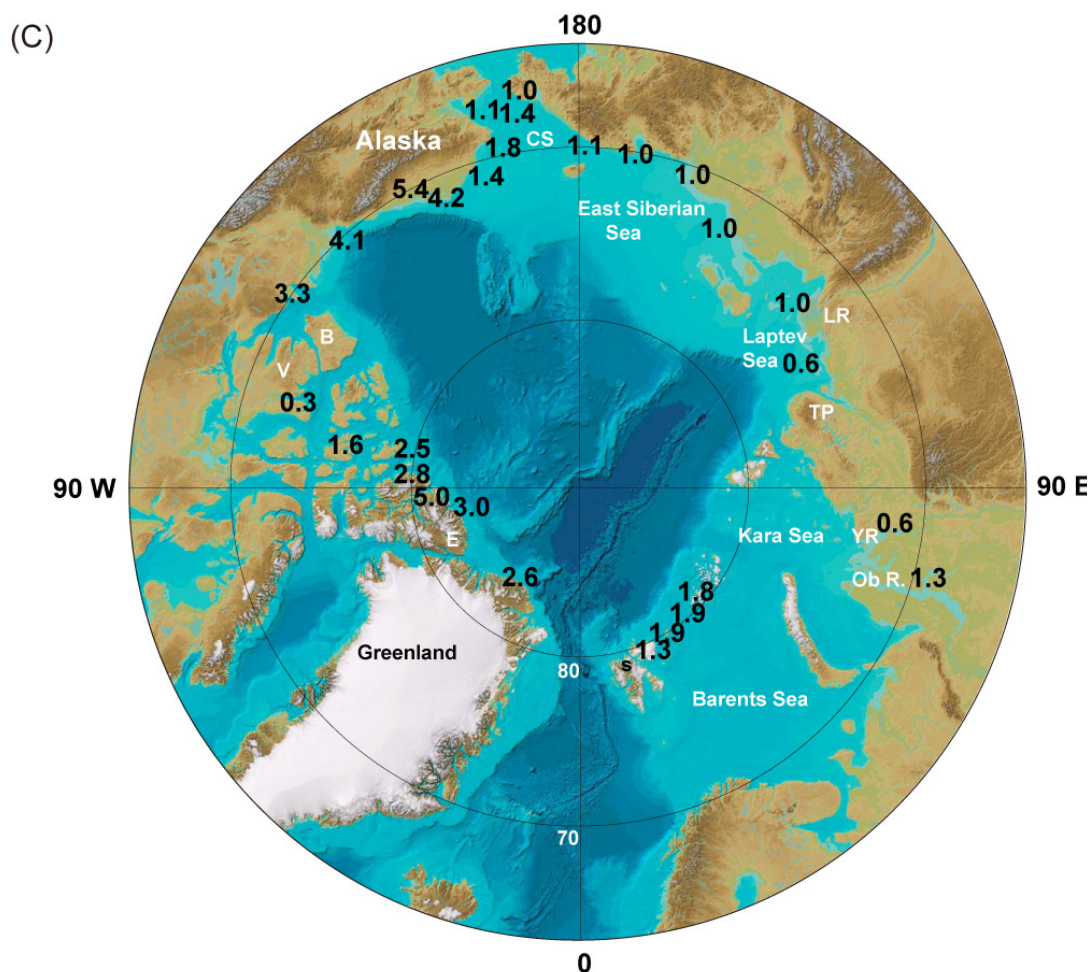


Fig 5.9 Distribution of Quartz/Feldspar in the surface sediments from Arctic Ocean and circum-Arctic source areas. (A) Contents ratio of Quartz/Feldspar from XRD bulk mineralogy results of surface sediments in the Arctic Ocean using RockJock in this study. (B) Peak ratio of Quartz/Feldspar of surface sediments from the Kara Sea, Laptev Sea continental margin and central Arctic Ocean (Vogt, 1997). (C) Contents ratio of Quartz/Feldspar from XRD mineralogy of the $<45\mu\text{m}$ size fraction from potential circum-Arctic source areas (calculated from Darby, 2011). E = Ellesmere Island, V = Victoria Island, B = Banks Island, CS = Chukchi Sea, LR = Lena River, TP = Taymyr Peninsula, YR = Yenisey River, and S = Svalbard.

Dolomite was found to be a common mineral in the Western Arctic and interpreted as an indicator for sediment input from the Canadian Archipelago (Bischof et al., 1996; Darby et al., 1989; Phillips and Grantz, 2001; Stein et al., 2010a; Vogt, 1997), especially the Banks Island and the Victoria Island. The regional geology survey (Okulitch, 1991) indicates that the Paleozoic carbonate terranes are the main sources for the dolomite in the Arctic Ocean. Results from this study also show dolomite enrichment in the samples from the Canadian Archipelago and the Alpha-Mendeleev

Ridge. Slightly high amount of dolomite appears around the Wrangel Island, which is likely transported by sea ice from the Beaufort Sea. It could also be from the Wrangel Island, due to the thick Paleozoic carbonate rocks on it (Kos'ko et al., 1990).

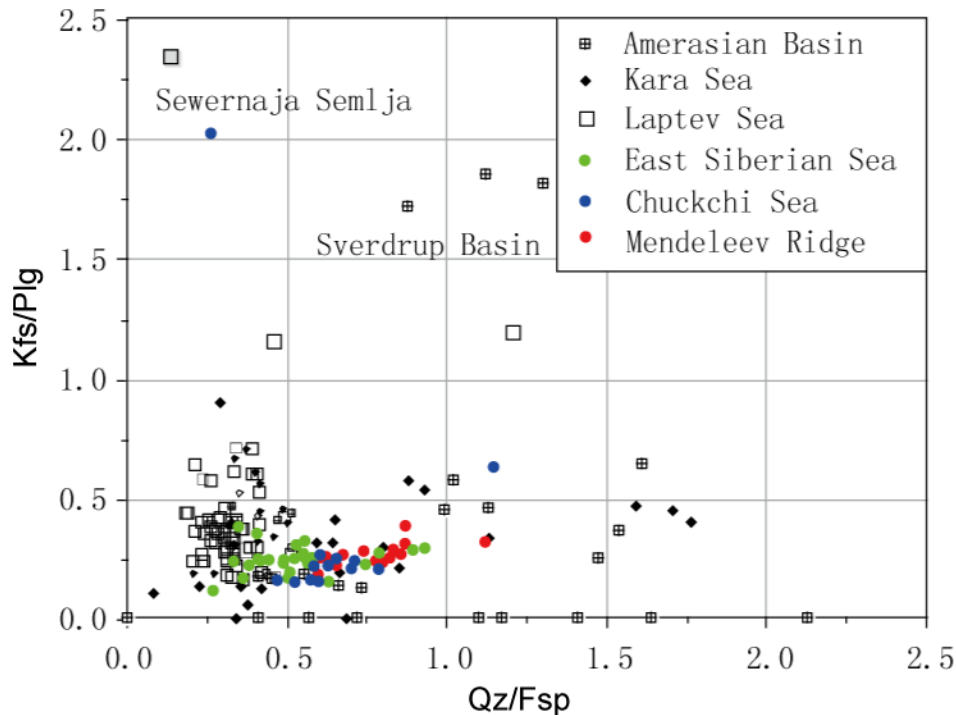


Fig 5.10 Kalifeldspar/plagioclase (Kfs/Plg) versus quartz/feldspar (Qz/Fsp) diagram in the Siberian Shelf Seas and the Central Arctic (black and white symbols are from Vogt, 1997 and color symbols are from this study).

Although the amphibole content in the bulk sample is so small that it's not possible to quantify, the occurrence of it may give important information on sediment provenance. In this study, amphibole occurs almost exclusively from the Eastern Siberian Sea and the eastern Laptev Sea (Fig 5.11). There's no amphibole in the western Arctic. This is in accordance with the heavy mineral data in previous studies (Behrends, 1999). Thus the amphibole occurrence could be an indicator of sediment from the Eastern Siberian Sea and the eastern Laptev Sea.

5.3.2 Bulk mineral assemblages

Combining the data in this study with literature data, it can be seen that the bulk mineral assemblages in different Arctic Ocean shelf seas are specific. Thus the

combination of quartz, Qz/Fsp, dolomite and kaolinite can be used to characterize the potential source areas surrounding the Arctic. However, due to the different methods and fractions used in these studies, it is not possible to make a quantitative conclusion.

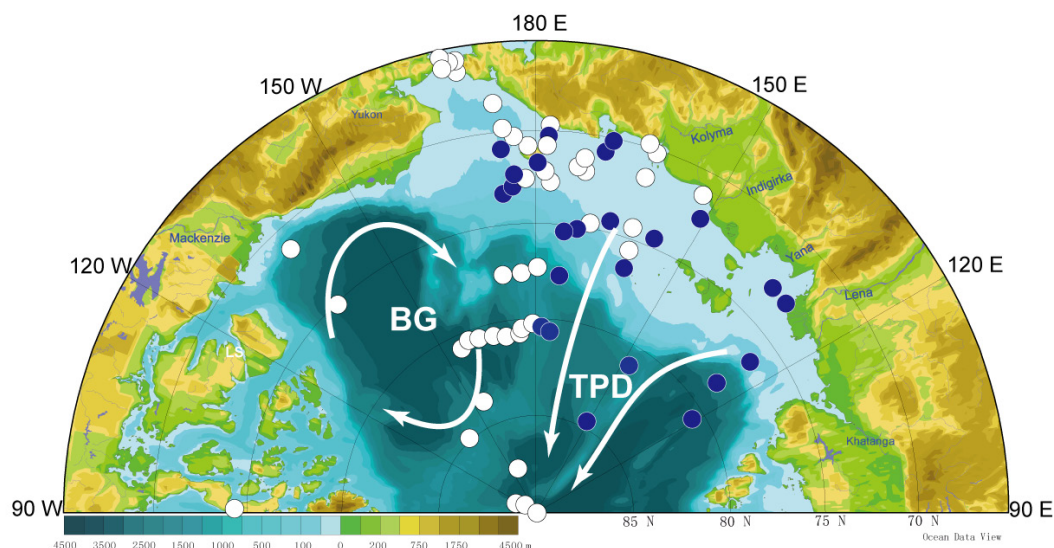


Fig 5.11 Locations of occurrences of amphibole. Blue dots represent samples in which amphibole occurs and white dots indicate samples without amphibole.

Sediment input from the Canadian Arctic is generally characterized by high dolomite and Qz/Fsp values. The Banks Island and Victoria Island are characterized by high dolomite and low Qz/Fsp values (Bischof et al., 1996; Darby et al., 2011; Phillips and Grantz, 2001; Vogt, 1997). Quartz values are very low due to dilution of dolomite. The Ellef Ringnes Island is characterized by elevated kaolinite and Qz/Fsp values and low dolomite value (Darby et al., 2011; Vogt, 1997). The Ellesmere Island is characterized by low kaolinite values and relatively low quartz, Qz/Fsp and dolomite values (Fig 5.12, Darby et al., 2011 and Vogt, 1997).

Sediment input from the Eurasian Arctic shelf seas is generally characterized by almost no dolomite, low Qz/Fsp and kaolinite values, and high quartz values. The Chukchi Sea and the Kara Sea, compared to the East Siberian Sea and the Laptev Sea, have relatively high Qz/Fsp values (Vogt, 1997). The East Siberian Sea and the Laptev Sea are also characterized by the occurrence of amphibole. The Barents Sea,

compared to other Siberian Shelf Seas, has high amount of kaolinite (Fig 5.12, Wahsner et al., 1999).

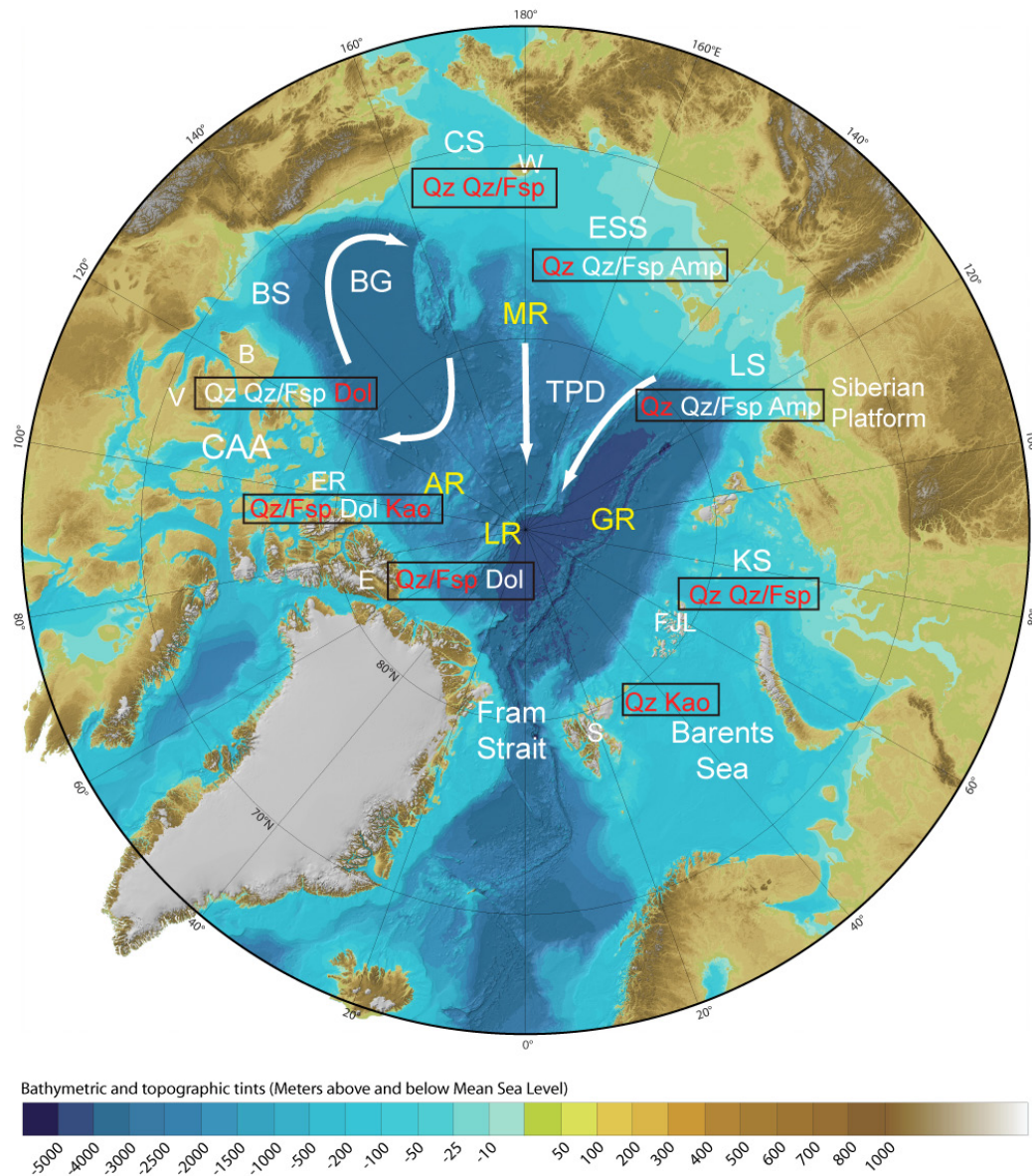


Fig 5.12 Bulk mineral assemblages in the specific areas around the Arctic. Qz – Quartz, Fsp – Feldspars, Dol – Dolomite, Kao – Kaolinite. White is for low value and red is for high value. The data from the CAA are from Darby et al. (2011). The data from the Chukchi Sea, the East Siberian Sea and the Laptev Sea are based on our research. The data from the Kara Sea and the Barents Sea are from Vogt (1997). White arrows show the two main surface circulation patterns: BG – Beaufort Gyre, TPD – Transpolar Drift. Names of shelf seas and major geographic names mentioned in the text are indicated in white colour: CS – Chukchi Sea, ESS – East Siberian Sea, LS – Laptev Sea, KS – Kara Sea, BS – Beaufort Sea, B – Banks Island, V – Victoria Island, ER – Ellef Ringnes Island, E – Ellesmere Island, W – Wangel Island, CAA – Canadian Arctic Archipelago, S – Svalbard, FJL – Frans Josef Land. Major geomorphologic features are indicated in yellow font: MR – Mendeleev Ridge, AR – Alpha Ridge, LR – Lomonosov Ridge, GR – Gakkel Ridge.

Besides dolomite, Qz/Fsp is also a good indicator for provenance in the Arctic. In general it decreases from the Canadian Arctic to the Eurasian Arctic as dolomite. But it also varies from different subdivided source regions, that is low Qz/Fsp values appear in the Victoria Island and the Ellesmere Island in the Canadian Arctic (Darby et al., 2011) and high values occur in the Chukchi Sea and the Kara Sea in the Eurasian Arctic (Vogt, 1997). However, the data from the source regions are still very limited, especially in the Canadian Arctic and more Qz/Fsp data should be investigated to prove the reliability of it being used as a source indicator. And bulk mineral assemblage is difficult to quantitatively identify source areas, and thus it should be combined with other indicators, such as clay mineralogy (Wahsner et al., 1999), heavy minerals (Behrends et al., 1999), major and minor elements (Schoster et al., 2000), and Nd and Pb isotope fingerprints (Fagel et al., 2014).

5.3.3 Comparison with other proxies

The previous clay mineral studies commonly used $<2\mu\text{m}$ fraction oriented samples and semi-quantitative XRD method to calculate the relative percentages of illite, chlorite, kaolinite and smectite. In this study, randomly oriented bulk samples and quantitative XRD method are used. It can also determine the amount of clay minerals besides non clay minerals. However, the results are difficult to compare as illite and chlorite are able to occur in the $>2\mu\text{m}$ fraction (Darby et al., 2011). Similar to the previous clay mineralogy study, in this study illite and chlorite is the most and second abundant clay minerals in the Arctic Ocean and the shelf seas. The content of kaolinite and smectite plays a minor role in the clay minerals, although they are both good provenance indicators as the potential source areas are limited (Darby et al., 2011; Krylov et al., 2014; Viscosi-Shirley et al., 2003a; Wahsner et al., 1999). However, due to the difficulty to distinguish illite from smectite in RockJock (Bazhenova, 2012; Eberl, 2003), the weight percentage of illite and smectite is added as micas when reported. Thus, illite and smectite are not qualified as good provenance indicators when using the RockJock result. The distribution of kaolinite in this study agrees with the previous clay mineralogy study (Fig 5.13). But as there are several potential

source

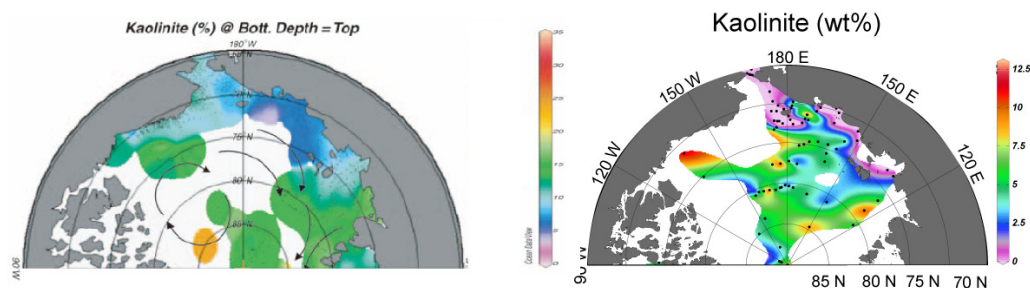


Fig 5.13 Comparison of kaolinite distribution between literature data (left, from Stein, 2008 and references therein) and our data (right).

areas for kaolinite, it is better to use kaolinite together with other proxies when tracing source areas. The distribution of chlorite in this study is similar to the previous clay mineralogy study (Fig 5.14). The maximum occurs in the Bering Sea in both figures. The contents in the East Siberian Sea are both high. And low amounts occur in the Beaufort Sea. In this study, the minimum occurs in the Laptev Sea, which is contradict to the previous study. However, it's only one data point and should not be overinterpreted.

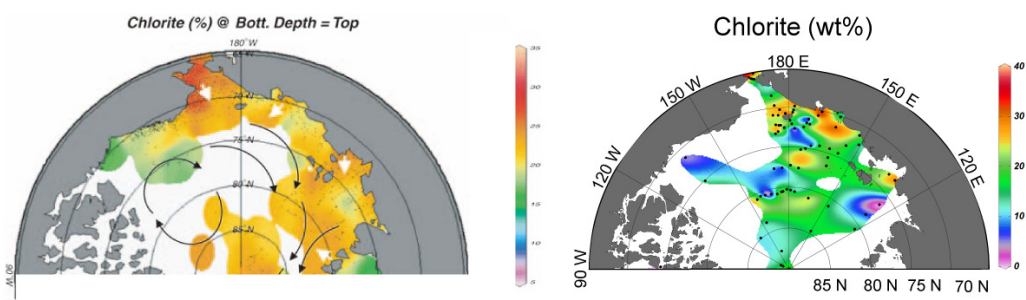


Fig 5.14 Comparison of chlorite distribution between literature data (left, from Stein, 2008 and references therein) and our data (right).

Compared to the heavy mineral studies, the contents of amphibole, clinopyroxene, epidote and garnet calculated from qXRD data in this study are very minor. They are usually beyond the detection limit and only at some locations small amount of them can be detected. Even for the few samples in which these minerals can be detected, it is difficult to quantify them because the amount is below 2%. However, the presence of these mineral can also give important information on source areas sometimes. In

this study, the samples in which amphibole can be detected are almost exclusively retrieved from the eastern Arctic (Fig 5.15), which suggests possible source areas of Siberian shelf seas. This is in accordance to the previous studies (Fig 5.15). As suggested in the previous studies that the main source areas for amphibole in the Arctic are the eastern Laptev Sea and the East Siberia Sea, the presence of amphibole can be possibly used as a provenance indicator.

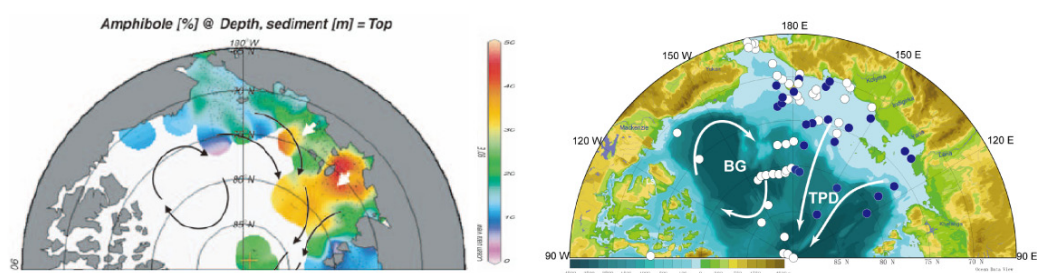


Fig 5.15 Comparison of amphibole distribution between literature data (left, from Stein, 2008 and references therein) and our data (right). In the right figure, blue dots represent locations where amphibole occurs and white dots represent locations where no amphibole occur.

Chemical fingerprint of Fe oxide grains has long been used as a proxy for determining sediment source areas (Darby, 2003; Darby and Bischof, 1996, 2004; Darby et al., 2011; Darby and Zimmerman, 2008; Myers and Darby, 2015). Compared to bulk mineral assemblages and other proxies, it has the advantage of being able to precisely trace the Fe grains to 41 potential circum-Arctic source areas and calculate the proportion of each source (e.g. Darby, 2003). Due to the lack of studies on surface sediments using Fe oxide fingerprint, the direct comparison between it and our bulk mineral assemblages data cannot be made. Wassmuth (2014) has compared the two proxies in tracing the variations in source areas. Piston core P1-92-AR-P1 (P1 for short) and its companion box core P1-92-AR-B3 (B3 for short) studied by Darby and Bischof (2004) are located close to core ARA2B-1B (1B for short) in the study of Wassmuth (2014) (Fig 5.16). Canada, East Siberia, Laptev Sea, Kara Sea or Canadian Archipelago, and Pacific are identified as the potential source areas using bulk mineral assemblages data for the time interval 5.6-0 ka (Table 5.1). Although the

resolution of the Fe grains is higher between 370 and 1300 years than the bulk mineral data, the correlation/anticorrelation between dolomite and amphibole (Fig 5.17) shows similar variability of changing source areas showed by Darby and Bischof (2004; Fig 5.18). Bulk mineral assemblages data fail to identify Laptev Sea as source areas, while the Fe grains do (Wassmuth, 2014).

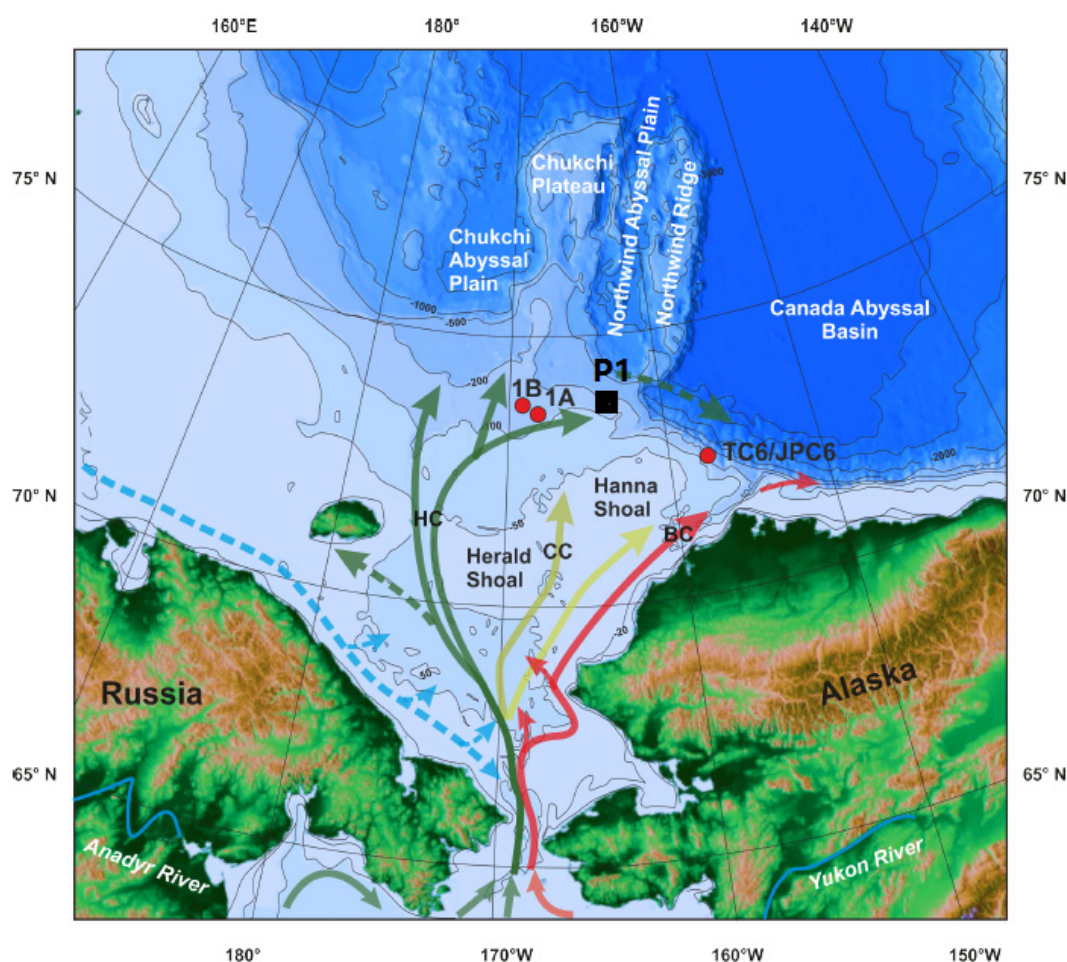


Fig 5.16 Core locations of ARA2B-1B (1B) and ARA2B-1A (1A) (Wassmuth, 2014), as well as core P1-92-AR-P1 (P1) studied by Darby and Bischof (2004). The figure is modified from Wassmuth (2014).

Viscosi et al. (2003a) identified five regions on the Siberian Shelf using multi-element chemistry and clay mineralogy. (1) The shale endmember in the Eastern Siberian Sea and eastern Laptev Sea. (2) The Basalt endmember in the Chuckchi Sea. (3) The mature sandstone endmember near the Wrangle Island and the Chukchi Sea's Siberian coast. (4) The immature endmember in the New Siberian Island region. (5) The

immature sandstone endmember in the western Laptev Sea. The bulk mineral

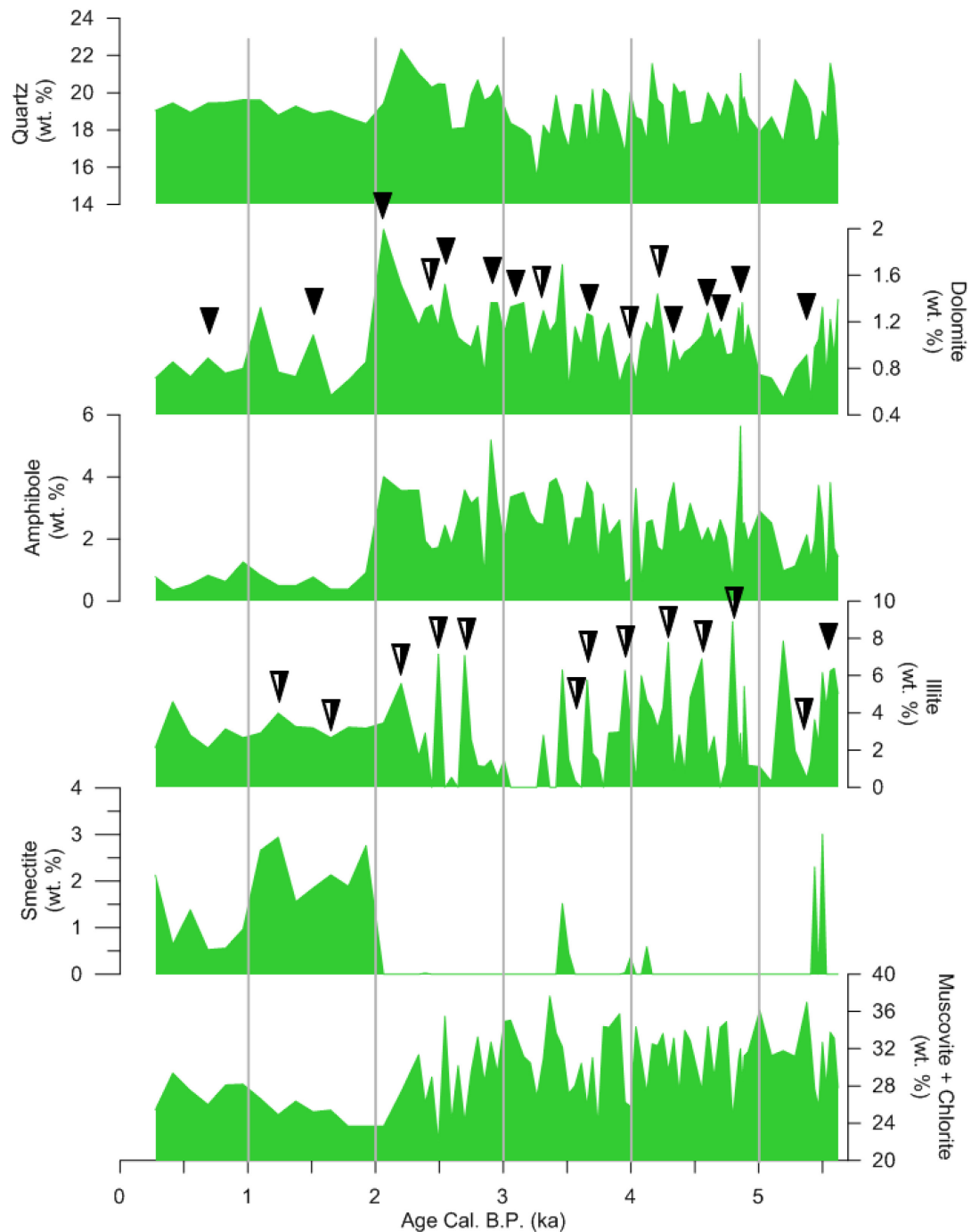


Fig 5.17 Trace minerals for source areas. Filled/half filled triangles indicate a correlation/anti-correlation between dolomite and amphibole respectively illite and muscovite + chlorite (Wassmuth, 2014).

assemblage of relatively low amount of quartz and Qz/Fsp ratio as well as the occurrence of amphibole in the Eastern Siberian Sea is similar to that in the eastern Laptev Sea (Fig 5.9 and Fig 5.11), which is in accordance with the geochemical

evidence. However, the bulk minerals used to characterize the source areas are difficult to confirm a shale source rock, further studies should be done. The high quartz content and Qz/Fsp ratio near the Wrangle Island and the Chukchi Sea's Siberian coast (Fig 5.9) is a support of the mature sandstone endmember in these regions. Due to the lack of samples near the New Siberian Island region and in the western Laptev Sea, only the distinct bulk mineral assemblage of the sample at the margin of the Laptev Sea shelf (Fig 5.9) may show the difference between the eastern Laptev Sea and the western Laptev Sea.

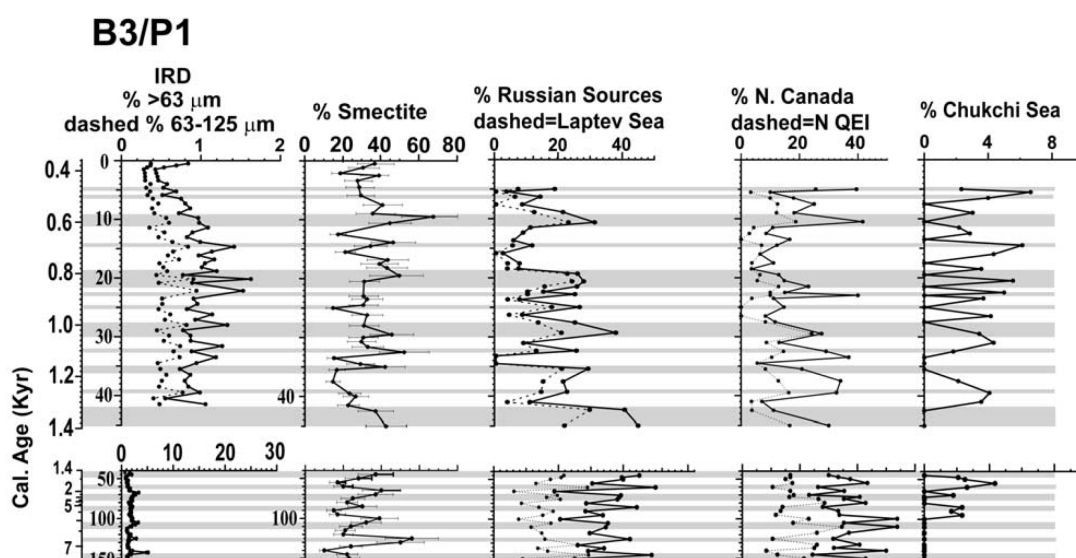


Fig 5.18 Changes of source areas indicated by Fe grains (Darby and Bischof, 2004). Shaded intervals are centered on the Russian Fe grain peaks.

Combining the isotopic signature and geochemical data, potential endmembers for the source of sediment on the Mendeleev Ridge were determined as the Lena River suspended matter (SPM), Mackenzie River SPM and Okhotsk-Chukotka Volcanic Arc (Bazhenova, 2012; Fagel et al., 2014). From the bulk mineral assemblage data in this study, the clear difference between the North American and Eurasian sources can also be seen, which is consistent with the isotopic proxy. However, the mineralogical difference between the East Siberian Sea and the Laptev Sea is not as distinct as shown by the isotope proxy. The advantage of the isotope proxy is that the strength of the provenance can be obtained using the three endmember mixing model.

Table 5.1 Attribution of the Source Areas (Canadian A. = Canadian Archipelago) for the time interval 5.6-2.2 ka and 2.2-0 ka on the basis of trace minerals. +/- symbolize elevated/decreased occurrence. Source Area Canada East Siberia Laptev Sea Kara Sea or Canadian A. Pacific

Source area	Canada	East Siberia	Laptev Sea	Kara Sea or Canada A.	Pacific
Trace mineral	Dolomite	Amphibole	Q/F<0.6	Q/F>0.6	Ch+Musc
2.2-0 ka	-	-	-	+	-
5.6-2.2 ka	+	+	-	+	+

Chapter 6. Provenance study of late Quaternary sediments on a transect across the Mendeleev Ridge as derived from grain size and bulk mineral assemblages

The Arctic Ocean plays an important role in global climate system. During the last decades, a lot of researches have been carried on in the Arctic Ocean (see Stein, 2008 for a review), however, the paleoclimatic and paleoceanographic history is still not fully understood. This is mainly due to the difficulty to get high-resolution sediment cores in this permanently ice-covered region. In recent years, many geological cruises have been performed in the Arctic (e.g. Darby et al., 2005; Jokat, 2009) to better understand the paleoenvironment conditions. Provenance studies can provide important information on the Late Quaternary history of circum-Arctic ice sheets and the paleoceanographic circulation patterns. Many provenance studies have been performed in the Arctic Ocean (as shown in Chapter 5). In this study, bulk mineral assemblages and grain size are used as provenance indicators as they provides important information on provenance and transport agent, and thus, the paleoceanographic circulation and paleoclimate reconstruction. Three sediment cores (PS72/396-5, PS72/410-3 and PS72/422-5) on a transect across the Mendeleev Ridge (for core locations see Fig 3.1 and Table 3.2) have been selected in order to identify the provenance of terrigenous sediments from the Central Arctic and to interpret the changes of the source areas during the past ~600ka in terms of paleoceanographic circulation changes in the Central Arctic. These cores have already been studied for bulk mineral assemblages within in the master thesis of Schulte-Loh (2009) based on the relative abundances estimated by single peak intensities (see Chapter 4). In this chapter, weight percentages calculated from the qXRD software packages of RockJock are used to study bulk mineral assemblages.

6.1 Down-core grain size distributions and bulk mineral variations

Table 6.1 shows the possible present minerals chosen for RockJock analysis and the grouped major minerals. The most abundant non-clay minerals are quartz, plagioclase, K-feldspar, calcite and dolomite. There are also some minor minerals such as pyroxenes, amphiboles, garnet, epidote and halite that can be identified. But the average contents are below 2% and thus excluded in this study. Clay minerals are grouped to illite, smectite, kaolinite and chlorite. Biotite and Muscovite are grouped into illite and vermiculite is grouped into smectite group (Darby et al., 2011).

Table 6.2 shows the basic statistics of the ice-rafted debris (IRD) and major minerals contents in the three cores. The $>63\mu\text{m}$ IRD abundance varies between 4.0% and 43.9% in core PS72/396-5 with an average of 17.2%. It decreases towards the Makarov Basin side of the Mendeleev Ridge. The average abundance in core PS72/410-3 is 11.1% and it decreases to 5.8% in core PS72/422-5. The minimal and maximal abundances also decrease from the west to the east. The same trend can also be found in the abundance of the $>250\mu\text{m}$ IRD. Quartz, dolomite, and plagioclase are the most abundant minerals in descending order in the three cores. Quartz and plagioclase are widely present in all three cores, while dolomite content is very low in core PS72/422-5. Like the IRD abundance, quartz and dolomite contents decrease from west to east. Plagioclase shows an opposite trend.

Down-core variations of coarse fraction, as well as major minerals contents in core PS72/396-5 are shown in Fig 6.1a. Quartz and dolomite correlate well with the 63-250 μm and $>250\mu\text{m}$ fraction respectively and dolomite shows reverse correlation with plagioclase (Table 6.3). In general, the 63-250 μm and $>250 \mu\text{m}$ fraction show similar distributions. It only shows mismatches at ~ 20 cm, ~ 32 cm, 66-83 cm and 183 cm (see detailed discussions in Chapter 6.3). The quartz content shows the largest variations and increases downward the section. Distinct peaks of $>40\%$ occur at ~ 20 cm, ~ 32 cm, 66-83 cm, ~ 168 cm, ~ 194 cm, ~ 225 cm and ~ 255 cm. Two prominent

Table 6.1 Non-clay and clay minerals possibly present in the samples that are selected to be calculated in the RockJock and the reduced and grouped minerals discussed in the context.

	Initial mineral selection	Reduced and consolidated
NON-CLAYS		
	Quartz	Quartz
	Kspar (ordered Microcline)	K-feldspar
	Kspar (intermediate microcline)	Plagioclase
	Kspar (sanidine)	Calcite
	Kspar (orthoclase)	Dolomite
	Plagioclase (albite, var. cleavelandite)	
	Plagioclase (oligoclase; NC)	
	Plagioclase (oligoclase; Norway)	
	Plagioclase (andesine)	
	Plagioclase (labradorite)	
	Plagioclase (bytownite)	
	Plagioclase (anorthite)	
	Calcite	
	Dolomite	
	Dolomite (Fe-rich)	
	Halite	
	Amphibole (ferrotschermakite)	
	Pyroxene (diopside)	
	Garnet (grossular)	
	Garnet (almandine)	
	Epidote	
CLAYS		
	Kaolinite (disordered)	Kaolinite
	Kaolinite (Dry Branch)	Smectite
	Smectite (Na-Kinney montmorillonite)	Illite
	Smectite (Ca-Kinney montmorillonite)	Chlorite
	Smectite (ferruginous)	
	Illite (1Md)	
	Illite (R>1, 70-80%I)	
	Illite (1M; RM30)	
	Biotite (1M)	
	Chlorite (CCa-2)	
	Chlorite (Mg; Luzenac)	
	Muscovite (2M1)	
	Vermiculite (Kent)	

dolomite peaks of >39% correlating with the >250 μm peaks, were found at 66 cm and 130 cm. Calcite starts to appear from ~200 cm.

Table 6.2 Basic statistics of the IRD and major minerals contents in the three cores.

	PS72/396-5			PS72/410-3			PS72/422-5		
	Average	Max	Min	Average	Max	Min	Average	Max	Min
Quartz	32.2	58.6	18.2	28.7	47.8	19.9	23.7	43.8	14.8
Ksp	4.6	10.7	1.3	4.5	9.4	2.2	5.1	10.6	2.4
Plg	8.2	17.8	2.4	11.9	18.1	2.7	13.6	23.4	8.1
Calcite	3.0	16.8	0.0	3.0	21.4	0.0	0.5	5.1	0.0
Dol	13.8	54.4	0.0	7.9	41.2	0.0	2.0	23.5	0.0
Q/F	2.9	9.0	1.2	1.9	5.5	1.2	1.3	3.9	0.9
63-250 μm	12.3	28.5	3.6	8.5	32.2	1.5	4.7	22.9	0.0
>250 μm	4.9	26.0	0.4	2.6	32.6	0.1	1.1	12.8	0.0
>63 μm	17.2	43.9	4.0	11.1	41.7	1.6	5.8	28.5	0.0

The distribution pattern of coarse fraction and major mineral contents in core PS72/410-3 is similar to core PS72/396-5 (Fig 6.1b), but the variations are less significant. Except for plagioclase, contents of other minerals decrease in core PS72/410-3 in comparison with those in core PS72/396-5. The major peaks in each proxy correlate well to the ones in core PS72/396-5. Calcite starts to appear from ~250 cm.

Core PS72/422-5 located at the Makarov Basin side of the Mendeleev Ridge, and the distribution pattern of coarse fraction and major minerals is quite different from the other two studied cores. The direct correlation of quartz, dolomite and coarse fractions and the reverse correlation of dolomite and plagioclase are still obvious, although less distinct. The most prominent difference is that in core PS72/422-5 the variation of the proxies is remarkably less significant than in other cores (Fig 6.1c). The background content of coarse fraction is less. Below the pink-white layer 1 (PW1), there is nearly no variations in all major minerals. The first occurrence of calcite is slightly before MIS6. Dolomite is rarely found in the core, except for the two distinct peaks in the two pink-white layers.

Table 6.3 Correlation coefficients of the minerals and grain size in a) core PS72/396-5 and b) core PS72/410-3.

a)

	Quartz	Ksp	Plg	Calcite	Dol	63-250um	>250um
Quartz	1.00						
Ksp	0.03	1.00					
Plg	0.04	0.24	1.00				
Calcite	-0.54	-0.27	-0.09	1.00			
Dol	-0.31	0.01	-0.76	0.22	1.00		
63-250um	0.71	0.29	0.08	-0.13	-0.07	1.00	
>250um	0.19	-0.01	-0.56	-0.13	0.62	0.19	1.00

b)

	Quartz	Ksp	Plg	Calcite	Dol	63-250um	>250um
Quartz	1.00						
Ksp	0.20	1.00					
Plg	0.19	0.11	1.00				
Calcite	-0.50	-0.11	-0.40	1.00			
Dol	-0.25	-0.06	-0.82	0.53	1.00		
63-250um	0.56	0.62	0.01	0.15	0.06	1.00	
>250um	-0.08	0.10	-0.60	0.38	0.75	0.13	1.00

For the three cores studied in this chapter, bulk mineral assemblages have been studied by Schulte-Loh (2009) using single peak intensities. As already shown in Chapter 4, the down-core variations of peak intensities and weight percentages of most major minerals (quartz, plagioclase, calcite, and dolomite) are very similar. The interpretation of K-feldspar peak intensities variations should be with care. If the sample preparation has been done properly, peak intensities can be used to estimate the relative abundances of major minerals of sediment except for K-feldspar.

6.2 Age model

Stein et al. (2010 a, b) has developed a preliminary age model for upper parts of the cores (above SL Unit K) mainly based on the correlations of upper 7 brown layers with other cores in which better age models has already been established. The age model based on the pink-white layer and sandy layers for the lower part (below SL

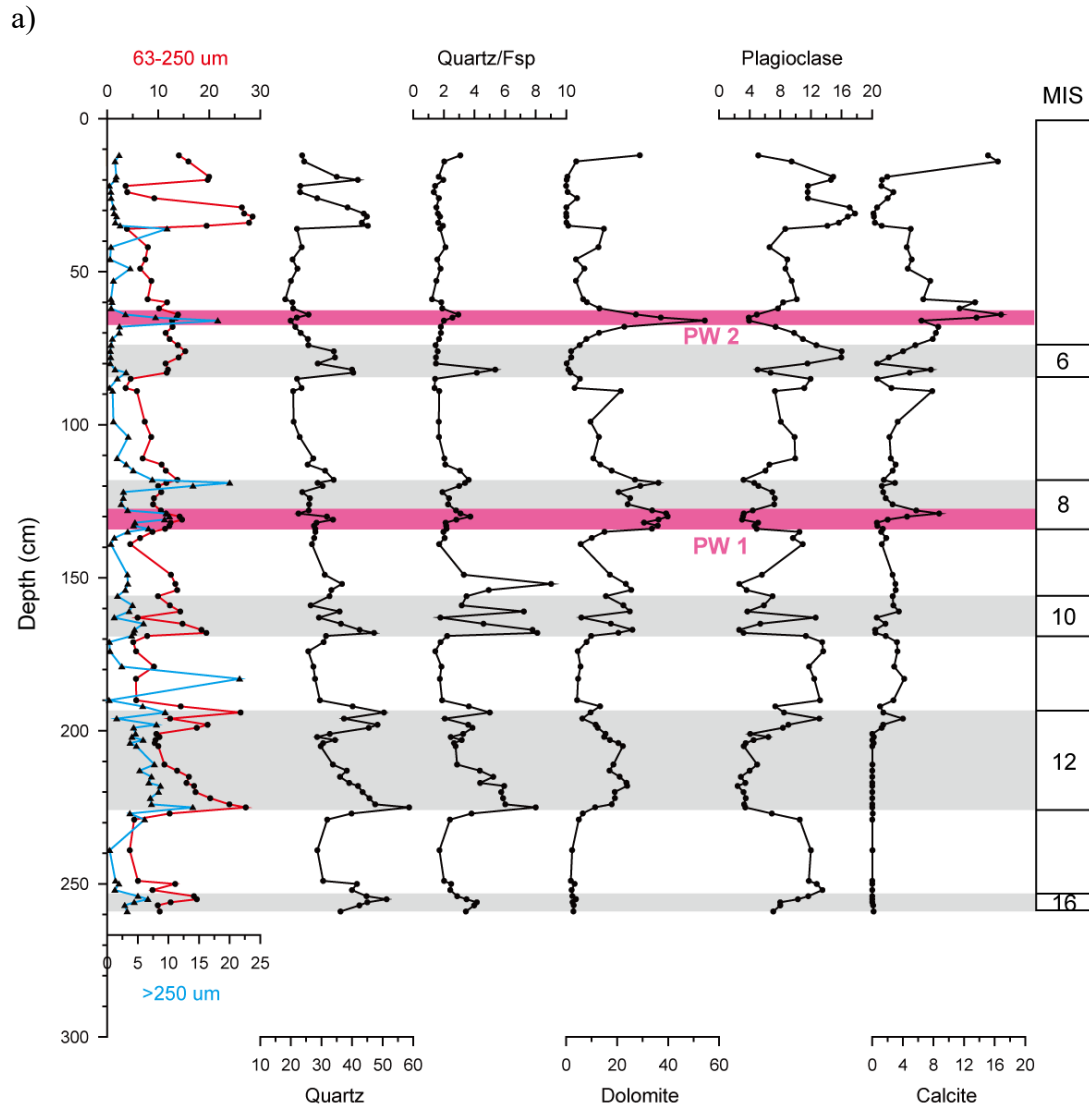


Fig 6.1 Down-core variations of coarse fraction and major minerals in a) core PS72/396-5, b) core PS72/410-3 and c) core PS72/422-5. MIS stratigraphy is according to the tentative age model proposed by Stein (2010a). Pink bars indicate the pink-white layers.

Unit K) is more tentative. As the lithology in core PS72/422-5 is quite different from other cores, the age model remains question mark (Stein et al., 2010a). In this chapter, independent correlation tools (XRF scanning and physical properties) are used to further support the preliminary age model and supplement the age model for core PS72/422-5.

6.2.1 Lithologies

A prominent characteristic of the sediment of these cores is the cyclical alternations of sediment color of brown to dark brown and light olive brown to grey (Fig 6.2; Stein et

al., 2010a), which is also found in other Central Arctic cores (Adler et al., 2009; Jakobsson et al., 2000; Phillips and Grantz, 2001; Polyak et al., 2004; Wang et al., 2013). The brown beds, characterized by moderate contents of coarse grained materials and elevated amount of biogenic components, are shown to represent interglacial or interstadial periods, whereas the grey beds are very fine grained with some coarse grain spikes and contain few biogenic materials, representing glacial or stadial periods (Adler et al., 2009; Polyak et al., 2009; Spielhagen et al., 2004; Stein et al., 2010a).

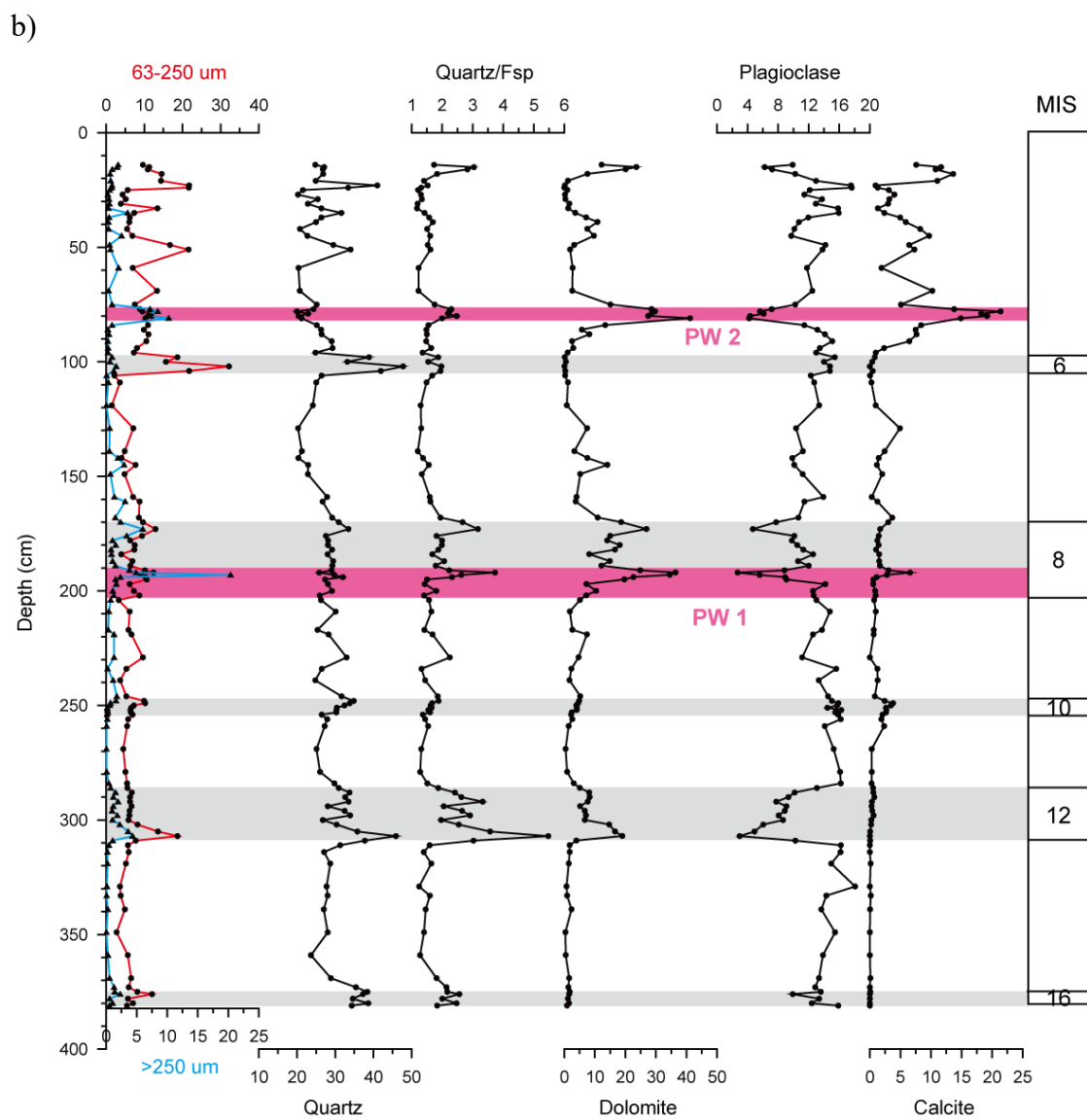


Fig 6.1 (continued)

For cores PS/72-396-5 and PS72/410-3, all the 13 standard lithostratigraphic (SL)

units A to M established by Clark et al. (1980) can be identified (Fig 6.2). The sandy layers (unit C, F, H, J, L and parts of M) and the prominent white or pink-white layer are key sedimentary features useful for core correlations within the Amerasian Basin. These layers form the Unit I of the two main sedimentary units, which is characterized by cycles of silty clay and sandy intervals. The Unit II is mainly featured by fine-grained sediments of brown/light olive brown colors (Stein et al., 2010a). For core PS72/422-5, the SL units and the two main sedimentary units cannot be identified and sandy intervals also occur in the lower part of the core.

c)

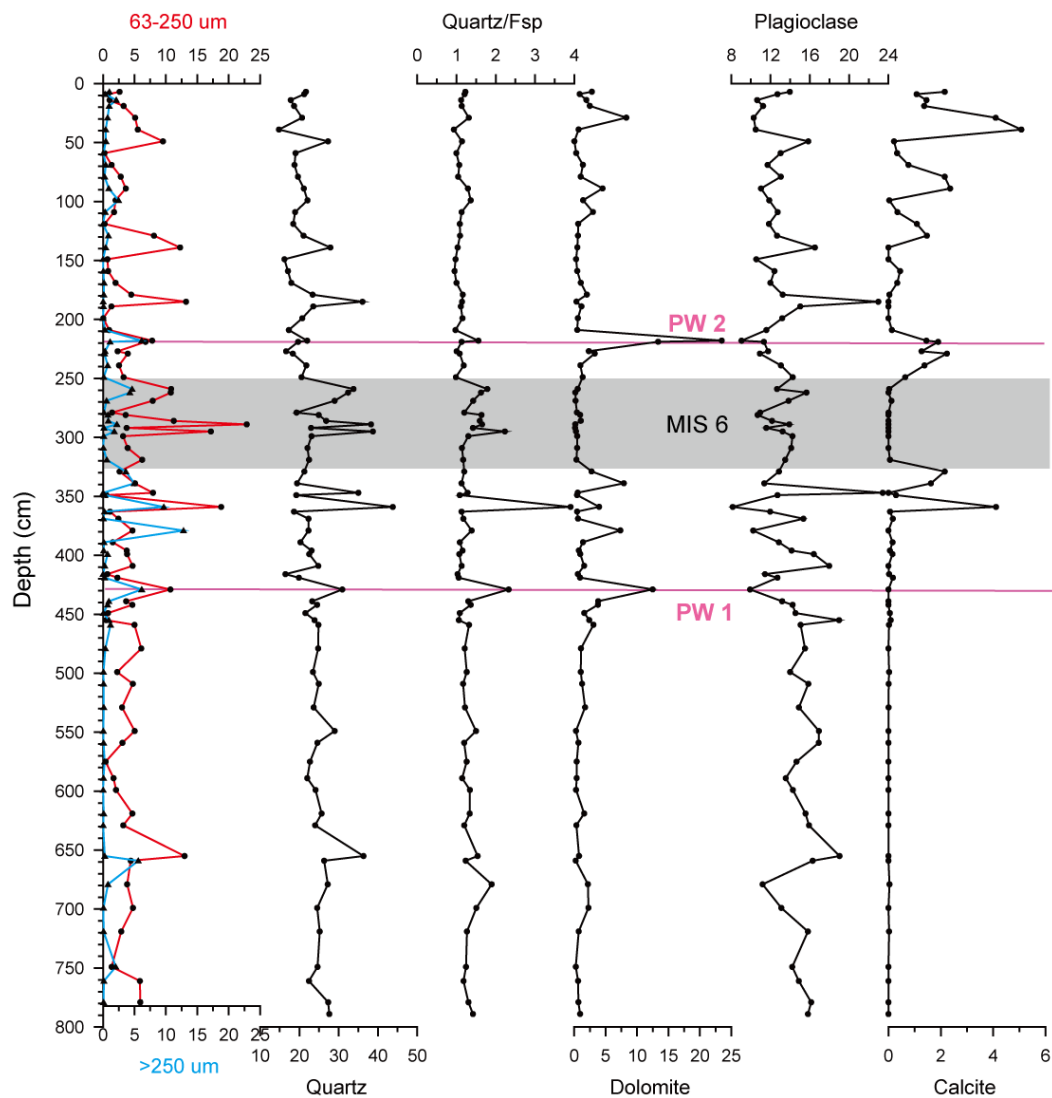


Fig 6.1 (continued)

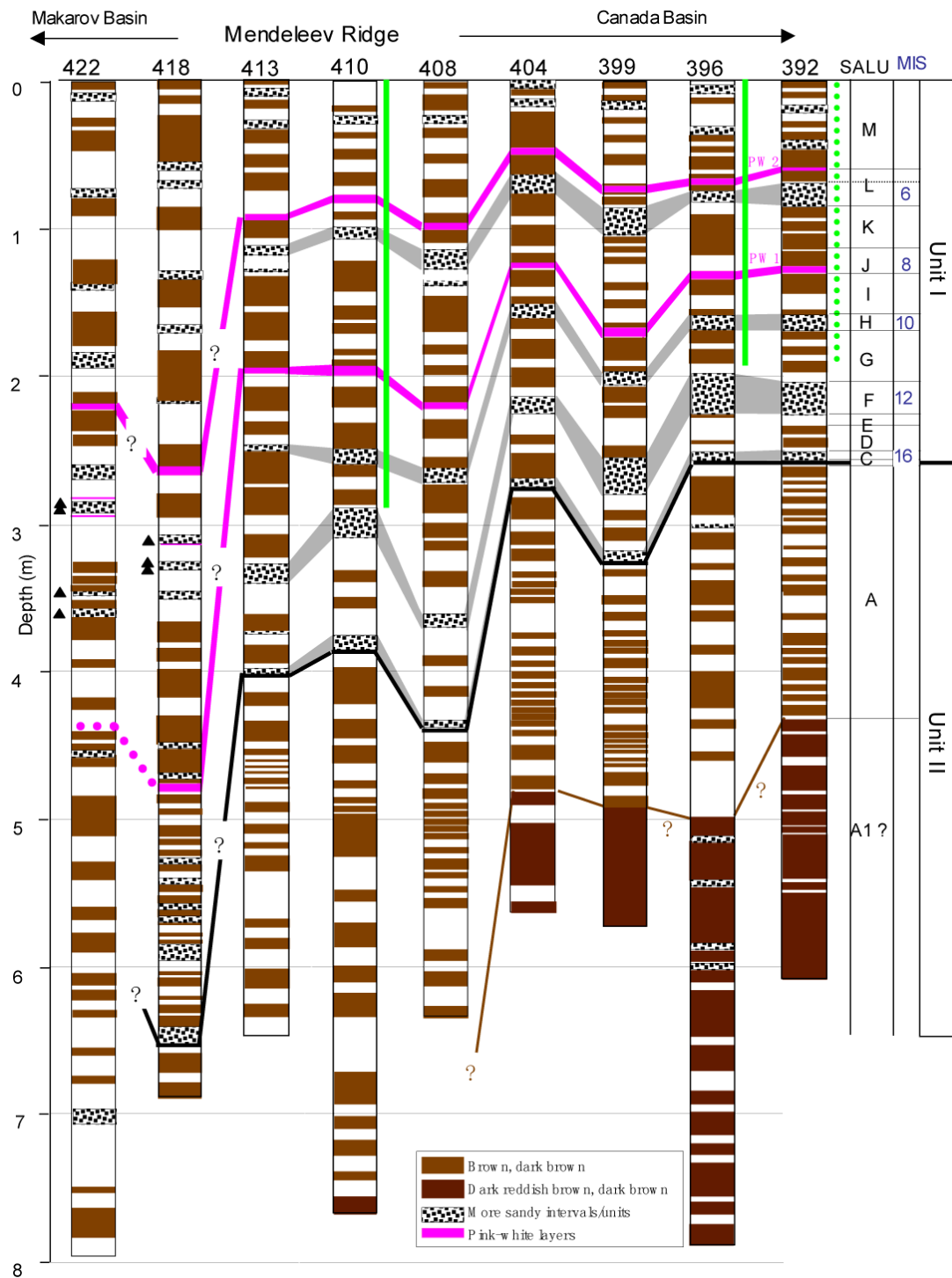


Fig 6.2 Simplified lithostratigraphy of the sediment cores in the northern transect from Polarstern ARK-XXIII/3 expedition (from Stein et al., 2010a). Cyclical alternations of sediment color of brown to dark brown and light olive brown to grey are shown. Standard lithostratigraphic (SL) units A1 to M (according to Clark et al. 1980), main lithological units I and II, and depths of main pink-white layers PW1 and PW2 are indicated.

6.2.2 Correlations based on X-ray Fluorescence (XRF) scanning data

X-ray fluorescence (XRF) core scanning is a fast semiquantitative method to obtain high-resolution (1cm interval) major and minor elements down-core variations data. Hanslik et al. (2013) has shown that central Arctic Ocean cores can be correlated using Ca concentrations measured by XRF. The cycles of Mn (manganese)-rich dark brown layers are often considered as representing glacial-interglacial cycles (Jakobsson et al., 2000; Löwemark et al., 2008; Löwemark et al., 2014; Löwemark et al., 2012; März et al., 2011b; Stein, 2015), and thus, can be used for correlation. The XRF scanning data of the three studied cores are from Matthiessen (2010a, b, c).

Fig 6.3 shows correlations of the three cores based on Ca intensity (XRF) and dolomite (XRD). Three distinct intervals of high Ca intensity can be seen in all three cores. Stein et al. (2010b) showed that the first onset of dolomite and calcite appears at the base of SL Unit C and middle part of SL unit G respectively in core PS72/392 located in the Canada basin. The major increase of dolomite occurs at the base of SL Unit F. In our cores, similar patterns can be found. In cores PS72/396-5 and PS72/410-3, the first Ca intensity peaks coincide with the first dolomite peaks, which is MIS12 based on the preliminary age model. The first Ca intensity peak in core PS72/422-5 doesn't coincide with the dolomite peak probably because the dolomite deposition is different at that location. The highest Ca peaks can be seen in the two dolomite rich layers – the pink-white layer – in all three cores. Another prominent pattern is the minimum of both Ca intensity and the dolomite concentration during MIS6. In glacial periods, the foraminiferal content is reduced and thus the Ca intensity due to the biological carbonate is significantly low. Meanwhile, the detrital carbonate is almost absent in MIS6, while the carbonate is abundant during other glacial periods, suggesting a different sediment source.

Fig 6.4 shows correlations of the three cores based on Mn intensity measured by XRF. The Mn-rich, brown layers are widespread features in the Arctic cores and Mn is

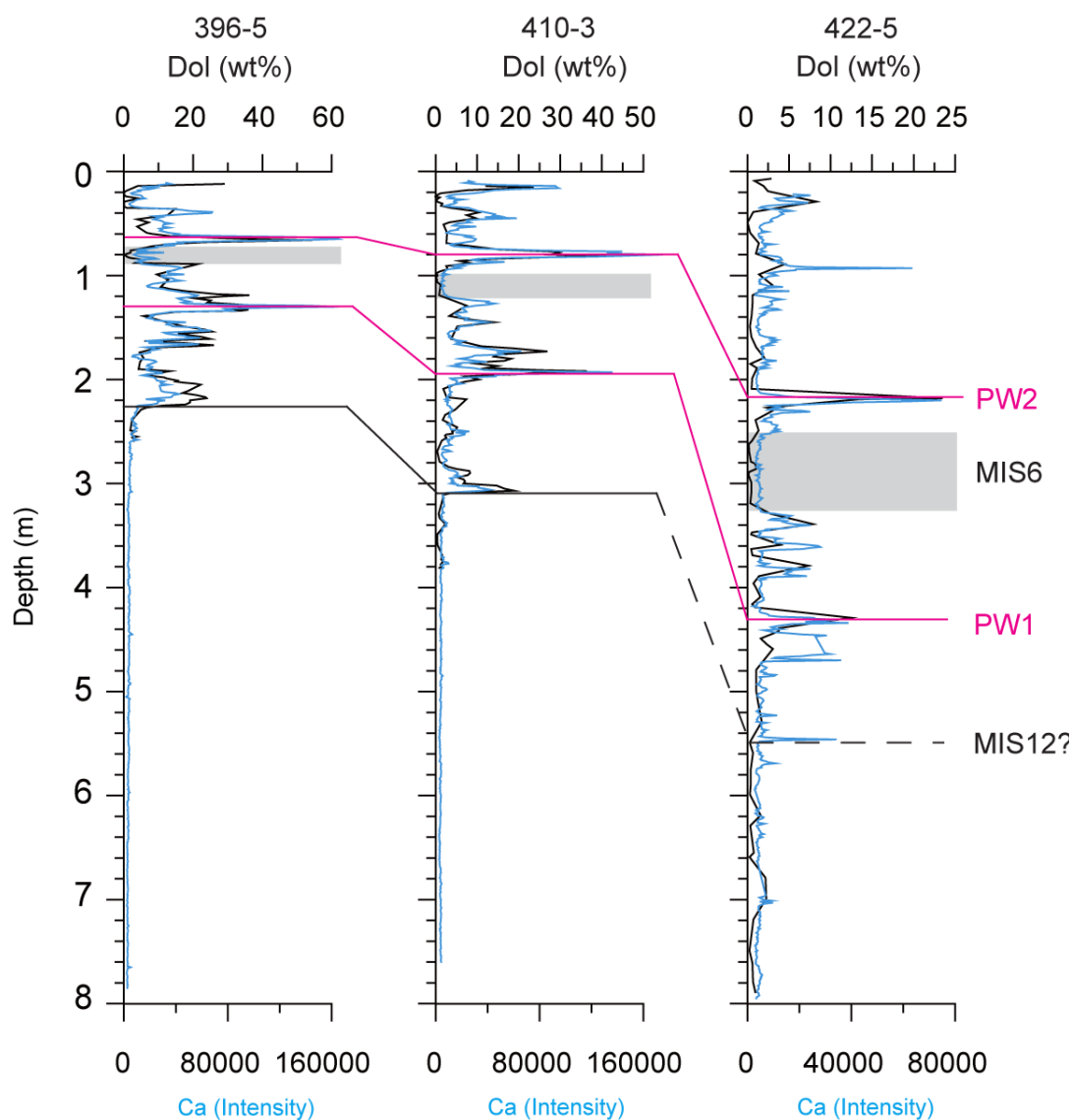


Fig 6.3 Stratigraphic correlations of core PS72/396-5, PS72/410-3 and PS72/422-5 based on Ca intensity (XRF) and dolomite (XRD). The two pink-white layers are identified in all three cores and marked as PW1 and PW2. The shaded areas represent MIS 6. The correlation of MIS 12 with core PS72/422-5 is more tentative. (Ca intensity data are from Matthiessen (2010a, b, c))

commonly believed to be deposited in interglacials (Darby et al., 2006; Jakobsson et al., 2000; Löwemark et al., 2008; Löwemark et al., 2012; O'Regan et al., 2008; Polyak et al., 2004). Therefore the Mn cycles may represent the glacial-interglacial cycles and thus can be a good correlation tool. But when using Mn cycles as a correlation tool, one should have in mind that diagenetic processes may alternate the preservation of Mn, and thus it should be combined with other independent proxies (März et al.,

2011b). The prominent cycles can be clearly seen in all three cores. In general, the Mn intensity peaks correspond to the brown layers. The pink-white layers can be identified by Mn intensity minimum in all three cores. Besides, distinct low Mn intensity intervals of 74-88cm, 117-133cm, 156-168cm, 194-225cm and 255-259cm can be seen in core PS72/396-5 and of 99-105cm, 173-202cm, 248-255cm, 286-309cm and 371-394cm in core PS72/410-3, representing MIS 6, 8, 10, 12 and 16 according to the tentative age model proposed by Stein et al.(2010a). In core PS72/422-5, Mn intensity minimum from 252 cm to 328 cm is quite conspicuous, which is MIS6 (Stein et al., 2010a). Below the first pink-white layer (PW1), prominent Mn intensity minimum intervals can also be seen at about 480 cm, 520 cm, and 550 cm (possibly representing MIS10, MIS12, and MIS16 (Stein et al., 2010a)). But they are more tentative and should be combined with other proxies.

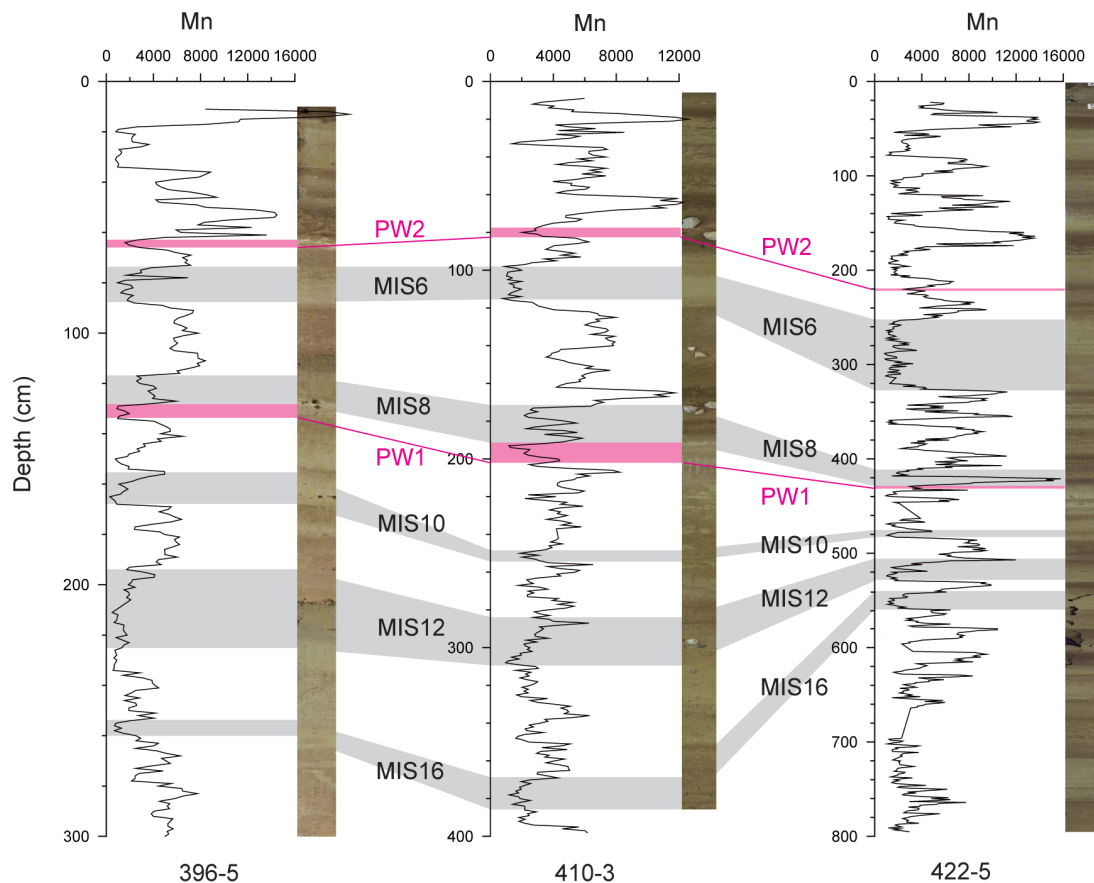


Fig 6.4 Stratigraphic correlations of core PS72/396-5, PS72/410-5 and PS72-422-5 based on Mn intensity measured by XRF. (Mn intensity data are from Matthiessen (2010a, b, c))

6.2.3 Correlations based on physical properties

Physical properties (i.e. magnetic susceptibility (MS), wet bulk density (WBD)) can be measured by a GEOTEK “Multi-Sensor-Core-Logger” (MSCL). The data can be acquired rapidly, non-destructively and continuously and are of high resolution (Weber et al., 1997). The data in this study were measured on board (Jokat, 2009). Physical properties data can be a useful tool to stratigraphically correlate cores within similar depositional environments from the Arctic Ocean (O'Regan et al., 2008; Sellén et al., 2010; Stein et al., 2001). The MS varies with the content of ferromagnetic material in the sample, because ferromagnetic minerals have a much higher susceptibility than other minerals (Thompson and Oldfield, 1986). In our cores, the MS peaks represent periods of high input from the Siberian, where volcanic rocks containing higher ferromagnetic minerals are widely present (Bazhenova, 2012). The BD is influenced by grain size, composition and porosity (Niessen et al., 2007; Weber et al., 1997). The long term variation of WBD reflects compaction (Niessen et al., 2007) and the short term variation is mainly due to the grain size variation (O'Regan et al., 2014).

Fig 6.5 shows correlations based on physical properties (i.e. MS and WBD). Throughout the cores, the MS inversely correlated with the WBD in general. The lows in the MS occur within the glacial periods. There are three prominent lows representing MIS10, 12, and 16 in all three cores. It can also be seen in other cores from the northern transect as shown in Fig 6.6. The WBD peaks are consistently associated with the increased coarse fraction contents ($> 63\mu\text{m}$). The depths of the three lows in the MS are the same as the Mn intensity lows, providing an independent support to the age model for PS72/422-5 based on Mn correlations.

6.3 The IRD events and their provenances

Ice-rafted debris (IRD), which is usually $>63\ \mu\text{m}$, can be used as an indicator of

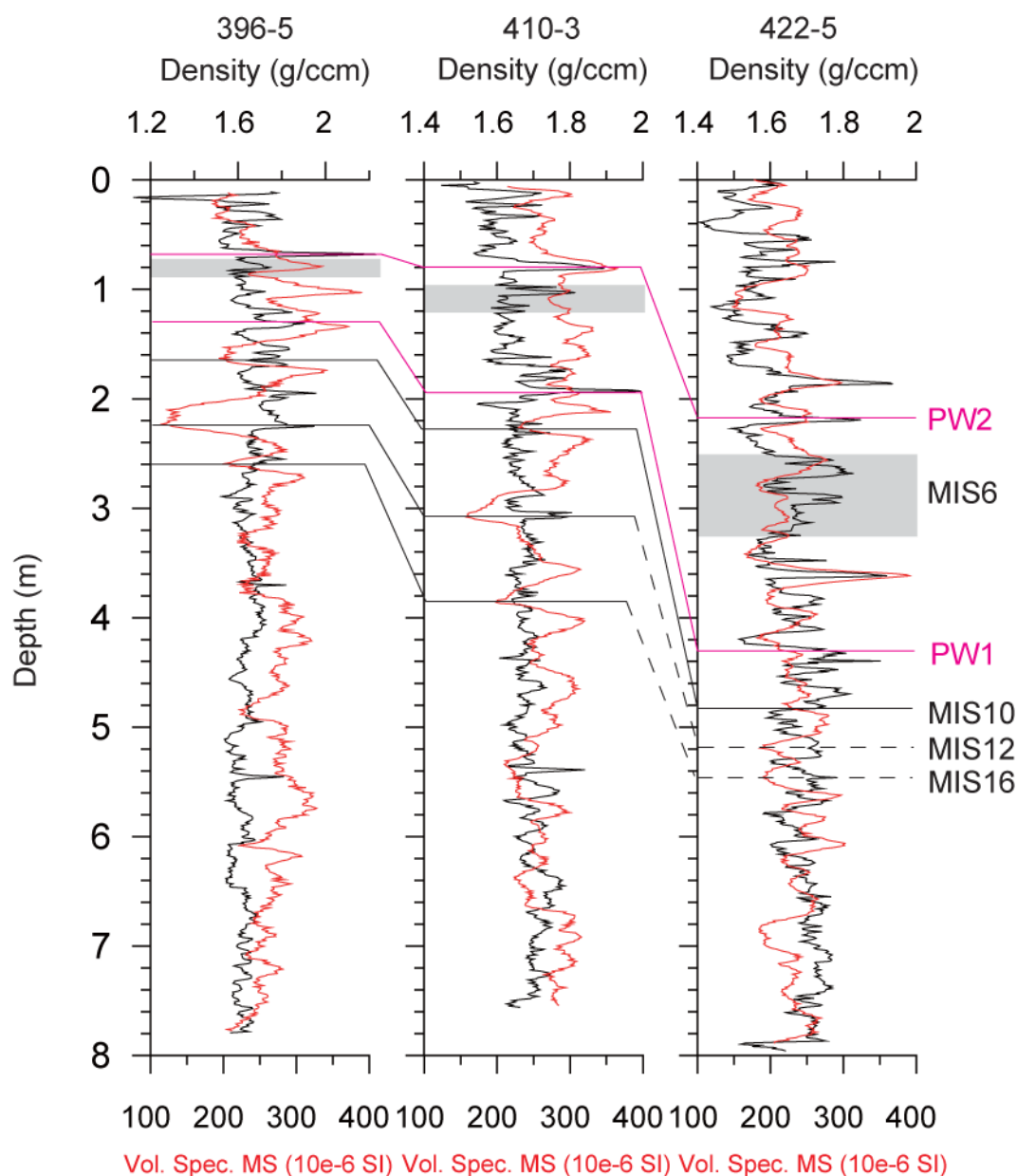


Fig 6.5 Stratigraphic correlations of core PS72/396-5, PS72/410-5 and PS72-422-5 based on wet bulk density and magnetic susceptibility measured by the multi-sensor core logger at 1-cm intervals. The tentative correlation of MIS12 and 16 in core PS72/422-5 is marked using dotted line. (Data are from Niessen et al. (2009))

materials transported by iceberg or sea ice (Lisitzin, 2002, and references therein). The $>63 \mu\text{m}$ fraction could be dominated by foraminifera shells, which is not IRD. But according to Stein et al. (2010a), sand-rich intervals in the studied cores correlate with cold periods that are depleted with foraminifers. Icebergs can transport sediment of all grain sizes ranging from clay to boulders, depending on the materials rafted by

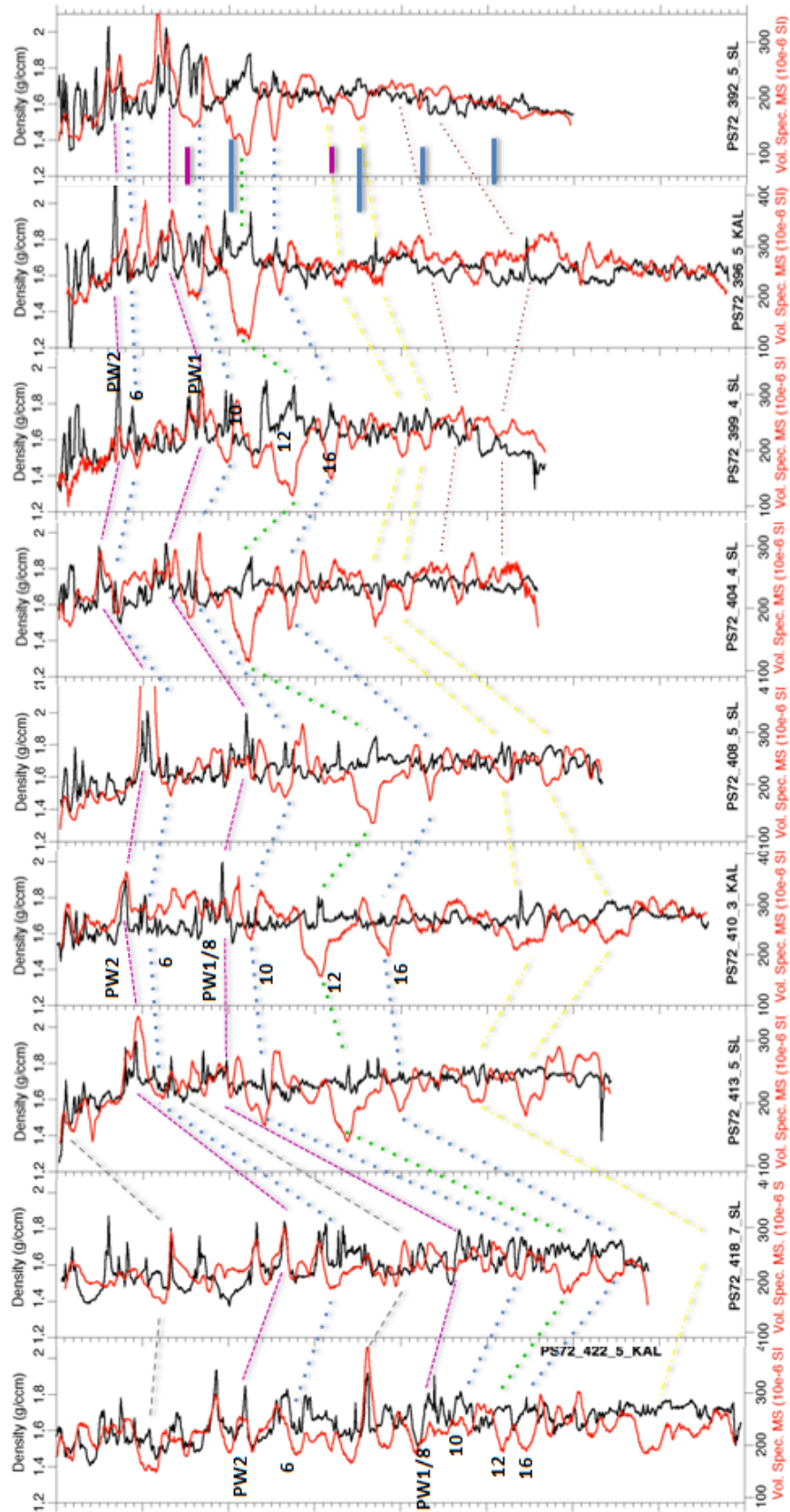


Fig 6.6 Stratigraphic correlations of the northern transect cores retrieved during Polarstern ARK-XXIII/3 expedition based on wet bulk density and magnetic susceptibility (from Dr. Frank Niessen, personal communication; data are from Niessen et al. (2009)).

the glaciers. Materials coarser than 250 μm are commonly believed to be transported by icebergs (Bischof et al., 1996; Darby et al., 2011; Spielhagen et al., 2004). Sediment entrainment in sea ice mainly occurs via frazil ice and anchor ice (Reimnitz et al., 1998). The sediment entrained via frazil ice is usually fine grained and do not exceed 30-60 μm (Clark and Hanson, 1983; Darby, 2003; Darby et al., 2011; Nürnberg et al., 1994), while anchor ice can entrain coarser materials if it is present on the sea floor (Darby et al., 2011). In this thesis, we assume that materials coarser than 250 μm are transported by icebergs and the 63-250 μm IRD is transported by both sea ice and icebergs. Therefore, intervals in which the 63-250 μm and >250 μm fractions are both high (for core PS72/396-5 and core PS72/410-3, it's in MIS5d, 8, 10, 12 and 16) are interpreted as IRD events that are transported by both iceberg and sea ice, whereas intervals in which the 63-250 μm fractions are dominant and the >250 μm fractions are low may suggest that the IRDs are transported mainly by sea ice.

Previous studies showed that coarse-grained IRD is transported and released in the Arctic Ocean during glacial periods (Bischof et al., 1996; Bischof and Darby, 1997), or during glacial terminations (Adler et al., 2009; Darby et al., 1997; Phillips and Grantz, 2001), or even during interglacial periods (Wang et al., 2013; Wang et al., 2010). This study shows fine-grained material is largely deposited during interglacial periods and major IRD events occur during the beginning and ending of glacial periods but also in the glacial periods. During the initial build-up phase of glacial periods, the ice sheet grows and extends. When reaching the coastline/shelf break, icebergs calve from the ice sheet and drift in the open water before sea-ice sheets were fully developed (Phillips and Grantz, 2001) and release sediments at the locations of the coring site. During the full glacial period, on one hand, the Arctic Ocean is completely covered by sea ice (Bradley and England, 2008; Polyak et al., 2010; Polyak et al., 2013), preventing icebergs from circulating in the Arctic Ocean. In this case, the IRDs are mostly transported by sea ice. On the other hand, in the weaker glacial periods, when there was no permanent sea-ice cover and icebergs could circulate freely in the Arctic Ocean, several IRD events might have occurred.

During the warming deglacial period, the sea level rises and the ice shelf collapses, producing massive icebergs. As a consequence, many IRD events occur in this period.

As discussed in Chapter 5, as well as concluded from various studies, bulk mineral assemblages are a good indicator of sediment provenance. Dolomite is commonly interpreted as an indicator for sediment input from the Canadian Archipelago, i.e. Banks Island and Victoria Island (Bischof et al., 1996; Phillips and Grantz, 2001). Plagioclase shows significant inverse correlation with dolomite in all three cores (Table 6.3 and Fig 6.1). Therefore, this might indicate the sediment input from the Eurasian side. Quartz, although widely present in the circum-Arctic regions, may suggest a Eurasian provenance (Adler et al., 2009; Polyak et al., 2004; Spielhagen et al., 1997; Vogt, 1996). When combined with feldspar, it can give more information on source areas (Moros et al., 2004; Vogt, 1997; Vogt et al., 2001). Although already shown in Chapter 5, the occurrence of amphibole can also be an indicator of sediment from Siberian shelf seas, it does not show any similar patterns as other minerals in the downcore variations. Therefore, it is excluded from the bulk mineral assemblages that are used to trace sediment source areas.

Unlike the cores from the Canada Basin side of the Mendeleev Ridge, in which the major coarse-grained materials are first deposited in MIS16, in core PS72/422-5 strong input of the IRD starts in MIS7, except for the pink-white layer that occurs in MIS8. This seems to be with the IRD distributions in cores located on the Lomonosov Ridge (Spielhagen et al., 2004), which may indicate similar source areas. In other words, it may suggest that the provenance of sediments deposited on the Makarov Basin side of the Mendeleev Ridge is different from that deposited on the Canada Basin side of the Mendeleev Ridge.

The IRD events in the inception and/or termination stage of MIS16, 12, 10, 8, as well as in the two pink-white layers, in core PS72/396-5 and PS72/410-3 are characterized by high dolomite contents, high quartz/feldspar ratios and low plagioclase contents. This indicates that in these time intervals IRD input from the Canadian Archipelago

plays an important role. Although in core PS72/422-5 there are almost no dolomite-rich layers, the two pink-white layers can be identified by increased dolomite contents, as outlined in Schulte-Loh (2009). These layers are also characterized by high amount of both 63-250 μm and $>250 \mu\text{m}$ fraction, indicating transport mainly by iceberg. These IRD events can also be found in other cores in the Canada Basin (Bischof and Darby, 1997; Phillips and Grantz, 2001; Stein et al., 2010a; Stein et al., 2010b). Similar coarse-grained, detrital-carbonate-rich layers, defined as “HS (Hudson Strait) Heinrich Events”, are found in IODP site U1308 and U1313 in the North Atlantic (Hodell et al., 2008; Stein et al., 2009). The pink-white layers that are rich in dolomite are common features in the cores retrieved from the Amerasian Basin (Clark et al., 1980). The dolomite rich IRD events occurred in the western Arctic Ocean and the North Atlantic both reflect the initiation and disintegration of the Laurentide Ice Sheet (Simon et al., 2013).

The MIS6 IRD events are characterized in all three cores by high quartz and low dolomite, which indicates IRD from Eurasian sources. These layers have prominently high amount of 63-250 μm fraction coarse-grained materials, coinciding with low amount of $>250\mu\text{m}$ fraction, which indicates IRD transported mainly by sea ice. Similar quartz-rich and dolomite-depleted layers are also found in other cores from the western Arctic Ocean (Adler et al., 2009; Polyak et al., 2004; Stein et al., 2010a), as well as on the Lomonosov Ridge (Spielhagen et al., 2004). The changes of provenances can be related to different circulation patterns during MIS6 in comparison to other glacial periods, i.e., MIS16, 12, 10, and 8 (Adler et al., 2009).

6.4 Implications for the ice-sheet history and paleoenvironment

The first onset of dolomite coincides with distinct peaks of coarse-grained materials ($>250\mu\text{m}$) starting in MIS16 in core PS72/396-5 and PS72/410-3, which is synchronous in core PS72/392-5 in the Canada Basin (Stein et al., 2010b) and in IODP sites U1308 and U1313 (Hodell et al., 2008; Stein et al., 2009) in the North Atlantic. Dolomite is commonly believed to be an indicator of Canadian Arctic

provenance, as Paleozoic limestones are widespread in the Canadian Arctic (Okulitch, 1991; Phillips and Grantz, 2001). The significant correlation between dolomite content and $>250\ \mu\text{m}$ coarse fraction (Table 6.3) indicates that the sediment is mainly transported by icebergs. This may suggest that MIS16 is the first time that the size of the Laurentide Ice Sheet is large enough to reach the shelf break and thus carving icebergs into the Central Arctic (Stein et al., 2010a). This is in accordance with the global benthic isotope record (Lisiecki and Raymo, 2005) which indicates that MIS16 is the first major Quaternary glaciation. The dolomite-rich material is then transported to the coring site via the Beaufort Gyre. The first major dolomite peaks occur in MIS12, as MIS12 is the most severe glaciation of the last 0.5Ma (Shackleton, 1987). Similar dolomite-rich coarse-grained intervals are also found during MIS12, 10, and 8, as well as in the two prominent pink-white layers probably occurring during MIS8 and MIS 5d (Stein et al., 2010a). These intervals may reflect the major iceberg discharge events during the initiation and disintegration of the Laurentide Ice Sheet. However, these layers, except for the pink-white layers, are absent from the core PS72/422-5 locating at the Makarov Basin side of Mendeleev Ridge. This may indicate that the provenance of IRD deposited during MIS16, 12, 10 and 8 in the Makarov Basin is different from that of the Canada Basin side of Mendeleev Ridge. It further indicates that the surface circulation patterns during these periods are different from that afterwards (Polyak and Jakobsson, 2011). The presence of the pink-white layers in the core PS72/422-5 suggests that during these periods the Beaufort Gyre is intensified and shifts towards the Lomonosov Ridge (see Fig 2.2).

In contrast to the IRD layers characterized by high dolomite content in MIS16, 12, 10 and 8, the IRD layers in MIS6 are characterized by high quartz contents and low Quartz/Fsp ratios. Quartz content is highly correlated to the 63-250 μm fraction (Table 6.3), which may indicate transport mainly by sea ice. Although quartz is widespread in circum Arctic source areas, it is usually recognized as indicator of Eurasian provenance (Polyak et al., 2004; Spielhagen et al., 1997). When combining with low Quartz/Fsp, it can be a more reliable indicator of Eurasian provenance (Vogt, 1997;

Vogt et al., 2001). The occurrence of Eurasian source sediment in the Canada Basin cores would imply that the surface circulation pattern during these periods was different from the present circulation pattern in the Central Arctic (Darby et al., 2002; Polyak et al., 2009; Polyak et al., 2004; Stein et al., 2010a). The location of the surface circulations are controlled by the Arctic Oscillation (AO) (Proshutinsky and Johnson, 1997; Thompson and Wallace, 1998), and these periods are probably related to the positive AO, when the Transpolar Drift (TPD) is intensified and shifts towards the North America (Darby and Bischof, 2004; see Fig 2.2). The lack of $>250\mu\text{m}$ IRD during these periods indicates that transport by iceberg plays no important role. It may suggest that during these periods there was very thick sea ice cover in the Amerasian Basin that prevent the icebergs to circulate freely in the Arctic Ocean (Polyak et al., 2009). Another possible reason is that during MIS 6 an ice shelf existing in the Amerasian Basin prevents the formation of icebergs (Jakobsson et al., 2010).

Chapter 7. Conclusions and outlook

The main aim of this thesis is to study in detail the quantitative X-Ray Diffraction (qXRD) software RockJock and the comparison of the two qXRD software RockJock and QUAX. And then we apply RockJock to quantify the mineral contents from XRD data to study the surface mineral assemblages in the Arctic Ocean. The bulk mineral assemblages in cores along the northern transect retrieved during the Polarstern expedition “ARK-XXIII/3” across the Mendeleev Ridge are used to reconstruct the paleoenvironmental changes in the Arctic Ocean.

During the study a lot of efforts have been paid to test the accuracy of the RockJock and look for the possible error sources. The RockJock has been checked for accuracy using artificial mixtures and the errors are generally within 1 or 2% (Eberl, 2003). However, these good results are derived using artificial mixtures that are composed of the same minerals as reference minerals and the same diffractometer. When using different diffractometers, the error bar goes apparently higher (Eberl, 2003), which can be further proved in this study. Reference minerals could also be an important error source. The best results will be obtained when minerals in samples are identical to the reference minerals. So extending the reference minerals database may be a good way to decrease the errors. Preferred orientation can be another source for errors and choosing a good preparation method can reduce preferred orientation.

New surface samples in the Arctic Ocean retrieved during two Polarstern cruises and two Russian cruises were analyzed using RockJock to test the possibility to use bulk mineral assemblages as provenance indicators. It shows that the combination of quartz, Qz/Fsp, dolomite and kaolinite can be used to identify source areas. Sediment input from the Canadian Arctic is generally characterized by high dolomite and Qz/Fsp values. Sediment input from the Eurasian Arctic shelf seas is generally characterized by low dolomite, Qz/Fsp, kaolinite values and high quartz values. However, it also shows that bulk mineral assemblage alone is difficult to distinguish specific source

areas, and thus should be combined with other proxies.

Three sediment cores on a transect across the Mendeleev Ridge that have been raised during the Polarstern cruise in 2008 were used in this thesis to study the provenance of terrigenous sediments from the Central Arctic. Quartz, dolomite, and plagioclase are the most abundant minerals and they can be used as provenance indicators. Dolomite is a common indicator for sediment input from the Canadian Archipelago. Plagioclase shows significant inverse correlation with dolomite and may suggest the sediment input from the Eurasian side. The IRD events in core PS72/396-5 are similar to that in core PS72/410-3 and different to that in core PS72/422-5. The major coarse-grained materials in core PS72/396-5 and PS72/410-3 are first deposited in MIS16, while in core PS72/422-5 strong input of the IRD starts from MIS7. This may suggest that the provenance of sediments deposited on the Makarov Basin side of the Mendeleev Ridge is different from that deposited on the Canada Basin side of the Mendeleev Ridge. The IRD events of MIS 16, 12, 10, 8 are characterized by high dolomite, high quartz/feldspar ratios and low plagioclase and may suggest IRD input from the Canadian Archipelago and the IRD events occur in MIS6 are characterized by high quartz and low dolomite, which indicates IRD from the Eurasian sources.

The age model before MIS7 is still tentative. Although correlations based on XRF scanning and physical properties data were used in this thesis to support the existing age model proposed by Stein (2010a), more independent proxies should be studied to establish a more convincing age model. Clay mineral assemblages should be investigated to further identify the major source areas and transport processes. Other proxies (e.g. Fe oxide grains and radiogenic isotopes of Sr, Nd and Pb) should also be combined to reconstruct the circum-Arctic ice-sheet extension and history.

References

- Aagaard, K., Coachman, L., Carmack, E., 1981. On the halocline of the Arctic Ocean. *Deep Sea Research Part A. Oceanographic Research Papers* 28, 529-545.
- Aagaard, K., Swift, J., Carmack, E., 1985. Thermohaline circulation in the Arctic Mediterranean seas. *Journal of Geophysical Research: Oceans (1978–2012)* 90, 4833-4846.
- Adler, R.E., Polyak, L., Ortiz, J.D., Kaufman, D.S., Channell, J.E.T., Xuan, C., Grottoli, A.G., Sellén, E., Crawford, K.A., 2009. Sediment record from the western Arctic Ocean with an improved Late Quaternary age resolution: HOTRAX core HLY0503-8JPC, Mendeleev Ridge. *Global and Planetary Change* 68, 18-29.
- Aitchison, J., 1986. *The statistical analysis of compositional data*. Chapman & Hall Ltd., New York.
- Alexander, L., Klug, H.P., 1948. Basic aspects of X-ray absorption in quantitative diffraction analysis of powder mixtures. *Analytical Chemistry* 20, 886-889.
- AMAP, 1998. AMAP assessment report: Arctic pollution issues. Arctic Monitoring and Assessment Programme (AMAP).
- Andrews, J., Barber, D., Jennings, A., Eberl, D., Maclean, B., Kirby, M., Stoner, J., 2012. Varying sediment sources (Hudson Strait, Cumberland Sound, Baffin Bay) to the NW Labrador Sea slope between and during Heinrich events 0 to 4. *Journal of Quaternary Science* 27, 475-482.
- Andrews, J.T., Eberl, D., Scott, D., 2010a. Surface (sea floor) and near-surface (box cores) sediment mineralogy in Baffin Bay as a key to sediment provenance and ice sheet variations. *Canadian Journal of Earth Sciences* 48, 1307-1328.
- Andrews, J.T., Eberl, D.D., 2007. Quantitative mineralogy of surface sediments on the Iceland shelf, and application to down-core studies of Holocene ice-rafted sediments. *Journal of Sedimentary Research* 77, 469-479.
- Andrews, J.T., Gibb, O.T., Jennings, A.E., Simon, Q., 2014. Variations in the provenance of sediment from ice sheets surrounding Baffin Bay during MIS 2 and 3 and export to the Labrador Shelf Sea: site HU2008029-0008 Davis Strait. *Journal of Quaternary Science* 29, 3-13.
- Andrews, J.T., Jennings, A.E., Coleman, G.C., Eberl, D.D., 2010b. Holocene variations in mineral and grain-size composition along the East Greenland glaciated margin (ca 67°-70°N): Local versus long-distance sediment transport. *Quaternary Science Reviews* 29, 2619-2632.
- Andrews, J.T., Vogt, C., 2014a. Results of bulk sediment X-ray diffraction analysis and quantification of mineral phases based on the RockJock and on the QUAX quantitative analysis, Supplement to: Andrews, John T; Vogt, Christoph (2014): Source to sink: Statistical identification of regional variations in the mineralogy of surface sediments in the western Nordic Seas (58°N-75°N; 10°W-40°W). *Marine Geology*, 357, 151-162, doi:10.1016/j.margeo.2014.08.005. PANGAEA.
- Andrews, J.T., Vogt, C., 2014b. Source to sink: Statistical identification of regional variations in the mineralogy of surface sediments in the western Nordic Seas (58°N–75°N; 10°W–40°W). *Marine Geology* 357, 151-162.
- Arrigo, K.R., Matrai, P.A., van Dijken, G.L., 2011. Primary productivity in the Arctic Ocean: Impacts of complex optical properties and subsurface chlorophyll maxima on large-scale estimates. *Journal of Geophysical Research: Oceans* 116, C11022.
- Asahara, Y., Takeuchi, F., Nagashima, K., Harada, N., Yamamoto, K., Oguri, K., Tadai, O., 2012. Provenance of terrigenous detritus of the surface sediments in the Bering and Chukchi Seas as

- derived from Sr and Nd isotopes: Implications for recent climate change in the Arctic regions. *Deep Sea Research Part II: Topical Studies in Oceanography* 61–64, 155-171.
- Bakhtmutov, V., Whitledge, T., Wood, K., Ostrovskiy, A., 2009. Report on the execution of marine research in the Bering Strait, East Siberian and the Chukchi Sea by the Russian-American Expedition under the program of "RUSALCA" during the period from 23 August through 30 September, 2009.
- Barry, R.G., 1996. The parameterization of surface albedo for sea ice and its snow cover. *Progress in Physical Geography* 20, 63-79.
- Batchelder, M., Cressey, G., 1998. Rapid, accurate phase quantification of clay-bearing samples using a position-sensitive X-ray detector. *Clays and Clay Minerals* 46, 183-194.
- Bazhenova, E., 2012. Reconstruction of late Quaternary sedimentary environments at the southern Mendeleev Ridge (Arctic Ocean). University of Bremen, Bremen, p. 83.
- Behrends, M., 1999. Reconstruction of sea-ice drift and terrigenous sediment supply in the late Quaternary Heavy-mineral associations in sediments of the Laptev-Sea continental margin and the central Arctic Ocean. *Berichte zur Polarforschung*, 164.
- Behrends, M., Hoops, E., Peregovich, B., 1999. Distribution patterns of heavy minerals in Siberian Rivers, the Laptev Sea and the eastern Arctic Ocean: An approach to identify sources, transport and pathways of terrigenous matter, *Land-Ocean Systems in the Siberian Arctic*. Springer, pp. 265-286.
- Bergmann, J., Kleeberg, R., 1998. Rietveld analysis of disordered layer silicates, *Materials Science Forum*. Trans Tech Publications, pp. 300-305.
- Biscaye, P.E., 1965. Mineralogy and sedimentation of recent deep-sea clay in the Atlantic Ocean and adjacent seas and oceans. *Geological Society of America Bulletin* 76, 803-832.
- Bischof, J., 2000. *Ice drift, ocean circulation and climate change*. Springer, New York.
- Bischof, J., Clark, D.L., Vincent, J.-S., 1996. Origin of Ice-Rafted Debris: Pleistocene Paleooceanography in the Western Arctic Ocean. *Paleoceanography* 11, 743-756.
- Bischof, J.F., Darby, D.A., 1997. Mid- to Late Pleistocene Ice Drift in the Western Arctic Ocean: Evidence for a Different Circulation in the Past. *Science* 277, 74-78.
- Bish, D.L., Chipera, S.J., 1988. Problems and solutions in quantitative analysis of complex mixtures by X-ray powder diffraction, *Advances in X-ray Analysis*. Springer, pp. 295-308.
- Bish, D.L., Chipera, S.J., 1995. Accuracy in quantitative X-ray powder diffraction analyses, *Advances in X-Ray Analysis*. Springer, pp. 47-57.
- Bish, D.L., Howard, S.A., 1988. Quantitative phase analysis using the Rietveld method. *Journal of Applied Crystallography* 21, 86-91.
- Bish, D.L., Post, J.E., 1993. Quantitative mineralogical analysis using the Rietveld full-pattern fitting method. *The American mineralogist* 78, 932-940.
- Bish, D.L., Reynolds, R.C., 1989. Sample preparation for X-ray diffraction. *Reviews in Mineralogy and Geochemistry* 20, 73-99.
- Bradley, R.S., England, J.H., 2008. The Younger Dryas and the Sea of Ancient Ice. *Quaternary Research* 70, 1-10.
- Calvert, C.S., Palkowsky, D.A., Pevear, D.R., 1989. A combined X-ray powder diffraction and chemical method for the quantitative mineral analysis of geological samples, In: Pevear, D.R., Mumpton, F.A. (Eds.), *Quantitative Mineral Analysis of Clays*. Clay Minerals Society, Colorado, USA, pp. 154-166.
- Chao, W., Chunde, P., Daqing, W., Aixia, S., Jihong, N., Shuhua, L., 1996. An improved method for

- quantitative analysis of sedimentary minerals by X-ray diffraction. *Powder Diffraction* 11, 235-239.
- Chipera, S.J., Bish, D.L., 1995. Multireflection RIR and intensity normalizations for quantitative analyses: Applications to feldspars and zeolites. *Powder Diffraction* 10, 47-55.
- Chipera, S.J., Bish, D.L., 2002. FULLPAT: a full-pattern quantitative analysis program for X-ray powder diffraction using measured and calculated patterns. *Journal of Applied Crystallography* 35, 744-749.
- Chung, F.H., 1974a. Quantitative interpretation of X-ray diffraction patterns of mixtures. I. Matrix-flushing method for quantitative multicomponent analysis. *Journal of Applied Crystallography* 7, 519-525.
- Chung, F.H., 1974b. Quantitative interpretation of X-ray diffraction patterns of mixtures. II. Adiabatic principle of X-ray diffraction analysis of mixtures. *Journal of Applied Crystallography* 7, 526-531.
- Clark, D., Whitman, R., Morgan, K., Mackey, S., 1980. Stratigraphy and Glacial-Marine Sediments of the Amerasian Basin, Central Arctic Ocean. *Geological Society of America Special Papers* 181, 1-65.
- Clark, D.L., Hanson, A., 1983. Central Arctic Ocean sediment texture: a key to ice transport mechanisms, Glacial-marine sedimentation. Springer, pp. 301-330.
- Clark, G.L., Reynolds, D.H., 1936. Quantitative analysis of mine dusts: an X-ray diffraction method. *Industrial & Engineering Chemistry Analytical Edition* 8, 36-40.
- Clark, P.U., Piasias, N.G., Stocker, T.F., Weaver, A.J., 2002. The role of the thermohaline circulation in abrupt climate change. *Nature* 415, 863-869.
- Comiso, J.C., 2006. Arctic warming signals from satellite observations. *Weather* 61, 70-76.
- Comiso, J.C., Parkinson, C.L., Gersten, R., Stock, L., 2008. Accelerated decline in the Arctic sea ice cover. *Geophysical Research Letters* 35.
- Cressey, G., Schofield, P.F., 1996. Rapid whole-pattern profile-stripping method for the quantification of multiphase samples. *Powder Diffraction* 11, 35-39.
- da Silva, A.L., de Oliveira, A.H., Souza, M.L., 2011. Influence of preferred orientation of minerals in the mineralogical identification process by X-ray diffraction, International Nuclear Atlantic Conference, Belo Horizonte, MG, Brazil.
- Dalrymple, R.W., Maass, O.C., 1987. Clay mineralogy of late Cenozoic sediments in the CESAR cores, Alpha Ridge, central Arctic Ocean. *Canadian Journal of Earth Sciences* 24, 1562-1569.
- Darby, D., Jakobsson, M., Polyak, L., 2005. Icebreaker expedition collects key Arctic seafloor and ice data. *Eos, Transactions American Geophysical Union* 86, 549.
- Darby, D., Naidu, A., Mowatt, T., Jones, G., 1989. Sediment composition and sedimentary processes in the Arctic Ocean, The Arctic Seas. Springer, pp. 657-720.
- Darby, D.A., 1975. Kaolinite and other clay minerals in Arctic Ocean sediments. *Journal of Sedimentary Research* 45, 272-279.
- Darby, D.A., 2003. Sources of sediment found in sea ice from the western Arctic Ocean, new insights into processes of entrainment and drift patterns. *Journal of Geophysical Research* 108, 3257.
- Darby, D.A., Bischof, J.F., 1996. A statistical approach to source determination of lithic and Fe oxide grains; an example from the Alpha Ridge, Arctic Ocean. *Journal of Sedimentary Research* 66, 599-607.
- Darby, D.A., Bischof, J.F., 2004. A Holocene record of changing Arctic Ocean ice drift analogous to the effects of the Arctic Oscillation. *Paleoceanography* 19, PA1027.
- Darby, D.A., Bischof, J.F., Jones, G.A., 1997. Radiocarbon chronology of depositional regimes in the

- western Arctic Ocean. *Deep Sea Research Part II: Topical Studies in Oceanography* 44, 1745-1757.
- Darby, D.A., Bischof, J.F., Spielhagen, R.F., Marshall, S.A., Herman, S.W., 2002. Arctic ice export events and their potential impact on global climate during the late Pleistocene. *Paleoceanography* 17.
- Darby, D.A., Myers, W., Herman, S., Nicholson, B., 2015. Chemical Fingerprinting, A Precise and Efficient Method To Determine Sediment Sources. *Journal of Sedimentary Research* 85, 247-253.
- Darby, D.A., Myers, W.B., Jakobsson, M., Rigor, I., 2011. Modern dirty sea ice characteristics and sources: The role of anchor ice. *Journal of Geophysical Research* 116, C09008.
- Darby, D.A., Polyak, L., Bauch, H.A., 2006. Past glacial and interglacial conditions in the Arctic Ocean and marginal seas - a review. *Progress In Oceanography* 71, 129-144.
- Darby, D.A., Zimmerman, P., 2008. Ice rafted detritus events in the Arctic during the last glacial interval, and the timing of the Innuitian and Laurentide ice sheet calving events. *Polar Research* 27, 114-127.
- Dieckmann, G.S., Hellmer, H.H., 2010. The importance of sea ice: An overview. *Sea Ice* 2, 1-22.
- Dudarev, O., 2008. Cruise report International Siberian Shelf Study 2008 (ISSS-08). Swedish Knut and Alice Wallenberg Foundation, the Far-Eastern Branch of the Russian Academy of Sciences, the Swedish Research Council, the Russian Foundation for Basic Research, NOAA, and the Swedish Polar Research Secretariat.
- Eberl, D., 2003. User's guide to RockJock, a program for determining quantitative mineralogy from powder X-ray diffraction data. US Geological Survey.
- Eberl, D., 2004. Quantitative mineralogy of the Yukon River system: Changes with reach and season, and determining sediment provenance. *American Mineralogist* 89, 1784.
- Eicken, H., Gradinger, R., Gaylord, A., Mahoney, A., Rigor, I., Melling, H., 2005. Sediment transport by sea ice in the Chukchi and Beaufort Seas: Increasing importance due to changing ice conditions? *Deep Sea Research Part II: Topical Studies in Oceanography* 52, 3281-3302.
- Eicken, H., Reimnitz, E., Alexandrov, V., Martin, T., Kassens, H., Viehoff, T., 1997. Sea-ice processes in the Laptev Sea and their importance for sediment export. *Continental Shelf Research* 17, 205-233.
- Emmertmann, R., Lauterjung, J., 1990. Double X-Ray analysis of cuttings and rock flour: a powerful tool for rapid and reliable determination of borehole lithostratigraphy. *Scientific Drilling* 1, 269-282.
- Fagel, N., Not, C., Gueibe, J., Mattielli, N., Bazhenova, E., 2014. Late Quaternary evolution of sediment provenances in the Central Arctic Ocean: mineral assemblage, trace element composition and Nd and Pb isotope fingerprints of detrital fraction from the Northern Mendeleev Ridge. *Quaternary Science Reviews* 92, 140-154.
- Grigoriev, M.N., Rachold, V., Schirrmeister, L., Hubberten, H.-W., 2004. Organic carbon input to the Arctic Seas through coastal erosion, In: Stein, R., Macdonald, R.W. (Eds.), *The Organic Carbon Cycle in the Arctic Ocean: Present and Past*. Springer, Berlin, pp. 37-65.
- Haley, B.A., Frank, M., Spielhagen, R.F., Fietzke, J., 2008. Radiogenic isotope record of Arctic Ocean circulation and weathering inputs of the past 15 million years. *Paleoceanography* 23, PA1S13.
- Haley, B.A., Polyak, L., 2013. Pre-modern Arctic Ocean circulation from surface sediment neodymium isotopes. *Geophysical Research Letters* 40, 893-897.
- Hanslik, D., Löwemark, L., Jakobsson, M., 2013. Biogenic and detrital-rich intervals in central Arctic Ocean cores identified using x-ray fluorescence scanning. *Polar Research* 32, 18368.

- Hill, R.J., Howard, C.J., 1987. Quantitative phase analysis from neutron powder diffraction data using the Rietveld method. *Journal of Applied Crystallography* 20, 467-474.
- Hillier, S., 1999. Use of an air brush to spray dry samples for X-ray powder diffraction. *Clay Minerals* 34, 127-135.
- Hodell, D.A., Channell, J.E.T., Curtis, J.H., Romero, O.E., Röhl, U., 2008. Onset of “Hudson Strait” Heinrich events in the eastern North Atlantic at the end of the middle Pleistocene transition (~640 ka)? *Paleoceanography* 23, PA4218.
- Hubbard, C.R., Evans, E.H., Smith, D.K., 1976. The reference intensity ratio, I/I_c , for computer simulated powder patterns. *Journal of Applied Crystallography* 9, 169-174.
- Hughes, R., Bohor, B., 1970. Random clay powders prepared by spray-drying. *American Mineralogist* 55, 1780-1786.
- Hull, A.W., 1919. A new method of chemical analysis. *Journal of the American Chemical Society* 41, 1168-1175.
- Jakobsson, M., 2002. Hypsometry and volume of the Arctic Ocean and its constituent seas. *Geochemistry, Geophysics, Geosystems* 3, 1-18.
- Jakobsson, M., Grantz, A., Kristoffersen, Y., Macnab, R., 2003. Physiographic provinces of the Arctic Ocean seafloor. *Geological Society of America Bulletin* 115, 1443-1455.
- Jakobsson, M., Lovlie, R., Al-Hanbali, H., Arnold, E., Backman, J., Morth, M., 2000. Manganese and color cycles in Arctic Ocean sediments constrain Pleistocene chronology. *Geology* 28, 23-26.
- Jakobsson, M., Macnab, R., Mayer, L., Anderson, R., Edwards, M., Hatzky, J., Schenke, H.W., Johnson, P., 2008. An improved bathymetric portrayal of the Arctic Ocean: Implications for ocean modeling and geological, geophysical and oceanographic analyses. *Geophysical Research Letters* 35, L07602.
- Jakobsson, M., Mayer, L., Coakley, B., Dowdeswell, J.A., Forbes, S., Fridman, B., Hodnesdal, H., Noormets, R., Pedersen, R., Rebesco, M., Schenke, H.W., Zarayskaya, Y., Accettella, D., Armstrong, A., Anderson, R.M., Bienhoff, P., Camerlenghi, A., Church, I., Edwards, M., Gardner, J.V., Hall, J.K., Hell, B., Hestvik, O., Kristoffersen, Y., Marcussen, C., Mohammad, R., Mosher, D., Nghiem, S.V., Pedrosa, M.T., Travaglini, P.G., Weatherall, P., 2012. The International Bathymetric Chart of the Arctic Ocean (IBCAO) Version 3.0. *Geophysical Research Letters* 39, L12609.
- Jakobsson, M., Nilsson, J., O'Regan, M., Backman, J., Löwemark, L., Dowdeswell, J.A., Mayer, L., Polyak, L., Colleoni, F., Anderson, L.G., Björk, G., Darby, D., Eriksson, B., Hanslik, D., Hell, B., Marcussen, C., Sellén, E., Wallin, Å., 2010. An Arctic Ocean ice shelf during MIS 6 constrained by new geophysical and geological data. *Quaternary Science Reviews* 29, 3505-3517.
- Jang, K., Han, Y., Huh, Y., Nam, S.-I., Stein, R., Mackensen, A., Matthiessen, J., 2013. Glacial freshwater discharge events recorded by authigenic neodymium isotopes in sediments from the Mendeleev Ridge, western Arctic Ocean. *Earth and Planetary Science Letters* 369–370, 148-157.
- Jokat, W., 2009. The Expedition ARK-XXIII/3 of RV Polarstern in 2008. *Report on Polar Marine Research* 597, 1-221.
- Jonas, E.C., Kuykendall, J.R., 1966. Preparation of montmorillonites for random powder diffraction. *Clay Minerals* 6, 232-235.
- Kahle, M., Kleber, M., Jahn, R., 2002. Review of XRD-based quantitative analyses of clay minerals in soils: the suitability of mineral intensity factors. *Geoderma* 109, 191-205.
- Kleeberg, R., Monecke, T., Hillier, S., 2008. Preferred orientation of mineral grains in sample mounts for quantitative XRD measurements: how random are powder samples? *Clays and Clay Minerals* 56, 404-415.

- Klug, H.P., Alexander, L.E., 1954. X-ray diffraction procedures. Wiley, New York.
- Kos'Ko, M.K., Lopatin, B.G., Ganelin, V.G., 1990. Major geological features of the islands of the East Siberian and Chukchi Seas and the northern coast of Chukotka. *Marine Geology* 93, 349-367.
- Krylov, A.A., Andreeva, I.A., Vogt, C., Backman, J., Krupskaya, V.V., Grikurov, G.E., Moran, K., Shoji, H., 2008. A shift in heavy and clay mineral provenance indicates a middle Miocene onset of a perennial sea ice cover in the Arctic Ocean. *Paleoceanography* 23, PA1S06.
- Krylov, A.A., Stein, R., Ermakova, L.A., 2014. Clay minerals as indicators of late quaternary sedimentation constraints in the Mendeleev Rise, Amerasian Basin, Arctic Ocean. *Lithology and Mineral Resources* 49, 103-116.
- Kwok, R., Spreen, G., Pang, S., 2013. Arctic sea ice circulation and drift speed: Decadal trends and ocean currents. *Journal of Geophysical Research: Oceans* 118, 2408-2425.
- Löwemark, L., Jakobsson, M., Mörth, M., Backman, J., 2008. Arctic Ocean manganese contents and sediment colour cycles. *Polar Research* 27, 105-113.
- Löwemark, L., März, C., O'Regan, M., Gyllencreutz, R., 2014. Arctic Ocean Mn-stratigraphy: genesis, synthesis and inter-basin correlation. *Quaternary Science Reviews* 92, 97-111.
- Löwemark, L., O'Regan, M., Hanebuth, T., Jakobsson, M., 2012. Late Quaternary spatial and temporal variability in Arctic deep-sea bioturbation and its relation to Mn cycles. *Palaeogeography, Palaeoclimatology, Palaeoecology*.
- Lapina, N., 1965. The determination of distribution paths of sediments, based on mineralogical investigations of marine deposits (example Laptev Sea), *Uchennye Zapiski NIIGA*, pp. 139-157.
- Levitan, I., Tarasov, G., Kukina, N., Burtman, M., 1999. Mineral composition of the St. Anna Trough surface sediments. *Oceanology* 39, 821-829.
- Levitan, M., Dekov, V., Gorbunova, Z., Gurvich, E., Muyakshin, S., Nurnberg, D., Pavlidis, M., Ruskova, N., Shelekhova, E., Vasilkov, A., 1996. The Kara Sea: a reflection of modern environment in grain size, mineralogy and chemical composition of the surface layer of bottom sediments, In: Stein, R., Ivanov, G.I., Levitan, M.A., Fahl, K. (Eds.), *Surface-sediment Composition and Sedimentary Processes in the Central Arctic Ocean and Along the Eurasian Continental Margin*. Reports on Polar Research, Bremerhaven, pp. 58-81.
- Lisiecki, L.E., Raymo, M.E., 2005. A Pliocene-Pleistocene stack of 57 globally distributed benthic $\delta^{18}\text{O}$ records. *Paleoceanography* 20, PA1003.
- Lisitzin, A.P., 2002. *Sea-ice and iceberg sedimentation in the ocean: Recent and Past*. Springer, Berlin.
- März, C., Stratmann, A., Matthiessen, J., Meinhardt, A.K., Eckert, S., Schnetger, B., Vogt, C., Stein, R., Brumsack, H.J., 2011b. Manganese-rich brown layers in Arctic Ocean sediments: Composition, formation mechanisms, and diagenetic overprint. *Geochimica Et Cosmochimica Acta* 75, 7668-7687.
- März, C., Vogt, C., Schnetger, B., Brumsack, H.-J., 2011a. Variable Eocene-Miocene sedimentation processes and bottom water redox conditions in the Central Arctic Ocean (IODP Expedition 302). *Earth and Planetary Science Letters* 310, 526-537.
- Macdonald, R., 1996. Awakenings in the Arctic. *Nature* 380, 286-287.
- Macdonald, R., Bewers, J., 1996. Contaminants in the arctic marine environment: priorities for protection. *ICES Journal of Marine Science: Journal du Conseil* 53, 537-563.
- Macdonald, R.W., Sakshaug, E. and Stein, R., 2004. The Arctic Ocean: Modern Status and Recent Climate Change, In: Stein, R., Macdonald, R.W. (Eds.), *The Organic Carbon Cycle in the Arctic Ocean*. Springer, Berlin, pp. 297-322.

- Matthiessen, J., 2010a. X-ray fluorescence on sediment core PS72/396-5 (raw data from XRF-core scanner), Unpublished Dataset ed. Pangaea.
- Matthiessen, J., 2010b. X-ray fluorescence on sediment core PS72/410-3 (raw data from XRF-core scanner), Unpublished Dataset ed. Pangaea.
- Matthiessen, J., 2010c. X-ray fluorescence on sediment core PS72/422-5 (raw data from XRF-core scanner), Unpublished Dataset ed. Pangaea.
- Maurer, J., 2007. Atlas of the Cryosphere. National Snow and Ice Data Center, digital media.
- Mauritzen, C., Häkkinen, S., 1997. Influence of sea ice on the thermohaline circulation in the Arctic - North Atlantic Ocean. *Geophysical Research Letters* 24, 3257-3260.
- McCarty, D.K., 2002. Quantitative Mineral Analysis of Clay-bearing Mixtures: The "Reynolds Cup" Contest. *Commission on Powder Diffraction Newsletters* 27, 12-16.
- Moore, D., Reynolds Jr, R., 1997. *X-Ray Diffraction and the Identification and Analysis of Clay Minerals*. Oxford University Press, Oxford, New York.
- Moritz, R.E., Bitz, C.M., Steig, E.J., 2002. Dynamics of Recent Climate Change in the Arctic. *Science* 297, 1497-1502.
- Moros, M., McManus, J.F., Rasmussen, T., Kuijpers, A., Dokken, T., Snowball, I., Nielsen, T., Jansen, E., 2004. Quartz content and the quartz-to-plagioclase ratio determined by X-ray diffraction: a proxy for ice rafting in the northern North Atlantic? *Earth and Planetary Science Letters* 218, 389-401.
- Myers, W.B., Darby, D.A., 2015. A new age model for the Central Arctic reveals brief intervals of extreme sedimentation rates over the last 140 kyr. *Arktos* 1, 1-20.
- Mysak, L.A., 2001. Patterns of Arctic circulation. *Science* 293, 1269-1270.
- Nørgaard-Pedersen, N., Mikkelsen, N., Kristoffersen, Y., 2007. Arctic Ocean record of last two glacial-interglacial cycles off North Greenland/Ellesmere Island -- Implications for glacial history. *Marine Geology* 244, 93-108.
- Nørgaard-Pedersen, N., Spielhagen, R.F., Erlenkeuser, H., Grootes, P.M., Heinemeier, J., Knies, J., 2003. Arctic Ocean during the Last Glacial Maximum: Atlantic and polar domains of surface water mass distribution and ice cover. *Paleoceanography* 18, 1063.
- Nørgaard-Pedersen, N., Spielhagen, R.F., Thiede, J., Kassens, H., 1998. Central Arctic Surface Ocean Environment During the Past 80,000 Years. *Paleoceanography* 13, 193-206.
- Nürnberg, D., Levitan, M., Pavlidis, J., Shelekhova, E., 1995. Distribution of clay minerals in surface sediments from the eastern Barents and south-western Kara seas. *Geologische Rundschau* 84, 665-682.
- Nürnberg, D., Wollenburg, I., Dethleff, D., Eicken, H., Kassens, H., Letzig, T., Reimnitz, E., Thiede, J., 1994. Sediments in Arctic sea ice: Implications for entrainment, transport and release. *Marine Geology* 119, 185-214.
- Naidu, A.S., Creager, J.S., Mowatt, T.C., 1982. Clay mineral dispersal patterns in the north Bering and Chukchi Seas. *Marine Geology* 47, 1-15.
- Naidu, A.S., Mowatt, T.C., 1983. Sources and dispersal patterns of clay minerals in surface sediments from the continental-shelf areas off Alaska. *Geological Society of America Bulletin* 94, 841-854.
- Naugler, F.P., Silverberg, N., Creager, J.S., 1974. Recent sediments of the East Siberian Sea, *Marine Geology and Oceanography of the Arctic Seas*. Springer, pp. 191-210.
- Niessen, F., Magens, D., Gebhardt, A., 2007. Physical properties of the AND-1B Core, ANDRILL McMurdo ice shelf project, Antarctica. *Terra Antarctica* 14, 155-166.

- Niessen, F., Poggemann, D., Schulte-Loh, I., 2009. Physical properties and core logging, In: Jokat, W. (Ed.), *The Expedition of the Research Vessel "Polarstern" to the Arctic in 2008 (ARK-XXIII/3)* Rep. Polar Res, pp. 23-26.
- O'Regan, M., King, J., Backman, J., Jakobsson, M., P like, H., Moran, K., Heil, C., Sakamoto, T., Cronin, T., Jordan, R., 2008. Constraints on the Pleistocene chronology of sediments from the Lomonosov Ridge. *Paleoceanography* 23, PA1S19.
- O'Regan, M., Sellén, E., Jakobsson, M., 2014. Middle to late Quaternary grain size variations and sea-ice rafting on the Lomonosov Ridge. *Polar Research* 33, 23672.
- Okulitch, A.V., 1991. Geology of the Canadian Archipelago and North Greenland, In: Tretteln, H.P. (Ed.), *Innuitian orogen and Arctic Platform: Canada and Greenland*.
- Omotoso, O., Eberl, D., 2009. Sample preparation and data collection strategies for X-ray diffraction quantitative phase analysis of clay-bearing rocks, 46th Annual Meeting of The Clay Minerals Society.
- Omotoso, O., McCarty, D.K., Hillier, S., Kleeberg, R., 2006. Some successful approaches to quantitative mineral analysis as revealed by the 3rd Reynolds Cup contest. *Clays and Clay Minerals* 54, 748-760.
- Ortiz, J.D., Polyak, L., Grebmeier, J.M., Darby, D., Eberl, D.D., Naidu, S., Nof, D., 2009. Provenance of Holocene sediment on the Chukchi-Alaskan margin based on combined diffuse spectral reflectance and quantitative X-Ray Diffraction analysis. *Global and Planetary Change* 68, 71-84.
- Parkinson, C.L., Comiso, J.C., 2013. On the 2012 record low Arctic sea ice cover: Combined impact of preconditioning and an August storm. *Geophysical Research Letters* 40, 1356-1361.
- Pawloski, G.A., 1985. Quantitative determination of mineral content of geological samples by X-ray diffraction. *American Mineralogist* 70, 663-667.
- Petschick, R., 2002. *MacDiff 4.2. 6. Manual*. Institut für Geologie, Universität Erlangen: Germany.
- Petschick, R., Kuhn, G., Gingele, F., 1996. Clay mineral distribution in surface sediments of the South Atlantic: sources, transport, and relation to oceanography. *Marine Geology* 130, 203-229.
- Pfirman, S., Lange, M., Wollenburg, I., Schlosser, P., 1990. Sea ice characteristics and the role of sediment inclusions in deep-sea deposition: Arctic—Antarctic comparisons, *Geological history of the polar oceans: Arctic versus Antarctic*. Springer, pp. 187-211.
- Phillips, R.L., Grantz, A., 2001. Regional variations in provenance and abundance of ice-rafted clasts in Arctic Ocean sediments: implications for the configuration of late Quaternary oceanic and atmospheric circulation in the Arctic. *Marine Geology* 172, 91-115.
- Pithan, F., Mauritsen, T., 2014. Arctic amplification dominated by temperature feedbacks in contemporary climate models. *Nature Geosci* 7, 181-184.
- Polyak, L., Alley, R.B., Andrews, J.T., Brigham-Grette, J., Cronin, T.M., Darby, D.A., Dyke, A.S., Fitzpatrick, J.J., Funder, S., Holland, M., 2010. History of sea ice in the Arctic. *Quaternary Science Reviews* 29, 1757-1778.
- Polyak, L., Best, K.M., Crawford, K.A., Council, E.A., St-Onge, G., 2013. Quaternary history of sea ice in the western Arctic Ocean based on foraminifera. *Quaternary Science Reviews* 79, 145-156.
- Polyak, L., Bischof, J., Ortiz, J.D., Darby, D.A., Channell, J.E.T., Xuan, C., Kaufman, D.S., Løvlie, R., Schneider, D.A., Eberl, D.D., Adler, R.E., Council, E.A., 2009. Late Quaternary stratigraphy and sedimentation patterns in the western Arctic Ocean. *Global and Planetary Change* 68, 5-17.
- Polyak, L., Curry, W.B., Darby, D.A., Bischof, J., Cronin, T.M., 2004. Contrasting glacial/interglacial regimes in the western Arctic Ocean as exemplified by a sedimentary record from the Mendeleev

- Ridge. *Palaeogeography, Palaeoclimatology, Palaeoecology* 203, 73-93.
- Polyak, L., Jakobsson, M., 2011. Quaternary sedimentation in the Arctic Ocean: Recent advances and further challenges. *Oceanography* 24, 52-64.
- Proshutinsky, A.Y., Johnson, M.A., 1997. Two circulation regimes of the wind-driven Arctic Ocean. *Journal of Geophysical Research* 102, 12493-12514.
- Rachold, V., 1999. Major, Trace and Rare Earth Element Geochemistry of Suspended Particulate Material of East Siberian Rivers Draining to the Arctic Ocean, In: Kassens, H., Bauch, H., Dmitrenko, I., Eicken, H., Hubberten, H.-W., Melles, M., Thiede, J., Timokhov, L. (Eds.), *Land-Ocean Systems in the Siberian Arctic*. Springer Berlin Heidelberg, pp. 199-222.
- Rachold, V., Eicken, H., Gordeev, V., Grigoriev, M.N., Hubberten, H.-W., Lisitzin, A.P., Shevchenko, V., Schirrmeister, L., 2004. Modern terrigenous organic carbon input to the Arctic Ocean, The organic carbon cycle in the Arctic Ocean. Springer, pp. 33-55.
- Reimnitz, E., Barnes, P., Weber, W., 1993. Particulate matter in pack ice of the Beaufort Gyre. *Journal of Glaciology* 39, 186-198.
- Reimnitz, E., McCormick, M., Bischof, J., Darby, D., 1998. Comparing sea-ice sediment load with Beaufort Sea shelf deposits: is entrainment selective? *Journal of Sedimentary Research* 68, 777-787.
- Rietveld, H., 1969. A profile refinement method for nuclear and magnetic structures. *Journal of Applied Crystallography* 2, 65-71.
- Rossak, B., Kassens, H., Lange, H., Thiede, J., 1999. Clay mineral distribution in surface sediments of the Laptev Sea: Indicator for sediment provinces, dynamics and sources, *Land-Ocean Systems in the Siberian Arctic*. Springer, pp. 587-599.
- Ruddiman, W.F., Bowles, F.A., 1976. Early interglacial bottom-current sedimentation on the eastern Reykjanes Ridge. *Marine Geology* 21, 191-210.
- Rudels, B., 2015. Arctic Ocean circulation, processes and water masses: a description of observations and ideas with focus on the period prior to the International Polar Year 2007-2009. *Progress In Oceanography* 132, 22-67.
- Schauer, U., 2012. The expedition of the research vessel "Polarstern" to the Arctic in 2011 (ARK-XXVI/3-TransArc). *Reports on Polar and Marine research* 649.
- Schlosser, P., Swift, J.H., Lewis, D., Pfirman, S.L., 1995. The role of the large-scale Arctic Ocean circulation in the transport of contaminants. *Deep Sea Research Part II: Topical Studies in Oceanography* 42, 1341-1367.
- Schoster, F., 2005. Terrigenous sediment supply and paleoenvironment in the Arctic Ocean during the late Quaternary: Reconstructions from major and trace elements. *Report on Polar Marine Research* 498, 149.
- Schoster, F., Behrends, M., Müller, C., Stein, R., Wahnert, M., 2000. Modern river discharge and pathways of supplied material in the Eurasian Arctic Ocean: evidence from mineral assemblages and major and minor element distribution. *International Journal of Earth Sciences* 89, 486-495.
- Schulte-Loh, I., 2009. *Paläoumweltbedingungen im spätquartären Arktischen Ozean: Rekonstruktion nach sedimentologischen Untersuchungen an Sedimentkernen vom Mendeleev-Rücken*, Fachbereich 8/Geographie. Universität Bremen, Bremen.
- Screen, J.A., Simmonds, I., 2010. The central role of diminishing sea ice in recent Arctic temperature amplification. *Nature* 464, 1334-1337.
- Sellén, E., O'Regan, M., Jakobsson, M., 2010. Spatial and temporal Arctic Ocean depositional regimes:

- a key to the evolution of ice drift and current patterns. *Quaternary Science Reviews* 29, 3644-3664.
- Serreze, M., Walsh, J., Chapin III, F., Osterkamp, T., Dyurgerov, M., Romanovsky, V., Oechel, W., Morison, J., Zhang, T., Barry, R., 2000. Observational evidence of recent change in the northern high-latitude environment. *Climatic Change* 46, 159-207.
- Serreze, M.C., Francis, J.A., 2006. The Arctic amplification debate. *Climatic Change* 76, 241-264.
- Serreze, M.C., Holland, M.M., Stroeve, J., 2007. Perspectives on the Arctic's shrinking sea-ice cover. *Science* 315, 1533-1536.
- Shackleton, N., 1987. Oxygen isotopes, ice volume and sea level. *Quaternary Science Reviews* 6, 183-190.
- Shevchenko, V.P., Lisitsin, A.P., Vinogradova, A., Vasil'ev, L., Ivanov, G., Klyuvitkin, A., Kriews, M., Novigatsky, A., 2004. New view on the influence of aeolian transport on the modern sedimentation and environment in the Arctic-results of studies of aerosols and snow (in Russian).
- Simon, Q., Hillaire-Marcel, C., St-Onge, G., Andrews, J.T., 2013. North-eastern Laurentide, western Greenland and southern Inuitian ice stream dynamics during the last glacial cycle. *Journal of Quaternary Science*, n/a-n/a.
- Smith, D.K., Johnson, G.G., Scheible, A., Wims, A.M., Johnson, J.L., Ullmann, G., 1987. Quantitative X-ray powder diffraction method using the full diffraction pattern. *Powder Diffraction* 2, 73-77.
- Smith, S.T., Snyder, R.L., Brownell, W., 1979a. Minimization of preferred orientation in powders by spray drying, *Advances in X-ray Analysis*. Springer, pp. 77-87.
- Smith, S.T., Snyder, R.L., Brownell, W., 1979b. Quantitative phase analysis of Devonian shales by computer controlled X-ray diffraction of spray dried samples, *Advances in X-ray Analysis*. Springer, pp. 181-191.
- Snyder, R.L., Bish, D.L., 1989. Quantitative Analysis, In: Bish, D.L., Post, J.E. (Eds.), *Modern powder diffraction*. Mineralogical Society of America *Reviews in Mineralogy*, pp. 101-144.
- Spielhagen, R., Bonani, G., Eisenhauer, A., Frank, M., Frederichs, T., Kassens, H., Kubik, P., Mangini, A., Nogaard Pedersen, N., Nowaczyk, N., 1997. Arctic Ocean evidence for late Quaternary initiation of northern Eurasian ice sheets. *Geology* 25, 783.
- Spielhagen, R.F., Baumann, K.-H., Erlenkeuser, H., Nowaczyk, N.R.N.R., Nørgaard-Pedersen, N., Vogt, C., Weiel, D., 2004. Arctic Ocean deep-sea record of northern Eurasian ice sheet history. *Quaternary Science Reviews* 23, 1455-1483.
- Środoń, J., Drits, V.A., McCarty, D.K., Hsieh, J.C., Eberl, D.D., 2001. Quantitative X-ray diffraction analysis of clay-bearing rocks from random preparations. *Clays and Clay Minerals* 49, 514-528.
- Stein, R., 2008. *Arctic Ocean Sediments: Processes, Proxies, and Paleoenvironment: Processes, Proxies, and Paleoenvironment*. Elsevier.
- Stein, R., 2015. The Expedition PS87 of the Research Vessel POLARSTERN to the Arctic Ocean in 2014. *Reports on Polar and Marine research* 688.
- Stein, R., Boucein, B., Fahl, K., Garcia de Oteyza, T., Knies, J., Niessen, F., 2001. Accumulation of particulate organic carbon at the Eurasian continental margin during late Quaternary times: controlling mechanisms and paleoenvironmental significance. *Global and Planetary Change* 31, 87-104.
- Stein, R., Dittmers, K., Fahl, K., Kraus, M., Matthiessen, J., Niessen, F., Pirrung, M., Polyakova, Y., Schoster, F., Steinke, T., Fütterer, D.K., 2004. Arctic (palaeo) river discharge and environmental change: evidence from the Holocene Kara Sea sedimentary record. *Quaternary Science Reviews* 23, 1485-1511.

- Stein, R., Hefter, J., Grützner, J., Voelker, A., Naafs, B.D.A., 2009. Variability of surface water characteristics and Heinrich - like events in the Pleistocene midlatitude North Atlantic Ocean: Biomarker and XRD records from IODP Site U1313 (MIS 16 - 9). *Paleoceanography* 24, PA2203.
- Stein, R., Matthiessen, J., Niessen, F., Krylov, A., Nam, S.-i., Bazhenova, E., 2010a. Towards a better (litho-) stratigraphy and reconstruction of Quaternary paleoenvironment in the Amerasian Basin (Arctic Ocean). *Polarforschung* 79, 97-121.
- Stein, R., Matthiessen, J., Niessen, F., 2010b. Re-coring at Ice Island T3 site of key core FL-224 (Nautilus Basin, Amerasian Arctic): sediment characteristics and stratigraphic framework. *Polarforschung* 79, 81-96.
- Stroeve, J., Holland, M.M., Meier, W., Scambos, T., Serreze, M., 2007. Arctic sea ice decline: Faster than forecast. *Geophysical Research Letters* 34.
- Stroeve, J., Serreze, M., Drobot, S., Gearheard, S., Holland, M., Maslanik, J., Meier, W., Scambos, T., 2008. Arctic sea ice extent plummets in 2007. *Eos, Transactions American Geophysical Union* 89, 13-14.
- Stroeve, J., Serreze, M., Holland, M., Kay, J., Malanik, J., Barrett, A., 2012. The Arctic's rapidly shrinking sea ice cover: a research synthesis. *Climatic Change* 110, 1005-1027.
- Tütken, T., Eisenhauer, A., Wiegand, B., Hansen, B.T., 2002. Glacial-interglacial cycles in Sr and Nd isotopic composition of Arctic marine sediments triggered by the Svalbard/Barents Sea ice sheet. *Marine Geology* 182, 351-372.
- Thompson, D., Wallace, J., 1998. The Arctic Oscillation signature in the wintertime geopotential height and temperature fields. *Geophysical Research Letters* 25, 1297-1300.
- Thompson, R., Oldfield, F., 1986. *Environmental magnetism*. Allen and Unwin, London.
- Ufer, K., Kleeberg, R., 2015. Parametric Rietveld refinement of coexisting disordered clay minerals. *Clay Minerals* 50, 287-296.
- Ufer, K., Kleeberg, R., Bergmann, J., Dohrmann, R., 2012a. Rietveld refinement of disordered illite-smectite mixed-layer structures by a recursive algorithm. I: One-dimensional patterns. *Clays and Clay Minerals* 60, 507-534.
- Ufer, K., Kleeberg, R., Bergmann, J., Dohrmann, R., 2012b. Rietveld refinement of disordered illite-smectite mixed-layer structures by a recursive algorithm. II: powder-pattern refinement and quantitative phase analysis. *Clays and Clay Minerals* 60, 535-552.
- Villaseñor, T., Jaeger, J.M., 2014. Data report: quantitative powder X-ray diffraction analysis from the Canterbury Basin, Expedition 317, Proceedings of the Integrated Ocean Drilling Program, pp. 1-38.
- Viscosi-Shirley, C., Mammone, K., Piasias, N., Dymond, J., 2003a. Clay mineralogy and multi-element chemistry of surface sediments on the Siberian-Arctic shelf: implications for sediment provenance and grain size sorting. *Continental Shelf Research* 23, 1175-1200.
- Viscosi-Shirley, C., Piasias, N., Mammone, K., 2003b. Sediment source strength, transport pathways and accumulation patterns on the Siberian-Arctic's Chukchi and Laptev shelves. *Continental Shelf Research* 23, 1201-1225.
- Vogt, C., 1996. Bulk mineralogy in surface sediments from the eastern central Arctic Ocean, In: Stein, R., Ivanov, G.I., Levitan, M.A., Fahl, K. (Eds.), *Surface-sediment Composition and Sedimentary Processes in the Central Arctic Ocean and Along the Eurasian Continental Margin*. Reports on Polar Research, Bremerhaven, pp. 159-171.
- Vogt, C., 1997. Regional and temporal variations of mineral assemblages in Arctic Ocean sediments as climatic indicator during glacial/interglacial changes. *Report on Polar Marine Research* 251, 309.

- Vogt, C., Knies, J., 2008. Sediment dynamics in the Eurasian Arctic Ocean during the last deglaciation — The clay mineral group smectite perspective. *Marine Geology* 250, 211-222.
- Vogt, C., Knies, J., Spielhagen, R.F., Stein, R., 2001. Detailed mineralogical evidence for two nearly identical glacial/deglacial cycles and Atlantic water advection to the Arctic Ocean during the last 90,000 years. *Global and Planetary Change* 31, 23-44.
- Vogt, C., Lauterjung, J., Fischer, R.X., 2002. Investigation of the Clay Fraction (<2 μm) of the Clay Minerals Society Reference Clays. *Clays and Clay Minerals* 50, 388-400.
- Wahsner, M., Müller, C., Stein, R., Ivanov, G., Levitan, M., Shelekhova, E., Tarasov, G., 1999. Clay-mineral distribution in surface sediments of the Eurasian Arctic Ocean and continental margin as indicator for source areas and transport pathways—a synthesis. *Boreas* 28, 215-233.
- Wang, R., Xiao, W., März, C., Li, Q., 2013. Late Quaternary paleoenvironmental changes revealed by multi-proxy records from the Chukchi Abyssal Plain, western Arctic Ocean. *Global and Planetary Change* 108, 100-118.
- Wang, R.J., Xiao, W.S., Li, W.B., Sun, Y.C., 2010. Late quaternary ice-rafted detritus events in the Chukchi Basin, western Arctic Ocean. *Chinese Science Bulletin* 55, 432-440.
- Wassmuth, S., 2014. (Sub-) Centennial variability of Holocene Pacific water inflow in the Chukchi Sea (Arctic Ocean): Reconstruction from mineralogical and XRF scanning data, Fachbereich 5/ Geowissenschaften. Universität Bremen, Bremen.
- Weber, M.E., Niessen, F., Kuhn, G., Wiedicke, M., 1997. Calibration and application of marine sedimentary physical properties using a multi-sensor core logger. *Marine Geology* 136, 151-172.